ROMA TRE
UNIVERSITÀ DEGLI STUDI

University of Roma Tre
Department of Physics "Edoardo Amaldi"
Doctoral School of Mathematics and Physics
XXV*th* Cycle

Analysis of the Global Radioxenon Background with Atmospheric Transport Modelling for Nuclear Explosion Monitoring

by
Michael Schöppner

ROME, ITALY - 2012

Tutor: Prof. Wolfango Plastino

Coordinator: Prof. Roberto Raimondi

The world was not meant to be a prison
in which man awaits his execution.

- John F. Kennedy, 1962

Abstract

Radioxenon plays an important role in the monitoring of nuclear explosions, particularly in the detection of nuclear tests. Due to its inert character as a noble gas it is a likely candidate to escape from the cavity of an underground nuclear explosions. In any case, once in the atmosphere it is subject to prevailing winds and can be transported over vast distances, while the dispersion in the atmosphere leads to a dilution of the concentration. Beta-gamma coincidence and high-resolution gamma techniques allow to detect concentration as small as $1\,^{\mathrm{mBq}}/_{\mathrm{m}^3}$ and below. A worldwide monitoring system is currently under construction by the Comprehensive Nuclear-Test-Ban Treaty Organization and already over 80% operational.

However, besides nuclear explosions also other sources of radioxenon exist. Nuclear fission processes involving heavy nuclei produce a certain yield of radioxenon isotopes. The strongest atmospheric emitters are nuclear power plants and medical isotope production facilities. Atmospheric Transport Modelling (ATM) has the potential to support the analysis of radioxenon detections. It is a relatively new tool that has come available in recent years due to improvements in computation power and data storage capabilities. The Lagrangian particle dispersion model FLEXPART can simulate the sensitivity between sources and receptors on a global scale.

The importance of ATM in radioxenon monitoring of nuclear explosions has increased since the existence and strength of background sources are known. The role of ATM in monitoring of nuclear explosions against this radioxenon background are examined in this work. The results can be divided in three parts.

First, the general radioxenon background was analysed. The background for all 39 IMS noble gas stations was simulated for the course of one year and the time series of each station follows a certain distribution. The simulated data are compared with experimental data for stations with available data. Regionally dominant emitters of radioxenon and the impact of the availability of known, time resolved source term - opposed to a yearly average - on the ATM prediction capability is validated. Also, using the Fukushima nuclear accident as an example it is demonstrated that it is possible to reconstruct a source term of known location. The problem of reconstruction is reduced to solving an overdetermined set of linear equations.

Secondly, possible roles of ATM in the automatic categorisation are suggested. ATM can be used to train categorisation schemes that inherently do not apply ATM. On the other hand ATM itself can be incorporated in such a scheme.

Third, the network coverage of the IMS noble gas component is defined in order to quantify its capability to detect nuclear explosions worldwide. Different emission and background scenarios are used to determine the ratio of detected and undetected hypothetical events, and recommendations to improve this value are given.

Contents

List of Figures

List of Tables

List of Abbreviations

ARIX	Automatic Radioanalyzer for Isotopic Xenon
ATM	Atmospheric Transport Modelling
CTBT	Comprehensive Nuclear-Test-Ban Treaty
CTBTO	CTBT Organization
HEU	Highly Enriched Uranium
IDC	International Data Centre
IMS	International Monitoring System
INGE	International Noble Gas Experiment
IPF	Isotope Production Facility
ITCZ	Intertropical Convergence Zone
LEU	Low Enriched Uranium
MDC	Minimum Detectable Concentration
NDC	National Data Centre
NPP	Nuclear Power Plant
NTS	Nevada Test Site
PTS	Provisional Technical Secretariat
SAUNA	Swedish Automatic Unit for Noble gas Acquisition
SPALAX	Système de Prélèvements Automatique en Ligne avec l'Analyse du Xénon
SRS	Source-Receptor Sensitivity
vDEC	virtual Data Exploitation Centre
WOSMIP	Workshop on Signatures of Medical and Industrial Isotope Production

Chapter 1

Introduction

1.1 Background and Motivation

In the past half century certainly some progress has been made in the fields of nuclear non-proliferation and disarmament. Already during the Cold War most nuclear weapon states have moved their nuclear weapon tests to underground. The absolute number of nuclear tests has been drastically reduced since the end of the Cold War and by today all official nuclear weapon states have stopped testing, with China and France being the last testers in 1996. Four countries have completely abolished their nuclear weapon programmes, namely South Africa, Kazakhstan, Ukraine and Belarus. The Non-Proliferation Treaty (NPT) has been extended indefinitely in 1995. As far as publicly known the ban of nuclear weapons in space is still complied.

On the other hand four countries successfully developed a nuclear weapons programme after the NPT entered into force. Of these India, Pakistan and North Korea were also the only countries to testing nuclear weapons since the official nuclear weapon states stopped doing so. The reasoning for the latest Iraq war showed that the sheer suspicion of possessing weapons of mass destruction, expressed by a single state, suffices to initiate a war. Today's civil, nuclear program of Iran runs in contradiction to a resolution of the United Nations. North Korea was the latest country to develop and test nuclear weapons, while expressing threats against other countries. Though, the absolute number of nuclear weapons has been clearly reduced after the end of the Cold War, especially by the USA and Russia, still about 12,000 warheads exist worldwide.

The beginning of the nuclear age is widely regarded to be July 16, 1945. On this date the Trinity test, the first nuclear explosion in history, has been conducted in New Mexico, USA, within the frame of the famous Manhattan Project. The Trinity test device was based on a ^{239}Pu implosion-design. About three weeks later, on August 6 and 9, 1945, the USA carried out the first and so far only nuclear attacks by bombing the Japanese cities of Hiroshima and Nagasaki. The nuclear bomb deployed at Hiroshima, known

Table 1.1: Known first tests of nuclear weapon states. The former five are the NPT-acknowledged nuclear weapon states, for which details are well known. The latter three are called de-facto nuclear weapon states with less confirmed details.

Country	First test		Total number of tests
	in year	yield	
USA	1945	20 kt	1,054
Soviet Union	1949	22 kt	715
Great Britain	1952	25 kt	45
France	1960	70 kt	210
China	1964	22 kt	45
India	1974	12 kt	6
Pakistan	1998	40 kt	6 or more
North Korea	2006	≈ 1 kt	2 or 3

as Little Boy, was of an ^{235}U gun-type design, which means that this was the unusual case of a previously untested type of weapon. For the bombing of Nagasaki a plutonium implosion-type design was used in a bomb known as Fat Man. This one was similar (but not identical) to the Trinity device. About 92,000 people were killed immediately by the two explosions, and it is estimated that further 130,000 people died due to the after effects, which are appearing in the population until today.

Since then new nuclear weapon states (NWS) have emerged from the international community; information about their nuclear testing is listed in Table 1.1. The spread of nuclear weapons in more and more countries is called horizontal proliferation. The probably most widely known measure against horizontal proliferation is the NPT from 1968. It has entered into force in 1970 and is overseen by the International Atomic Energy Agency (IAEA). The build-up of existing nuclear arsenals and improvement of nuclear weapon technology is called vertical proliferation. This happened for example especially during the Cold War as part of the arms race between the USA and the Soviet Union. Newly developed weapons are usually tested before entering a state's arsenal. An internationally pursued measure to prevent vertical proliferation is the Comprehensive Nuclear-Test-Ban Treaty (CTBT), which was adopted by the United Nations General Assembly in 1996. Once into force it will prohibit its ratifying member states to conduct nuclear explosions and thus discourages to develop new nuclear weapons. The compliance with the treaty will be overseen by the CTBT Organisation (CTBTO) based in Vienna, Austria. In order to effectively do this the International Monitoring System (IMS) is designed to monitor nuclear explosions worldwide, see Figure 1.1. It is currently under construction and of the total of 337 facilities already over 80% are operational [`http://www.ctbto.org/map/`].

In general it is conceivable that (a) a state tests a nuclear bomb and publicly admits it, (b) a state tests a nuclear bomb, but does not admit it, or (c) conducting a conventional/chemical explosion and claiming it to be nuclear. In any case the true nature of the event must be independently assessed not from a political but a physical point of view as it is necessary for a sound decision making of the international community.

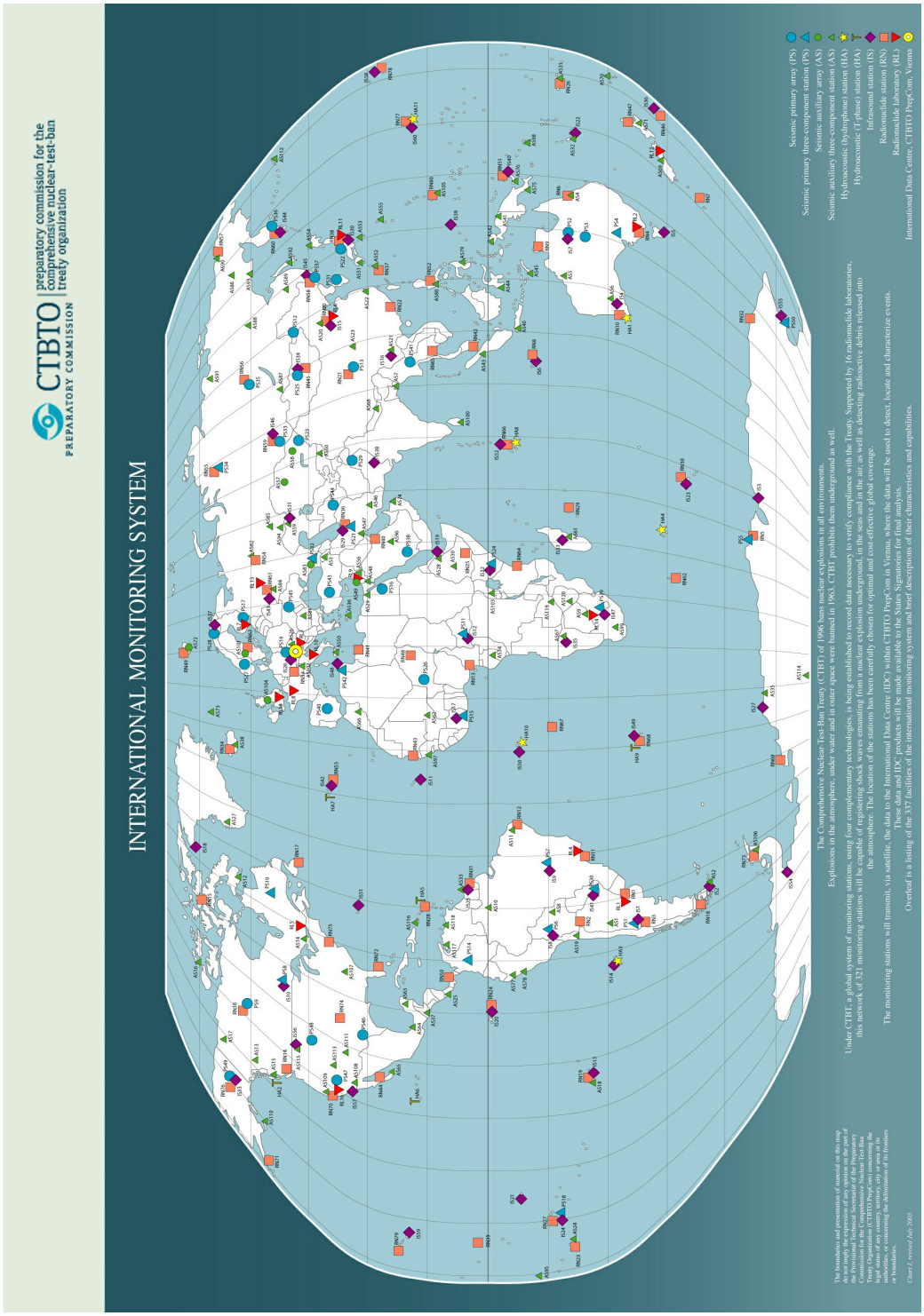

Figure 1.1: Map of IMS facilities. [`http://www.ctbto.org/`] Shown are seismic, hydroacoustic, infrasound and radionuclide stations, and the International Data Centre in Vienna, Austria.

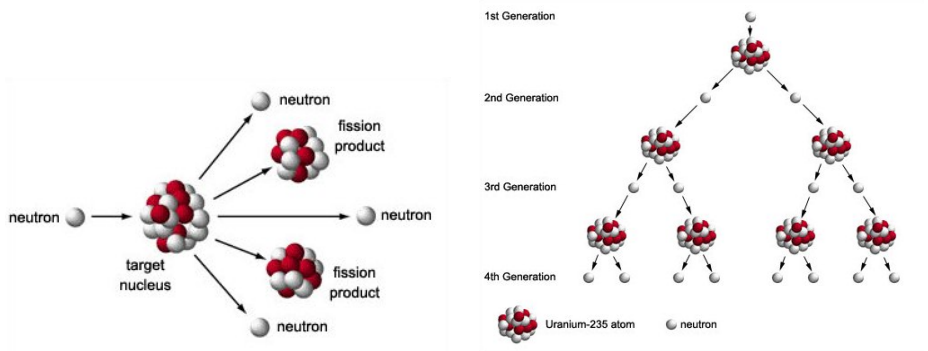

(a) (b)

Figure 1.2: Nuclear fission (a) and a fission chain reaction (b). (`www.atomicarchive.com`) If a critical mass and density of fissile material is exceeded, one fission process can trigger a chain reaction.

1.2 Basics of Nuclear Explosion Monitoring

The excess energy from a nuclear explosion is released by the exothermic chain reaction of induced nuclear fission. As opposed to spontaneous nuclear fission, where an isotope decays without external influence due to its own instable nucleon configuration, the induced fission is initiated by an external neutron. In this case an incoming neutron is absorbed by the nucleus, excites it to an unstable state and thus causes the fission process. Due to the conservation of energy

$$E = (m_{original} - m_{final})\,\mathrm{c}^2 \tag{1.1}$$

the binding energies are released as the nucleus breaks into fragments, e.g.

$$^{235}\mathrm{U} + n \quad \rightarrow \quad X_1 + X_2 + 2.4\,\mathrm{n} + 192.9\,\mathrm{MeV} \tag{1.2}$$

or

$$^{239}\mathrm{Pu} + n \rightarrow X_1 + X_2 + 2.9\,\mathrm{n} + 198.5\,\mathrm{MeV}\,, \tag{1.3}$$

where X_1 and X_2 represent sample fragments, see Figure 1.2a. In bulk material the additional neutrons can initiate further fission processes, which can lead to a chain reaction, see Figure 1.2b, if a certain material-dependent mass is exceeded. The fission products are created due to certain yields that depend on the fission material and the energy of the fission inducing neutrons. As seen in Figure 1.3 the fission product yield varies between $< 0.01\,\%$ for isotopes with mass numbers $A \lesssim 75$ and $A \gtrsim 155$, and values up to $\approx 10\,\%$ for isotopes with mass numbers around $A \approx 95$ and $A \approx 140$. The excess energy is released into the environment as heat, air blast etc.

A high-energetic event like a nuclear explosion couples in many ways into its environment. The coupling into the solid surroundings, e.g. in the case of an underground nuclear explosion, can create a seismic wave that can be detected. Foremost, multiple

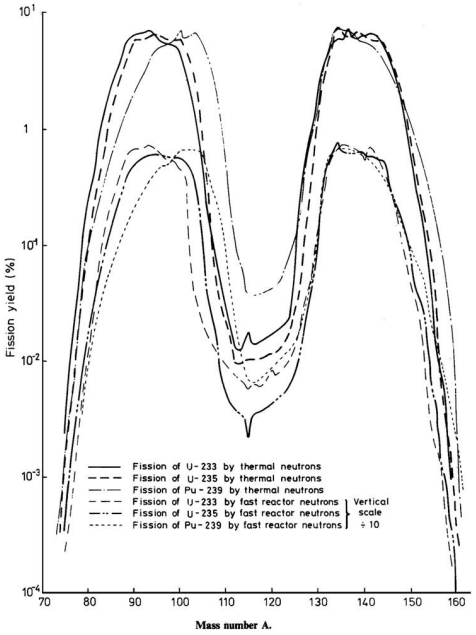

Figure 1.3: The fission yield depending on the mass number A. [Sow12] The probability distribution depends on the fission material and the neutron energy. ^{235}U and ^{239}Pu are common as fuel products for nuclear reactors and as material for nuclear weapons. ^{233}U is used in the thorium fuel cycle.

stations make it possible to locate a seismic event. With seismic monitoring it is also possible to distinguish between explosions and earthquakes due to their different excitation characteristics, see Figure 1.4. However, it is not possible to deduct the nature of the explosion, e.g. chemical or nuclear, from seismic data. On the other hand, seismic monitoring allows to reconstruct the yield of the explosion. This has been demonstrated for example with a Kazakh seismic station near Borovoye (BRV) that has monitored the US Nevada Test Site (NTS) during periods of nuclear tests [Adu93]:

$$\begin{aligned} m_b\,(BRV - NTS) &= 0.52 \cdot \log q + 4.78\,, \text{ for } q < 20\,\text{kt}\,, \\ m_b\,(BRV - NTS) &= 1.07 \cdot \log q + 4.13\,, \text{ for } 20 \leq q \leq 150\,\text{kt}\,, \\ m_b\,(BRV - NTS) &= 0.53 \cdot \log q + 5.48\,, \text{ for } q > 150\,\text{kt}\,. \end{aligned} \tag{1.4}$$

From estimating the yield of an explosion-like event certain assumptions can be made about the nature of the explosion. Chemical explosions are technically and logistically difficult to realize beyond a certain yield, whereas nuclear explosions cannot be made arbitrarily small. However, both overlap in the region below 1 kt TNT equivalent. Thus, explosions within this range can usually not be clearly identified. The strength of the IMS seismic component is the ability to locate events. The IMS design includes a total of 170 seismic stations for worldwide coverage [Bar01], see Figure 1.1.

In case of an underwater nuclear explosion hydroacoustic waves are created. Due to special characteristics of sea water these waves can travel vast distances in the so-called

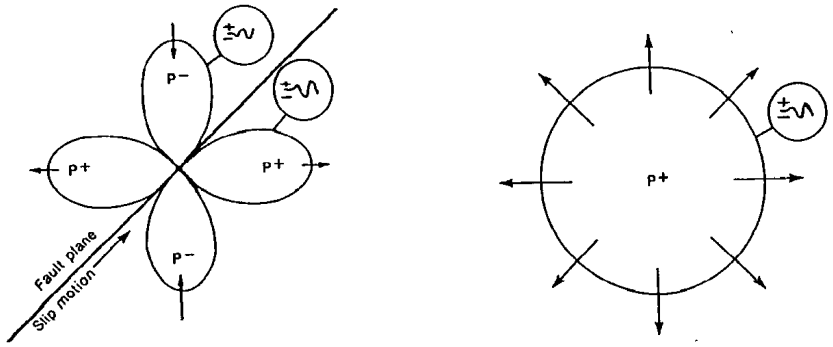

(a) (b)

Figure 1.4: Radiation patterns of P-waves. [**Ric90**] Seismic waves that are created in earthquakes (a) usually radiate their energy in a transversal, vibrating mode. Explosion-like events (b) tend to release their energy in a radial mode.

Sound Frequency and Ranging channel (SOFAR channel). The SOFAR channel is located in a certain depth, where temperature, pressure and salinity create a minimum of sound speed in the water column. Due to the depth-dependent gradient of the sound speed in the SOFAR channel hydroacoustic waves have an especially high range within this depth of minimum sound speed. Therefore, the IMS design has eleven hydroacoustic monitoring stations to cover the world's oceans [Law01], see Figure 1.1.

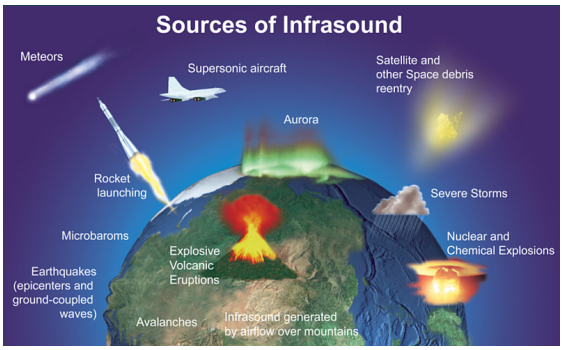

Figure 1.5: Man-made and natural sources of infrasound. [`www.ctbto.org`]

Infrasound are atmospheric sound waves below human audible frequencies, i.e. with long wavelengths. These are produced by various natural and man-made events, see Figure 1.5, including nuclear explosions, especially above- or near-surface ones. They can travel and be detected over long distances, so that 60 stations are foreseen in the IMS design to cover the world's atmosphere [Chr01], see Figure 1.1. Infrasound monitoring allows to determine the nature of an event, e.g. volcanic or explosion-like, but not whether an explosion was nuclear or chemical.

Since all three waveform technologies can only provide evidence for the explosion-like character of an event, but not the nuclear character of the explosion, another method is needed to scientifically prove or disprove the nuclear character. This is especially true, because the yield range of conventional/chemical and nuclear explosions can overlap below the order of 1 kt TNT equivalent. The nuclear character of an event can be verified by detecting one or more of various radionuclides that are created during the fission process.

Table 1.2: Cumulative fission yields (%) of relevant radioxenon isotopes. [Sae12] Shown are the six fission modes relevant for nuclear explosions, including fission spectrum neutrons (f) and high energy neutrons (he) of 14.7 MeV.

Isotope	Half life	^{235}U(f)	^{235}U(he)	^{238}U(f)	^{238}U(he)	^{239}Pu(f)	^{239}Pu(he)
^{131m}Xe	11.93 d	0.05	0.06	0.05	0.06	0.05	0.07
^{133m}Xe	2.19 d	0.19	0.29	0.19	0.18	0.24	0.42
^{133}Xe	**5.24 d**	**6.72**	**5.53**	**6.76**	**6.02**	**6.97**	**4.86**
^{135}Xe	9.14 h	6.60	5.67	6.97	5.84	7.54	6.18

When choosing a set of suitable isotopes for monitoring nuclear explosions, one has to consider certain characteristics: Fission yield (see Figure 1.3), decay rate, gamma emission intensity and detector efficiency. Furthermore the occurrence of natural and man-made backgrounds can hinder the monitoring process. Apart from the background these characteristics can be used to calculate the isotope-specific Detection Probability Index (DPI) in order to assess the suitability of each isotope [Mat05]. The significant particulate fission products have been determined to be

- ^{95}Nb, ^{95}Zr, ^{97}Zr, ^{99}Mo, ^{103}Ru, ^{105}Rh, ^{115}Cd, ^{126}Sb, ^{127}Sb, ^{131}I, ^{131m}Te, ^{132}Te, ^{133}I, ^{136}Cs, ^{140}Ba, ^{140}La, ^{141}Ce, ^{143}Ce, ^{144}Ce, and ^{147}Nd,

and validated with historical experimental data. However, these radionuclides are existent in particulate form and in case of an underground nuclear explosion they can be contained - intentionally or unintentionally - in the subsurface. Also, they are subject to various deposition effects while being airborne, e.g. dry and wet deposition. This can prevent a successful detection by the IMS. Nevertheless, if an atmospheric concentration of one or more of these radionuclides is detected, it can be strong indicator of a nuclear explosion [DeG12]. A total number of 80 radionuclide monitoring stations are planned to be incorporated in the IMS [Mat01].

In this work the focus is on the radioactive noble gases, in particular radioxenon, that are created during nuclear fission of weapon-grade radioactive material. Monitoring noble gases has the advantage that they are chemically inert and therefore, have a higher probability to leak from underground explosions through the surface. In terms of fission yield xenon is the noble gas element of choice. There exist a total of 38 isotopes and 6 meta-stable isomers of xenon. Unlike the usual case, when radioactive fallout is undesired, the radioactivity is advantageous for monitoring purposes, i.e. it allows to detect atmospherically diluted concentrations. Of the 44 variations of xenon isotopes 9 are stable and 27 have half-lives below 6 hours, which is considered the lower limit to be relevant for CTBT monitoring purposes. Thus 8 isotopes/isomers fulfil the radioactivity and half-live criteria. Four of these are not produced in fission or by activation in a nuclear explosion [DeG02], leaving four isotopes/isomers with suitable characteristics:

- ^{131m}Xe, ^{133m}Xe, ^{133}Xe, and ^{135}Xe, see also Table 1.2.

Within the context of this work, the term radioxenon refers to these four specific xenon radionuclides, if not noted otherwise, and although two of these radionuclides are isomers,

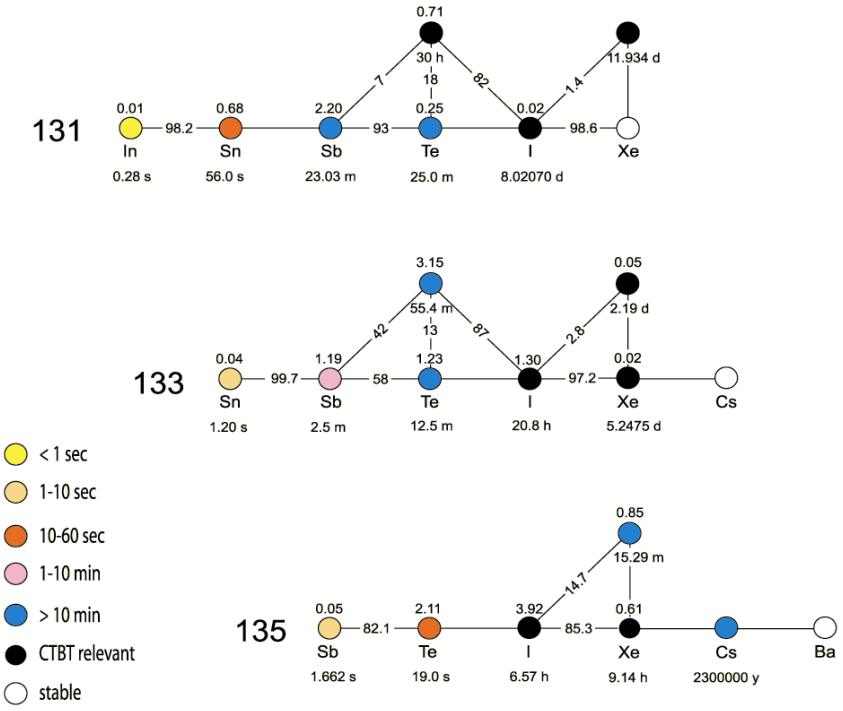

Figure 1.6: Isobaric decay chains for mass numbers 131, 133 and 135. [DeG02] Shown are all nuclides with an integrated decay flow of at least 0.01 %. The decay flow is from left to right. The independent fission yield (%) for fission spectrum neutrons from ^{239}Pu are given above the nuclide symbol, half-lives are given below. Numbers between nuclide symbols represent the branching factor.

they will also be referred to as such. The isobaric decay chains for the mass numbers of the relevant xenon isotopes are shown in Figure 1.6. As seen there radioxenon is not only produced directly during the fission process, but is also subject to feeding from precursors in the decay chains.

Radioxenon isotopes have a history of being used as indicators for nuclear activities since the Second World War in order to monitor clandestine nuclear activities, e.g. in aerial reconnaissance over Germany in 1944 [Ric06, Sae10a]. They have also been chosen by the state parties of the CTBTO as a tracer for nuclear explosions. The current IMS design foresees 40 noble gas monitoring stations around the world in order to provide a 90 % detectability of a 1 kt nuclear explosions within 14 days [Sch00]. These 40 stations are included in the aforementioned 80 radionuclide monitoring stations. In Appendix A all IMS radionuclide stations and the current status of its noble gas component (as of the end of 2012) are listed. Those, which are certified or in their testing phase, already monitor the atmospheric activity concentrations of the four radioxenon isotopes. Depending on the geographical location detections are regularly made also when no nuclear explosion has occurred.

Table 1.3: Typical releases from strong emitters of radioxenon. [Kal06, Sae09]

Type of emitter	Typical emission of ^{133}Xe
Nuclear Power Plants	$\approx 10^{9}\,\mathrm{Bq/d}$
Isotopic Production Facilities	$\approx 10^{11} - 10^{13}\,\mathrm{Bq/d}$
Underground 1 kt nuclear explosion	$0- \approx 10^{15}\,\mathrm{Bq}$
Atmospheric 1 kt nuclear explosion	$\approx 10^{16}\,\mathrm{Bq}$

Noble gas monitoring of nuclear explosions is impeded by a legitimate, man-made background of radioxenon. As mentioned above radioxenon is created during nuclear reactions and therefore also released from e.g. reactors and hot cells. Significant emitters are Nuclear Power Plants (NPP) and Isotope Production Facilities (IPF). Table 1.3 gives an overview over the order of magnitude of emissions that can be expected from such sources in comparison with a 1 kt nuclear explosions. Though the amount of radioxenon created in a nuclear explosion exceeds that from legitimate sources, the the spatial distribution of the latter can create a disguising background. In certain regions of the world nuclear facilities have a higher density and/or are in vicinity of an IMS noble gas station. Also, the amount of radioxenon leaking from underground explosions can vary over many orders of magnitude, depending on the environmental characteristics of the surrounding earth.

The emissions from those legitimate sources can strongly vary in time. Experience with monitoring stations has shown that a signal from a nuclear explosion can possibly be covered under a higher concentration originating from legitimate sources. The worldwide distribution of nuclear reactors is mainly set in developed countries with nuclear industry. A high percentage of these are found in the northern hemisphere and in western countries. The emissions also depend on the mode of operation and may be continuous releases or batch releases with a frequency of a few times per year. However, information about radioxenon emissions are not centrally accessible and much had to be learned about sources and their emission strength since the CTBT opened for signature. There is a strong need in the CTBT community to further explore the impact of the legitimate radioxenon background sources on the verification regime.

The radioxenon concentration picked up by a detector is not only dependent on the source emissions, but also on the prevailing winds. Due to the improvements in computation power and availability of data in the last decade Atmospheric Transport Modelling (ATM) has become a valid and important tool that is able to help to understand, simulate and predict the global background. The purpose of ATM is to calculate the sensitivity between a certain source and a certain receptor, so that if the concentration at either one is known the other one can be determined. However, ATM is a relatively young method and its possibilities in nuclear explosion monitoring have not been fully exploited yet. This work investigates possible roles and benefits of ATM in the noble gas monitoring of nuclear explosions. The legitimate radioxenon background is characterized, opportunities for categorization are developed, and the capability of the IMS noble gas component to detect nuclear explosions is quantified.

1.3 Outline

Having established the role of radioxenon in the general monitoring of nuclear explosions and having set the goal of examining the roles of ATM in it, the structure of the following chapters is summarized here:

Chapter 2 covers the physical processes in emission, detection and analysis of atmospheric radioxenon concentrations. Known emitters are identified and their emissions quantified; detection methods as well as existing analysis methods are introduced.

Chapter 3 contains the description of how ATM has been employed for this work. The theory of ATM is presented; used software and methods of validation are specified. Also sources of used data are described; a radioxenon emission inventory, meteorological data and radioxenon sampling data are needed.

Chapter 4 revolves around the characterisation of the worldwide radioxenon background. Concentration levels and their distribution at all IMS noble gas stations are simulated. The impact of the source term time resolution of strong emitters is examined, and the reconstruction of a source term of a single, known source is demonstrated.

Chapter 5 covers the possibilities and roles that ATM can fulfil in categorisation of radioxenon monitoring data. It can be used to train non-ATM methods, as well as within a categorisation method itself.

Chapter 6 presents the definition of the network coverage as a quality parameter to assess the capability of the IMS noble gas component to detect nuclear explosions. This network coverage is calculated for different explosion scenarios and radioxenon backgrounds.

Chapter 7 contains a summary of the presented work and its results. From these the recommendations for further research and noble gas monitoring of nuclear explosions in general are devised.

The appendix includes an overview over the IMS radionuclide component, the applied radioxenon emission inventory, and the used hard- and software.

Chapter 2
2 Noble Gas Monitoring of Nuclear Explosions

In the following chapter the main sources of radioxenon - including nuclear explosions - are identified. The knowledge of different sources of radioxenon is needed when the signature of a nuclear explosion has to be identified against a background resulting from legitimate sources. Subsequently the available detection methods and systems are presented, which are necessary to gather and interpret radioxenon concentration data. Furthermore, currently used analysing methods are briefly explained. The reasons why radioxenon is suitable for this purpose are summarised:

- Their **half lives**, see Table 1.2, are suitable, i.e. neither too short nor too long. The isotopes must still be detectable after a few days, but a possible memory effect in the earth's atmosphere is not desired.

- The **noble gas characteristic** of xenon makes it difficult to retain the isotopes, e.g. in an underground nuclear explosion. Due to their inertness they are likely to leak also out of underground cavities and are also not subject to deposition processes during the atmospheric transport.

- The **fission yields** for radioxenon isotopes are the highest among the noble gases, e.g. ^{133}Xe has a 5-7% cumulative fission yield for ^{235}U or ^{239}Pu devices [Eng93]. This can result in amounts that are still detectable in an atmospheric dilution, which typically is in order of $10^{-14} - 10^{-15}$[Wot03a].

- Significant occurrences of the four isotopes in question are **synthetic**[1]. Therefore, there is no natural background imposing on daily sampling procedures, and only anthropogenic sources must be considered.

[1] Isotopes of radioxenon are also produced in the radioactive processes in the earth's crust resulting from natural deposits, e.g. of uranium. However, this contribution is very small compared to man-made sources [Sau12].

2.1 Sources of Radioxenon

Radioxenon can be created in various ways. The four radioxenon isotopes in question can be created directly in nuclear reactions, such as fission of heavy nuclei, e.g. ^{235}U, or (n,p) reactions in general [Sae10b]. All four relevant radioxenon isotopes are created in significant yields in fission induced by thermal, i.e. slow, neutrons. Apart from ^{131m}Xe the other three isotopes also have significant yields, when fission is induced by fission-originated or fast neutrons. Thus the isotope composition depends also on the neutron energy and thus also on the type of source. Possible sources of radioxenon isotopes are presented in the following subsections.

2.1.1 Nuclear Explosions

2.1.1.1 Background

As mentioned before there are reasons to carry out a nuclear explosion other than as an offensive weapon. So-called peaceful nuclear explosions have been in discussion, e.g. for large-scale earth moving also known as geoforming. However, *testing* a nuclear explosion device is usually done, when a state believes in the deterrence effect or when it develops its weapons arsenal further. The latter is called vertical proliferation and has led from the earliest uranium gun-type and plutonium implosion-type design to today's advanced fusion and boosted fission designs. The main motivation to develop new types of nuclear weapons is to have access to different yields, bomb weights and sizes, as well as effects on the surroundings (i.e. humans, vehicles, buildings).

In the ongoing of this the arms race between the USA and the Soviet Union various variations have been seen. Not only the absolute number of available warheads were important for each side. The biggest yield has been detonated by the Soviet Union in 1961 with the Soviet Tsar bomb with a yield of 50 Mt. Nowadays, the focus is rather on minimizing the yield of the explosion. So-called mini nukes with yields below 1 kt are in principle more difficult to build than devices with higher yields. Also bunker busters are the result of more recent developments as they first penetrate the surface to maximize the explosion depth in order to reach deep infrastructure. However, also the respective arsenals of the USA and the Soviet Union drastically increased during the Cold War, see Fig 2.1a. Until today over 2,000 tests have been conducted, mainly by the USA and the USSR, see Table 1.1. Famous test sites of these parties are the Nevada Test Site (NTS) in the USA and the Semipalatinsk Test Site (STS) in today's Kazakhstan.

The Partial Test Ban Treaty (PTBT) from 1963 has banned nuclear weapon tests in the atmosphere, in outer space and under water for the signature states USA, UK and USSR. After the CTBT has opened for signature only India, Pakistan and North Korea have conducted known tests, see Figure 2.1b. As of today nuclear testing is not as usual as it has been in the past, especially during the Cold War, but tests in the future are plausible in various scenarios.

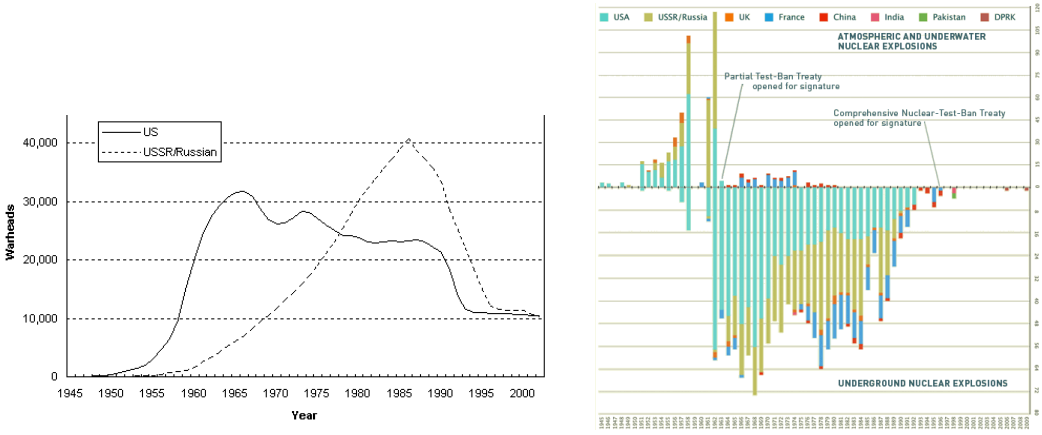

(a) US and USSR/Russian stockpiles of nuclear warheads, 1945-2002. [`www.nrdc.org`]

(b) Worldwide nuclear testing, 1945-2009. [`www.ctbto.org`]

Figure 2.1: Time development of nuclear arsenals and nuclear tests. Stockpiles and number of tests decreased after the end of the Cold War. Test explosions moved largely underground after the PTBT.

2.1.1.2 Emissions

The chain reaction creating a nuclear explosion is based on induced fission. Opposed to spontaneous fission an induced fission is initiated by an incoming neutron, which excites the nucleus into an unstable state. The following fission usually produces two heavy fragments and two or three free neutrons. This multiplication of neutrons can lead to a chain reaction, if a fissile material dependent critical mass is exceeded. The excess energy from the chain reaction is passed to the environment. In a typical nuclear fission explosion the released energy splits approximately [Aue12] in

- 50% for air blast and shock waves,
- 35% for thermal radiation,
- 15% in ionizing radiation,
  - with 5% initially within a minute mainly in form of neutrons and gamma rays,
  - and 10% residual over time from fission product decay in form of beta and gamma radiation.

The fission during a nuclear explosion is induced by fast neutrons. Since the full chain reaction is completed within a microsecond, there is not enough time for complex activation processes to build up. A 1 kt nuclear explosion creates about $1.08 - 1.33 \cdot 10^{16}$ Bq of ^{133}Xe directly [Sae07]. The exact value also depends on the used fissile material, e.g. ^{233}U, ^{235}U or ^{239}Pu. In order to estimate emissions from explosions with higher yields, in a first approximation a linear behaviour is assumed.

The behaviour of the products and the effects of the released energy from a nuclear explosion on the environment depend strongly on the surroundings. Explosions above the earth's surface (also explosions on or a few meters below the surface belong in this category) are called atmospheric explosions and can pass their output directly into the atmosphere. The most visible outcome is a mushroom cloud carrying dust and radioactive material into the air. From there on the aerosol and gaseous particles are subject to prevailing meteorological conditions. Whereas part of the particulate fallout can be deposited on-site, it can be assumed that 100% of the created noble gases are released immediately into the atmosphere.

When detonating underwater the released energy is transferred to the surrounding water masses. Particulate fallout will most likely be contained underwater, but traces could emerge. Regarding noble gases it is certain that they are not chemically bound in the sea water, but radioxenon atoms being trapped physically within carrier molecules cannot be excluded. However, in absence of any experimental data it is assumed that 100% of the created noble gases are transported to the surface and released into the atmosphere. Common sense dictates that this release into the atmosphere must be slower than for an atmospheric explosion, but faster than for an underground explosion.

The processes during and after an underground nuclear explosion are more complex. The released energy leads to an increase in pressure and temperature, which are transmitted into the surrounding, and an isotropic shock wave is created. Milliseconds after the detonation the outward directed pressure and shock wave create an underground cavity. The inside wall of the cavity is coated with fused earth, but since the inside of the cavity is pressurized the surrounding walls are likely to get fractured. When gas is leaking through these cracks, the pressure decreases and rubble can fall down. By repeating this the cavity can migrate towards the surface. The shifting of earth material downwards can cause a crater to be formed on the surface. The amount of gas that leaks through the earth to the surface can vary widely. It can hardly be predicted, because it depends on many parameters such as the rock composition and depth, yield and kind of explosion. Common scenarios assume a total leakage between 1% and 10% [Kal09, Wot10]. The time dependence of the atmospheric release from underground nuclear tests has been examined with experimental data from the Nevada Test Site [Kal11]. Controlled releases usually have a significant delay between detonation and emission, e.g. between one day and one week [Sch96]. However, uncontrolled test releases occur typically with a delay of a few minutes or a few hours. This means that the main leakage of radioxenon can be assumed within one time step of ATM, which is 3 h.

2.1.2 Isotope Production Facilities

Potentially the strongest, legitimate emitter of radioxenon is an Isotope Production Facility (IPF). Their common purpose is to produce ^{99}Mo for medical applications by irradiating Highly Enriched Uranium (HEU) or Low Enriched Uranium (LEU) with neutrons. About 95% of the world's ^{99}Mo supply is produced in this way [Sae10b, Uns09].

The uranium targets normally consist of uranium metal between two aluminium plates. The targets are irradiated in a nuclear reactor with a neutron flux of $10^{13} - 5 \cdot 10^{14}\,\mathrm{n/cm^2 s}$

for 2-12 days. The irradiation time depends on maximising the returns of the desired isotopes and minimizing undesirable isotope by-products [Sae10b]. After the irradiation time the total dose rate is reduced by removing any short-lived isotopes by leaving the targets to decay for typically 1 day. Then an acid or a base hot-cell is used to dissolve the uranium for about 1-2 h and the fission products are separated for purification, see Figure 2.2. During this dissolution the created noble gases are released and, depending on the process, can be recovered with helium as a carrier to either krypton, xenon and/or iodine recovery cells [Sal85]. Once in the recovery cell the created noble gases can be separated from the helium by freezing them out with liquid nitrogen (77 K) due to the boiling point of helium of 4 K. The noble gases can be separated from each other by various methods such as adsorption, trapping or during the warming process. In some cases noble gases are handled as waste products and released into the atmosphere directly or after passing through a charcoal delay line to reduce the activity.

The isotope composition of hypothetical nuclear explosions from ^{235}U and ^{239}Pu were calculated and compared with that from IPF releases. In cases of short irradiation times of the uranium target at the IPF and a separation of the radioxenon isotopes after more than one day after an explosion, the isotope compositions are similar if not identical [Sae10b]. Thus, longer irradiation times of targets are in favour of the CTBT verification regime as it would make the two kind of signals more distinguishable in terms of isotope composition (not due to signal strength). Also, during start-up of a cold reactor the isotope composition of radioxenon may be very similar to that of nuclear explosions. Some facilities also host a $^{130}\mathrm{Te}\,(\mathrm{n},\gamma)^{131}\mathrm{Te}$ process in order to produce ^{131}I from the subsequent decay of ^{131}Te [Sae10b]. From the produced ^{131}I an amount of 1.2% decays to ^{131m}Xe, which changes the composition of the four radioxenon isotopes.

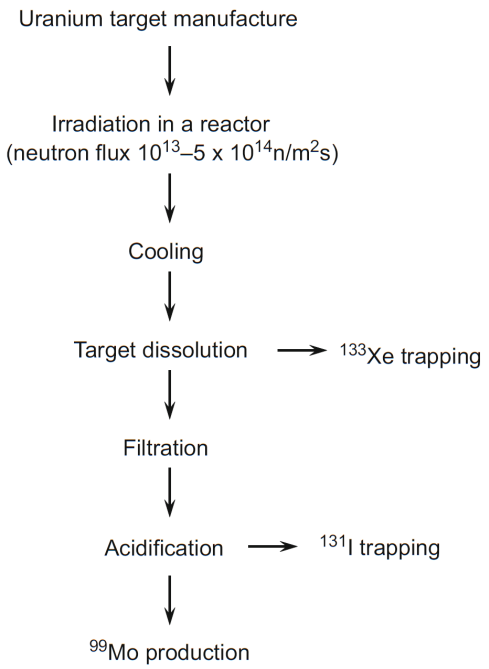

Figure 2.2: Common ^{99}Mo production technique. [Sae10b]

Measures such as basic target dissolution processes and charcoal traps for the trapping and decay of xenon help to reduce the overall radioxenon emissions. Stack and emission monitoring are also supportive actions as these data could be used to explain the background at nearby monitoring stations [Sam87, Sch12a, Sch12b]. However, the total amount of created radioxenon depends on the amount of produced ^{99}Mo [Kal12], and a large IPF can have average emissions of up to $10^{16}\,\mathrm{Bq/a}$ of ^{133}Xe, see Appendix B. Shut-downs due to maintenance or instalments of new processes can lead to a noticeable decrease of radioxenon levels at close IMS noble gas stations [Sae10c].

Anyway, IPFs are usually driven by commercial actors on a worldwide and complex market, and therefore follow other operation modes than e.g. research or power reactors. This means that most likely the radioxenon emissions of an IPF are not constant, but are rather released in batches and in a frequency dependent on work shifts, week days, economical situation etc.

2.1.3 Nuclear Power Plants

A Nuclear Power Plant (NPP) is a thermal power station that uses heat from nuclear reactions. In a nuclear power reactor normally thermal, i.e. slow, neutrons are used for the fission of uranium or plutonium. The excess energy from these fission processes, see Equations 1.2 and 1.3, supply the heat from which the electrical energy is derived. The reactor must provide a sustained nuclear chain reaction, which distinguishes it from the uncontrolled chain reaction in a nuclear explosion. To avoid the uncontrolled chain reaction in a nuclear power reactor the neutrons are moderated (or poisoned) in order to change the fission rate. Common moderators are light water, graphite and heavy water. Alternatively the reactor core may contain moveable rods that are filled with a neutron absorbing material in order to reduce their flow rate.

Opposed to nuclear explosions there is sufficient time to produce many activation products in the reactor fuel, including radioxenon. Common NPPs produce an average electrical power output between a few hundred MW and some tens of GW. With that they have average radioxenon emissions (^{131m}Xe, ^{133m}Xe, ^{133}Xe and ^{135}Xe) of between a few $10^{9}\,{}^{\mathrm{Bq}}/_{\mathrm{a}}$ and a few $10^{13}\,{}^{\mathrm{Bq}}/_{\mathrm{a}}$. However, commercial power plants normally operate with batch emissions instead of continuously emitting into the atmosphere. A detailed overview over the used radioxenon emissions is given in Section 3.2.1 and Appendix B.

The total ^{133}Xe inventory of a reactor can be in the range of a few EBq. In non-explosion scenarios these orders of magnitudes are usually only released in accidents at nuclear facilities, as happened e.g. in Chernobyl on 26 April 1986 and Fukushima on 11 March 2011. Today's estimations of the Chernobyl ^{133}Xe source term are 6.5 EBq [Nea02]. Recent atmospheric simulations [Sto11] showed the total ^{133}Xe release from Fukushima is 16.7 ± 3.3 EBq.

Since the very first nuclear reactor Chicago Pile-1 in 1942 and the first power plant for civil usage AM-1 Obninsk in 1954 several variants have been developed. Today's reactors are usually classified by their type of (e.g.)

- fission process: thermal or fast neutrons;
- the moderator material: light or heavy water, graphite;
- and/or the coolant: water, gas, liquid metal, molten salt.

Starting from the 1950s the number of nuclear power plants steadily increased until the end of the 1980s. Since then the growth reduced or at one point turned even negative. Although new reactors are continuously planned and constructed all over the world, also an significant number of reactors are shut-down or deconstructed. Today the IAEA database lists 435 operating nuclear power reactors worldwide with increased densities in

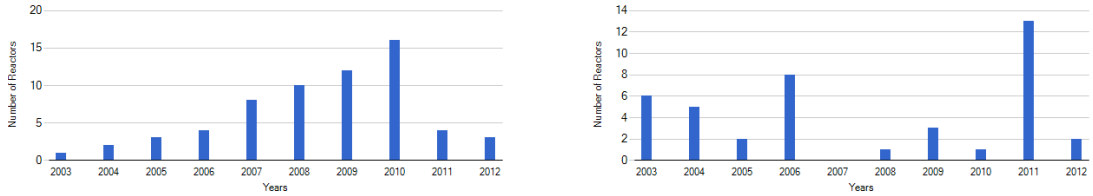

(a) Construction starts.

(b) Permanent shut-downs.

Figure 2.3: Status development of nuclear reactors worldwide. [Iae12] Shown are number of new constructions (a) and number of permanent shut-downs (b), displaying a decrease/increase in the Fukushima year 2011.

North America, Europe and East Asia. Beside these a total of 64 are under construction and 5 are reported to be in long-term shut-down. Though, the rate of newly started constructions has drastically reduced since 2011, supposedly due to the Fukushima accident following the Tōhoku earthquake and tsunami on 11 March 2011, see Figure 2.3. Also the number of permanent shut-downs has considerably peaked in that year.

2.1.4 Other Sources of Radioxenon

The above listed emitters are considered to be the sources of radioxenon with a noticeable impact on the global background. Other sources that have too small power output (i.e. small radioxenon emissions) and are too randomly in their emission times or are mobile cannot be included here. These are for example:

- Nuclear driven ships and submarines (up to a few hundred MW of power output),
- Research reactors (usually power output between a few hundred kW and a few MW),
- Reprocessing plants (for large facilities up to 10^8 Bq of ^{133}Xe per day [Kal09]),
- Hospitals (from one medical application typically 10^8 Bq of ^{133}Xe [Hei02]),
- Radioactive material in the earth crust (traces of radioxenon from spontaneous fission processes),
- Unknown facilities of known types of sources (e.g. newly built IPFs),
- Unconsidered types of sources.

All of the aforementioned known sources usually emit only a fraction of what operating NPPs emit, and are therefore not further considered in the simulation of the global radioxenon background.

Table 2.1: Operational parameters of IMS noble gas stations. [Aue10]

Characteristic	Minimum requirement	SPALAX	SAUNA	ARIX
Airflow	$0.4\,^{m^3}/_{h}$	$15-20\,^{m^3}/_{h}$	$1.2\,^{m^3}/_{h}$	$1.6\,^{m^3}/_{h}$
Sample volum	$10\,m^3$	$50-75\,m^3$	$25-30\,m^3$	$36\,m^3$
Collection time	$\leq 24\,h$	$\leq 24\,h$	$12\,h$	$12\,h$
Measurement time	$\leq 24\,h$	$\leq 24\,h$	$11\,h\ 10\,min$	$18\,h$
Time before report	$\leq 48\,h$	$\leq 48\,h$	$30\,h$	$34\,h$
Report frequency	Daily	Daily	Twice daily	Twice daily
Detection system	n/a	Hi-res-γ-spectrometry	β-γ-coincidence	β-γ-coincidence
MDC for ^{133}Xe	$1\,^{mBq}/_{m^3}$	$0.2-0.6\,^{mBq}/_{m^3}$	$0.2-0.4\,^{mBq}/_{m^3}$	$0.2-0.3\,^{mBq}/_{m^3}$

2.2 Detection of Atmospheric Radioxenon

Atmospheric concentrations of radioxenon are measured by its radioactivity. The following sections describe the used detection systems and the status of worldwide monitoring.

2.2.1 Methods of Detection

After emitted into the atmosphere and being subject to mesoscale atmospheric transport the concentration of radioxenon is diluted typically by factors of $10^{-14} - 10^{-18}$. The concentration of radioxenon isotopes in air is determined by detecting the radioactive decay products. A globally uniform monitoring system for radioxenon requires a high time resolution ($\leq 24\,h$) as well as a high sensitivity ($\leq 1\,^{mBq}/_{m^3}$ for ^{133}Xe) [Aue10]. At the moment three different noble gas monitoring systems are in use within the IMS: the French SPALAX[2], the Swedish SAUNA[3] and the Russian ARIX[4], each using different techniques to monitor atmospheric radioxenon concentrations, see Table 2.1.

2.2.1.1 Sampling and Processing

Each sample will consist mostly of natural, stable xenon as it is found in the atmosphere at a constant 0.087 ppm by volume. In order to extract xenon (stable and radioactive) from air the most common method is to use activated charcoal as an adsorber, because the adsorption coefficient is higher for xenon than for other air constituents. The air is passed with certain temperature and flow rate through a column filled with activated charcoal so that finally the xenon is filtered from it. In order to maximise the adsorption process, each of the three systems follows a different approach. Because adsorption is more efficient at lower temperatures, the ARIX system has been designed to to perform the adsorption at temperatures below $-100\,°C$. The SAUNA system on the other hand has been designed with higher amounts of the adsorbent, i.e. charcoal, in order to allow

[2]Système de Prélèvements Automatique en Ligne avec l'Analyse du Xénon
[3]Swedish Automatic Unit for Noble gas Acquisition.
[4]Automatic Radioanalyzer for Isotopic Xenon.

sampling at a more moderate temperature of −5 °C [Rin03]. In the SPALAX system the ambient air is pre-enriched in xenon to 1 ppm by volume through a semi-permeable membrane [Fon04]. Thus an effectively higher volume can be sampled without increasing the amount of charcoal nor decreasing the temperature.

The xenon is then removed from the charcoal traps by heating these up to $250 - 300$ °C and flushed out with an inert gas, e.g. He or N_2. The xenon is now available in a higher concentration. Further processing includes removing impurities such as Rn, H_2O and CO_2 by system specific gas traps in order to further increase the xenon concentration.

2.2.1.2 Measurement of Activity Concentration

Determining the activity concentration of radioxenon from the obtained sample can be done with high-resolution gamma-spectrometry, as used in SPALAX, or with beta-gamma coincidence spectrometry, as used in ARIX and SAUNA.

In high-resolution gamma-spectrometry the radioxenon isotopes are detected and quantified with a high-purity germanium (HPGe) detector by their distinctive gamma lines, see Table 2.2. The radioxenon spectrum may only be disturbed by traces of atmospheric radon (^{222}Rn) that made it through the purification process and its daughter products, namely ^{214}Pb and ^{214}Bi. The resulting spectrum is simple in terms of peak location and identification, but the quantification of ^{131m}Xe and ^{133m}Xe is made difficult due their low gamma intensities (1.95% and 10.0% respectively). However, this does not apply to ^{133}Xe and ^{135}Xe. For all isotopes the detection of X-rays can help to increase the sensitivity, but for ^{131m}Xe and ^{133m}Xe only in an integral manner since their X-ray spectra peak at the same energies, see Table 2.2.

In beta-gamma coincidence systems a plastic scintillator tube for beta detection is surrounded by a NaI(Tl) gamma detector. Relying on coincidence measurements significantly reduces the background. In order to detect radioxenon the following coincidences are measured, see also Figure 2.4:

^{131m}Xe: Sum of 29.46 to 34.61 keV X-rays and 129 keV e^-,

^{133m}Xe: Sum of 29.46 to 34.61 keV X-rays and 199 keV e^-,

^{133}Xe: 31.63 keV X-ray + 45 keV e^- + 346 keV beta, and

80.98 keV gamma + 346 beta,

^{135}Xe: 31.63 keV X-ray + 214 keV e^- + 910 keV beta, and

249.8 gamma + 910 keV beta.

Today's IMS noble gas stations utilise the beta-gamma-energy correlation method[5]. It measures the energies of gamma rays, X-rays, beta particles and conversion electrons. The latter are particular importance for detecting the decay of the isomers ^{131m}Xe and

[5]Previous versions of the ARIX system included the beta-gated gamma systems.

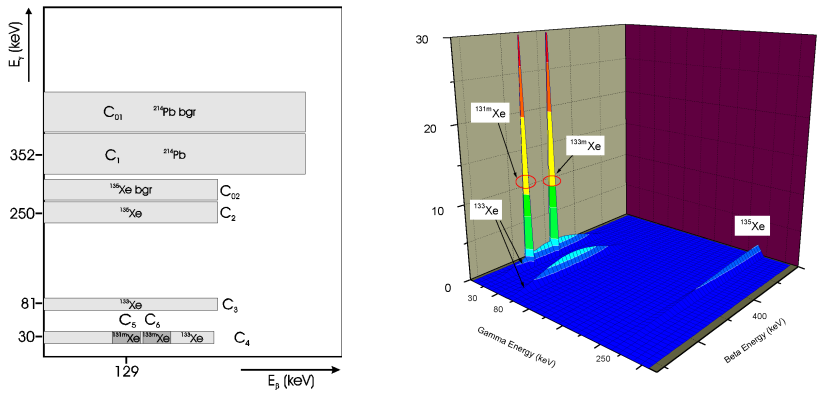

Figure 2.4: Regions of interest for radioxenon in a beta-gamma spectrum. [Ing03]

Table 2.2: Characteristic decays of radioxenon. [Aue10]

Isotope	Decay product	Energy (keV)	Branching (%)
^{131}Xe	X-rays	29.46	15.4
		29.78	28.6
		33.60	10.2
		34.61	1.85
	Gamma	163.93	1.95
	Conversion e^-	129.4	61
^{133m}Xe	X-rays	29.46	16.1
		29.78	29.8
		33.60	10.6
		34.61	1.9
	Gamma	233.2	10.0
	Conversion e^-	198.7	64
^{133}Xe	X-rays	30.62	14.1
		30.97	26.2
		35.00	9.4
		36.01	1.7
		80.99	37.0
		45	55.1
	Beta	max. 346	100
^{135}Xe	X-rays	30.62	1.45
		30.97	2.69
		35.00	0.97
		36.01	0.185
	Gamma	249.8	90
		608.2	2.90
	Conversion e^-	214	5.7
	Beta	max. 910	100

^{133m}Xe. This allows to improve the Minimum Detectable Activity (MDA) below 10 mBq for an 18 h measurement [Aue10].

Anyway, all monitoring systems are affected by the decay products of ^{222}Rn. With an average atmospheric activity concentration of 10 $^{\mathrm{mBq}}/_{\mathrm{m}^3}$ and a half life of 3.82 days, significant amounts can survive the sample processing and contaminate the detector. The relevant daughter products are ^{214}Pb and ^{214}Bi. With half lives of $T_{1/2}\left(^{214}\mathrm{Pb}\right) = 26.8\,\mathrm{min}$ and $T_{1/2}\left(^{214}\mathrm{Bi}\right) = 19.9\,\mathrm{min}$, and gamma and X-rays energies similar to radioxenon they can alter the detection of radioxenon. In order to minimize this factor all detection systems reduce the concentration of ^{222}Rn in the purification process by a factor of about 10^5.

For the final determination of the activity concentration also the sample's air volume is needed. Since the concentration of stable xenon in the earth's atmosphere is constant, the actual air volume can be deducted from the volume of stable xenon gas, which is measured with a gas chromatograph or a Thermal Conductivity Detector (TCD). Uncertainties of volume measurements of stable gases are typically 10-15%. The activity concentration c [$^{\mathrm{Bq}}/_{\mathrm{m}^3}$] is calculated by

$$c = \frac{A\,[\mathrm{Bq}]}{V_{\mathrm{Xe}}\,[\mathrm{cm}^3]} \cdot \frac{V_{\mathrm{Xe}}[\mathrm{cm}^3]}{V_{\mathrm{air}}\,[m^3]}\,, \tag{2.1}$$

with A being the sample activity, V_{Xe} the xenon volume,$^{V_{\mathrm{Xe}}}/_{V_{\mathrm{air}}}$ the concentration of stable xenon in the atmosphere ($= 0.087\,^{\mathrm{cm}^3}/_{\mathrm{m}^3} = const.$).

A common practise, also required by the CTBTO, is to define a confidence level, in this case 95%. This means that it has to be assumed that 5% of false-positive detections occur. This has also influence on the Minimum Detectable Concentration (MDC). The MDC is defined as [Bie01]

$$MDC = \frac{L_D}{\varepsilon \cdot I \cdot V \cdot \lambda^{-2} \cdot (1 - e^{-\lambda t_c}) \cdot e^{-\lambda t_d} \cdot (1 - e^{-\lambda t_a})}\,, \tag{2.2}$$

with the following parameters:

L_D detection limit, defined as

$$L_D = k^2 + 2 \cdot L_C\,, \tag{2.3}$$

with k being the confidence factor, accordant to the demanded confidence level of 95% set to $k = 1.645$, and L_C the critical level defined as $L_C = k \cdot \sqrt{B + \sigma_B^2}$, where B is the baseline counts and σ_B the according uncertainty [Cur68],

and ε detection efficiency, I intensity, V sample volume, λ decay constant, t_c collection time, t_d decay time, t_a acquisition time.

Due to varying conditions of these parameters the MDC must be determined for every sample. In case of e.g. a mechanical failure of the air venting system the MDC increases. The sample-specific value of the MDC is important to validate the reliability of the measured activity concentration.

In ARIX and SAUNA systems a memory effect can occur due the porosity of the plastic scintillator material that allows xenon to diffuse through the walls of the detector, and can amount to around 5% [Bea07]. This means that especially after a high activity measurement the memory effect has to be accounted for. This is done by doing a background measurement before the actual sample measurement. However, subtracting the background counts from the measurement counts reduces the MDA. The SPALAX systems with their aluminium casing do not show this type of memory effect.

2.2.1.3 Maintenance

According to the CTBT the IMS noble gas stations are required to deliver data with an availability of at least 95%. Down-times are only allowed for no more than seven consecutive days and not more than a total of 15 days per year. Stations need to be especially reliable since they are often in remote locations with limited infrastructure, and qualified operators might not always be available. Experience showed the reasons for down-times are most often due to the detector system, the sampling and processing, computer and software and organisational issues [Aue10].

2.2.2 Status of Radioxenon Monitoring

The Preparatory Commission of the CTBTO has defined the minimum requirements for the IMS noble gas component. They include operational requirements for the network and detection requirements for the stations. Summarized they result in the requirement that the IMS noble gas component should have 90% detection probability of a 1 kt nuclear explosion within 14 days after the explosion [Sch00]. This is important, when later drawing the boundary conditions for determining the network coverage of the IMS noble gas component. The Preparatory Commission has two working groups, one for financial (Working Group A) and one for verification matters (Working Group B). The main activities of the latter are performed by the Provisional Technical Secretariat (PTS). The PTS has been established in 1997 to assist the Preparatory Commission in the assembly of the International Monitoring System (IMS). Since verification and monitoring compliance are a basic interest of the CTBT, the IMS is built so that it will be operational once the Treaty enters into force. Out of the the total 337 stations 80 of them will sample radionuclides in the environment transported through the atmosphere. Present planning foresees that 40 of the 80 radionuclide stations will also monitor atmospheric radioxenon concentrations, see Figure 2.5 and Appendix A. The task of the PTS is to gather IMS data and distribute them to the National Data Centres (NDC) of the CTBT member states. Then it is up to the NDCs to interpret the data. This division of responsibilities is an important mechanism within the CTBTO as it is not allowed to assess, if a nuclear explosion has occurred, or distribute such an opinion. However, certain screening procedures have already been adopted to categorize the data and thus support the member state in their interpretation.

The International Noble Gas Experiment (INGE) was founded in 1999 as an informal group overseen by staff from the CTBTO. Until today within INGE research, development

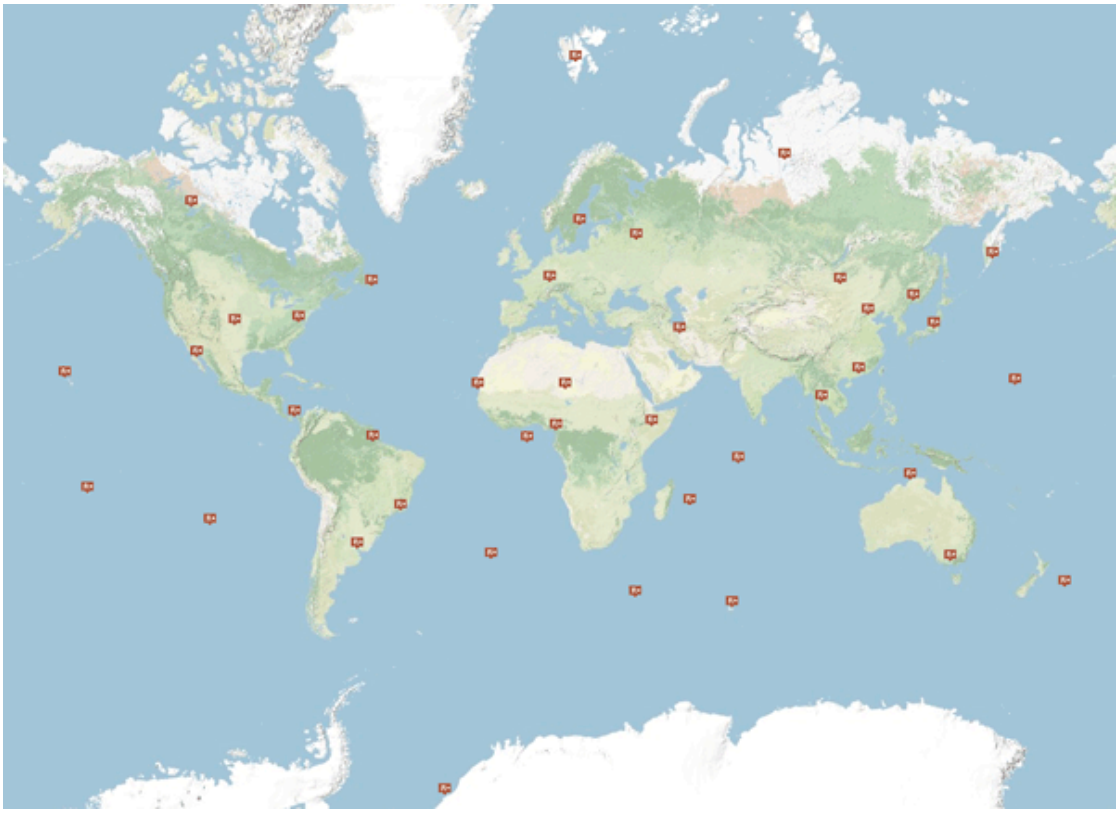

Figure 2.5: Map of the currently appointed 39 IMS noble gas stations. [http://www.ctbto.org/map/] The network is designed to equally cover and monitor the earth's surface. A 40th stations is appointed to be located in India.

and testing of the detection systems that are necessary for the verification of the CTBT are accomplished.

Since 2009 the Workshop on Signatures of Medical and Industrial Isotope Production (WOSMIP) has taken place three times. Its goal is to bring the community of emitters of radioxenon (mainly from IPFs) and the monitoring community of radioxenon together in order to improve the detection capability of the IMS noble gas component.

2.3 Analysis of Radioxenon Concentrations

By protocol, the (Provisional) Technical Secretariat of the CTBTO does not judge whether the IMS monitoring data indicate a nuclear explosion or not; only state parties are allowed to do so. Therefore, all IMS monitoring data is only distributed by the CTBTO to its member states. Anyway, the CTBTO is allowed to prepare the data and give additional information to support the decision process.

This section gives an overview over existing and already applied methods to detect and identify nuclear explosions. However, as of today it has not been decided yet by the CTBTO how exactly the different analysis techniques for radioxenon will be arranged in a screening procedure.

2.3.1 Absolute Concentrations

The forty IMS noble gas stations will be distributed over the earth's surface as to cover it more or less equally. Since the legitimate radioxenon sources are not equally distributed over the globe, each station will detect different typical concentrations.

2.3.1.1 Quality Control

As seen in the previous section, the task of periodic monitoring of atmospheric radioxenon activity concentrations is not straightforward. Before the concentration can be used for further analysis, the quality of the sample has to be checked. Each sample's state of health is validated by a number of criteria to ensure its reliability. For a good quality of the sample the following criteria have to be fulfilled (still acceptable boundaries are given in brackets):

- The MDC has to be equal or below 1 $^{\mathrm{mBq}}/_{\mathrm{m}^3}$ (5 $^{\mathrm{mBq}}/_{\mathrm{m}^3}$),
- the reporting time must be below 48 h (96 h),
- the sampled xenon volume must be above 0.87 ml (for SAUNA also 0.2 ml is acceptable),
- the sampling and the acquisition time must be
  - for SAUNA systems between 10.8 h and 13.2 h (6 h and 24 h),
  - for SPALAX systems between 21.6 h and 26.4 h (12 h and 48 h).

When these criteria are met, the basic requirements for a good state of health of the sample are fulfilled. Anyway, this does not exclude false-positive detections, e.g. as these can appear when the real radioxenon concentration is below or near the MDC.

2.3.1.2 Categorisation

Due to chaotic nature of atmospheric transport trajectories it is possible that even low emissions from a legitimate source result in a high concentration at a detector site;

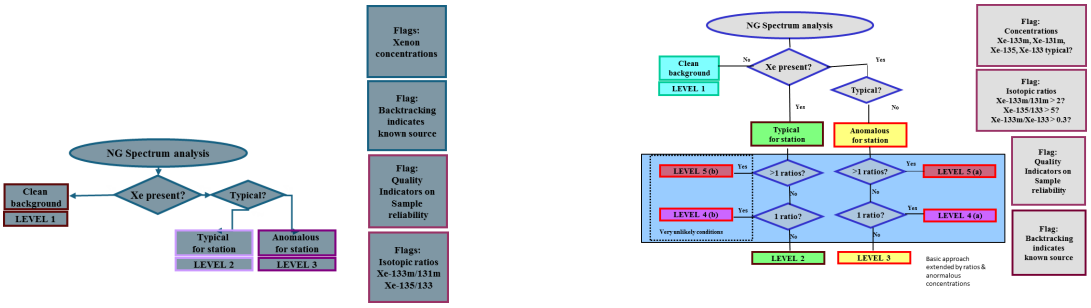

(a) 3-level categorisation scheme. [Zäh09]

(b) 5-level categorisation scheme. [Nik11a]

Figure 2.6: Possible categorisation schemes for radioxenon samples. These have been proposed during meetings of the Working Group B. Beside the actual level they also include flags to give further information on the sample.

but also that some high emission does not necessarily result in high detection but can also be missed by any detector. This means that a categorisation based solely on the concentration of a single sample can only indicate an abnormal concentration, which on the other hand is not necessarily a sign of a nuclear explosion. In a fully operational IMS noble gas component the concentration of about 60 samples[6] is measured every day. To overcome the daily, manual analysis of these samples, a categorisation scheme would help to screen out samples that are uninteresting in the CTBT sense and highlight the important ones.

Present suggestions for a categorisation scheme are shown in Figure 2.6. Each sample would be assigned with a level based on an absolute threshold concentration (and eventually isotopic ratios, see below). Additionally to further characterise the sample certain flags can be added that supply information about e.g. the isotopic ratios, results from ATM etc.

2.3.1.3 Time Series Analysis

Two ^{133}Xe data sets, one from CAX17 (St. John's, Canada) and one from USX75 (Charlottesville, USA), were statistically analysed and de-trended from local meteorological patterns [Pla10]. For both stations the air temperature, air pressure, relative humidity, rainfall, wind direction and wind speed were available for the same time periods as the radioxenon data.

A power-spectrum estimator is applied on the radioxenon and the meteorological time series; the Blackman-Turkey method reduces the estimation's variance and bias. The coupled frequencies are removed from the time series. The residual of the radioxenon time series is checked for white noise in order to test the randomness of the distribution with the Kolmogorov-Smirnov and the Ljung-Box tests.

[6] Assuming 20 stations with 12h and 20 stations with 24h sampling time. The exact number depends on which detection systems will be used in the remaining stations that are to be built.

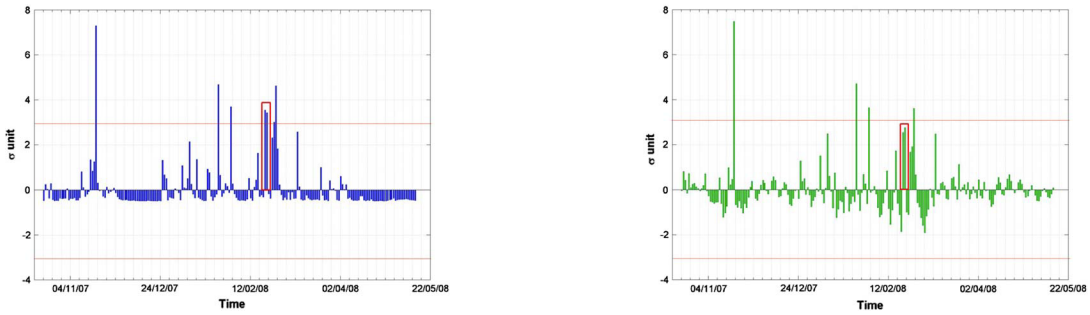

(a) Original time series. **(b)** Residual time series.

Figure 2.7: The original (a) and residual (b) time series for radioxenon data from CAX17. [**Pla10**] Both data sets are normalised to null mean value and standard deviation; values beyond the 3σ line are defined as outliers. The time series analysis can reduce the number of outliers, see red rectangle.

For the data from CAX17 a white noise and for USX75 a more complex not fully characterized noise were identified [Pla10]. Furthermore, this approach could remove wrong outliers from the raw data and thus reduce the number of false-positive alarms, see Figure 2.7. This showed that local meteorological patterns play a role in radioxenon event categorization.

2.3.2 Isotopic Activity Ratios

Due to the man-made background of radioxenon in the world, a detection of one or more radioxenon isotopes does not necessarily mean that a nuclear explosion took place. Even the detection of unusually high concentrations could be e.g. the result from a batch release from a legitimate facility. Therefore, the task of source discrimination is relevant to the screening process. The radioxenon emissions of reactors differ in their isotopic composition from that of nuclear explosions . This allows to take into account not only the absolute concentration of radioxenon, but also the activity ratios between the four isotopes [Kal10]. If it was possible to determine the concentration of three or four radioxenon isotopes, the ratios of their activity can give information about the type of source. The carried source information is preserved during transport, since the different isotopes decay with different half-lives and can be used as an inherent clock. This method is robust against the decay of the isotopes, it is also independent of the transport time and the dilution from source to receptor.

In the optimum case, when four isotopes are detected, two independent isotopic activity ratios can be calculated. When choosing the ratios in a way that the shorter-lived isotope is in the numerator, the ratios always decrease for an initial concentration of all four radioxenon isotopes. In a plot of one ratio against another a data point always moves towards the origin with time. Reactor emissions and nuclear explosion emissions differ fundamentally in the ratios of their radioxenon isotopes. As seen in Figure 2.8, after an initial start-up phase the emissions of typically operating reactor can be found in

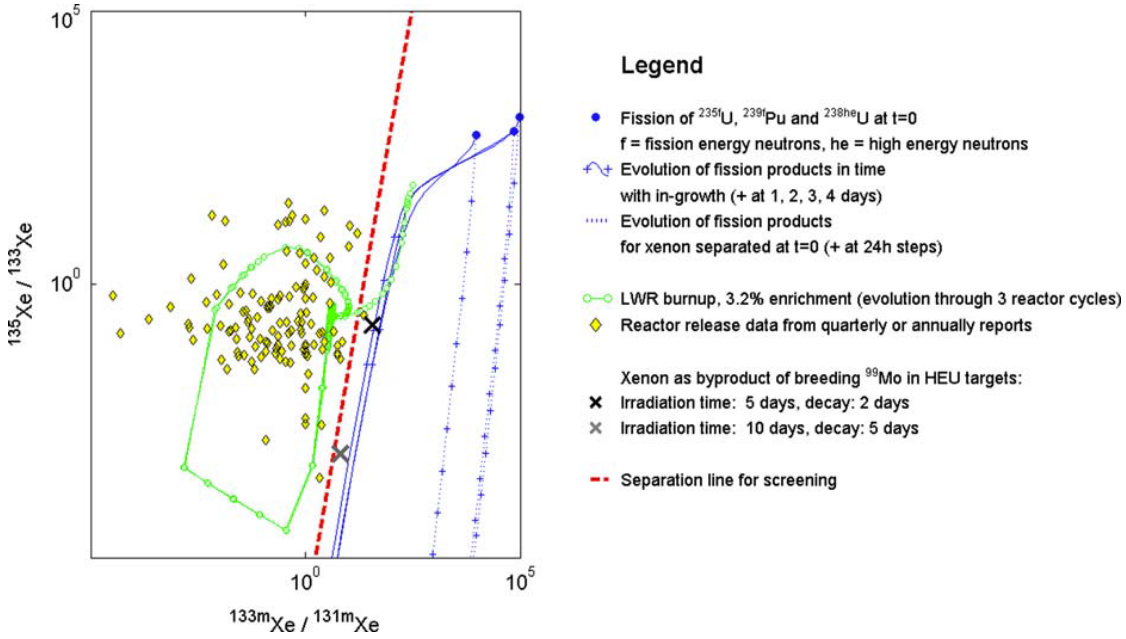

(a) Based on reactor emission data.

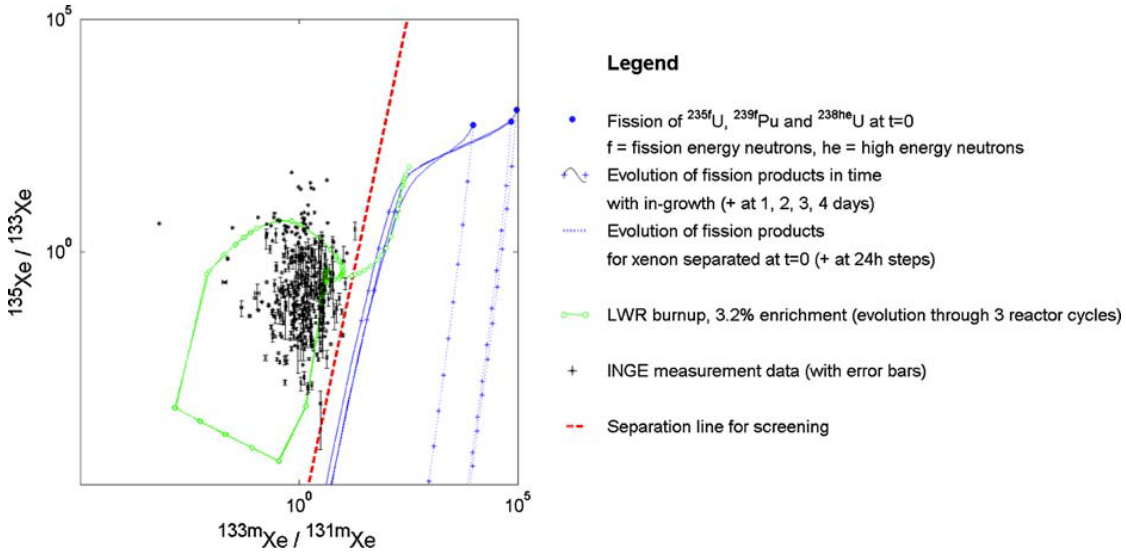

(b) Based on atmospheric detections.

Figure 2.8: Time-invariant source discrimination based on xenon isotopic activity ratios. [Kal10] The two plots show reactor emission data (a) and atmospheric detections (b). The dashed separation line divides the reactor domain (upper/left) and the nuclear explosion domain (lower/right). Samples that are found to be in reactor domain can be screened out, when assuming a single source. Samples that are found in the explosion domain must be subject to further analysis.

Table 2.3: ATM-based flagging by the PTS. [**Nik11b**] The simulations take into account constant emissions from known radioxenon sources.

Simulated Concentration	Flag value	Comment
$0\,\mathrm{mBq/m^3} \leq c_{sim} < 0.1\,\mathrm{mBq/m^3}$	0	not influenced
$0.1\,\mathrm{mBq/m^3} < c_{sim} < 1.0\,\mathrm{mBq/m^3}$	1	slightly influenced
$1.0\,\mathrm{mBq/m^3} < c_{sim}$	2	influenced

a certain area of the isotopic activity ratio plot. On the other hand the emissions of nuclear explosions are found in a different area on the same plot with higher ratios of c_{Xe135}/c_{Xe133} and c_{Xe133m}/c_{Xe131m}. Also plotted (in dashed red) is the separation line that divides the two domains. Nuclear explosions can never create a signal that crosses the separation line, whereas reactor emissions can be ambiguous. The separation line can be used as a screening method to screen out all events of no interest for nuclear explosion monitoring, i.e. above/left of the separation line in the reactor domain:

$$\frac{c_{\mathrm{Xe135}}}{c_{\mathrm{Xe133}}} - \sigma_{\mathrm{Xe135,Xe133}} > \left(\frac{c_{\mathrm{Xe133}m}}{c_{\mathrm{Xe131}m}} - \sigma_{\mathrm{Xe133}m,\mathrm{Xe131}m}\right)^{4.4388} \cdot 10^{-6}\,. \tag{2.4}$$

If the detected radioxenon concentrations originated from one single source, it is a robust method of source discrimination [Kal10]. When the emissions of different type of sources are mixed, the concentration of each isotope adds up independently so that the ratios are shifted according to the relative concentrations. This means that in mixed scenarios the ratios are found closer or even across the separation line. Thus it becomes less probable to clearly identify any nuclear character within the signal. This has been examined with the conclusion that it is still possible to detect the nuclear explosion signal in mixed air masses under certain circumstances [Pos12]. Furthermore, this has led to the proposal of a five-level based categorisation scheme, see Figure 2.6b, including isotopic activity ratios in the screening process.

Opposed to the analysis based on absolute concentrations, which strongly depend on emissions and atmospheric dilution, the categorization based on isotopic activity ratios is in principle capable of source discrimination. The isotopic ratios can be used as an inherent clock also for longer distances and longer transport times, i.e. in cases of higher dilution.

2.3.3 Flagging based on Atmospheric Transport Modelling

The PTS uses ATM to simulate the impact of known noble gas sources to the IMS noble gas component. The simulated concentrations are used to set a flag, which can be used as additional information for the sample analysis. The flag knows three values depending on absolute threshold values, see Table 2.3.

In order to determine the arriving concentration at the detector site the source terms of known radioxenon emitters and the accordant source-receptor-sensitivities must be known. Normally constant source terms are assumed for known emitters, both for IPFs and NPPs. If available, information about time resolved source terms as well as special,

temporary sources can be incorporated. The resulting flag value represents the expected contribution from known sources to the measurement. Thus, it is useful for e.g. explaining a detection of high concentration. The experience with this flagger shows that stations can be categorised due to their typical background [Nik11b]:

- Not influenced: AUX04, AUX09, CMX13, FRX27, FRX29, NZX46, GBX66, GBX68, USX77, USX79.
- Rarely influenced: ARX01, CAX16, CNX20, FRX31, MNX45, RUX58.
- Influenced: CNX22, NOX49, USX74.
- Rich and variable time series: CAX17, DEX33, JPX38, RUX61, SEX63, USX75.

Of course, ATM can serve for many other purposes in the framework of nuclear explosion monitoring. However, other, standardised possibilities of ATM have not been realized and incorporated yet. Examples of manual application of ATM include the case of the assumed nuclear test in North Korea on 9 October 2006, where simulations showed that radioxenon detections in Canada possibly have originated from the North Korean test site [Rin09], and the interpretation of unusual detections of certain radioisotopes including radioxenon in East Asia in May 2010 [DeG12].

Chapter 3
3 Utilisation of Atmospheric Transport Modelling

3.1 Simulation of Atmospheric Transport

The motions of air masses in the earth's atmosphere are determined by the gravity, the pressure gradient, and the Coriolis effect [Mar06]. The horizontal movements are determined primarily by pressure gradients and the Coriolis force. The resulting steady flow is called geostrophic flow and an imbalance between these two forces can create an inward bound circular motion of air masses. The vertical dynamics are subject to gravity and the pressure gradient. Buoyant movements of air masses are caused by an unbalance between these forces. Vertical transport is mainly happening up to a height of about 7 km, while the horizontal motions are responsible for the general circulation of the atmosphere. The friction with the surface influences the motions below 1 km altitude. Transport times for both dimensions can vary greatly; vertical transport times depend strongly on the season, the latitude and the climate [Sal12]. Typical time scales for horizontal directions are shown in Figure 3.1.

The Intertropical Convergence Zone (ITCZ) is an equatorial area of a few hundred kilometres width and characterised by persistent convergence of air masses. The associated clouds can build up into the tropopause. The location of the ITCZ depends on the season of the year. From January to July it moves northwards. In northern and southern direction of the ITCZ the trade winds are the predominant patterns. They are found about between $20° - 30°$ of latitude. These have a prevailing direction from east to west. Belts of high pressure are found usually at about 30° in both hemispheres, particularly over oceans. For higher latitudes, the so-called mid-latitudes, the winds have a general direction from west to east [Mar06]. Due to the latitudinal heating gradient the accordant wind speeds are typically as high as $10\,\mathrm{m/s}$, resulting in a transport time around the globe of a few weeks. Meridional transport mechanisms produce only wind speeds of $1\,\mathrm{m/s}$. Thus, the exchange of air masses between the mid-latitudes and the tropics usually happens on a time scale of 1-2 months. The exchange of air between the hemispheres takes significantly longer with a time scale of up to 1 year, although shiftings of meteorological patterns can

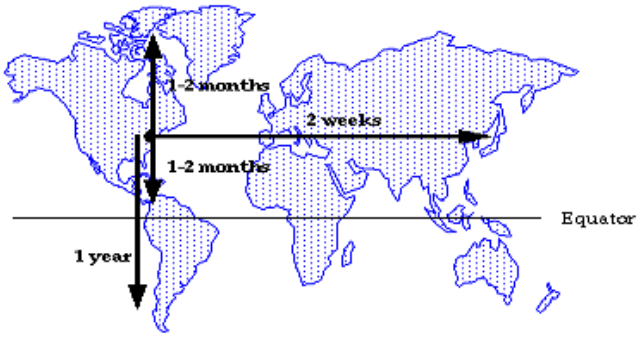

Figure 3.1: Global, atmospheric transport times. **[Jac99]** Shown are expectations of maximal transport times; experiences with e.g. the emissions from the Fukushima nuclear accident [Orr12] have shown that already after 6-8 weeks it can be possible to detect transported material due to shifts of seasonal meteorological patterns.

allow transport times of under 2 months [Orr12]. This is caused by horizontal mixing of convective storm outflows at the ITCZ, with increasing mixing effect during its seasonal shift [Sal12].

3.1.1 Theory of Atmospheric Transport Modelling

When particles are emitted into the atmosphere they are subject to the prevailing atmospheric conditions such as wind, precipitation etc. Thus they can be transported through the atmosphere and detected at a remote location. The dilution of the concentration depends on the various trajectories of the particles. The general purpose of ATM is to reproduce the relation between the emission S from a source and the concentration c at the receptor:

$$\frac{c_{reality}}{S_{reality}} \equiv \frac{c_{model}}{S_{model}} \,. \tag{3.1}$$

The right hand side can be merged into the factor M that describes the theoretical dilution of the concentration between source and receptor, also known as the source-receptor sensitivity (SRS):

$$M = \frac{c_{model}}{S_{model}} \,. \tag{3.2}$$

Thus the concentration at the receptor can be expressed as the product depending on emissions of the source S at the location (i,j) and during the time interval (n), and the accordant SRS value [Wot03a]:

$$c = M_{ijn} S_{ijn} \,. \tag{3.3}$$

When emissions from multiple sources at various locations and time intervals can contribute to the concentration at the receptor, the respective products of the above formula have to be added up:

$$c = \sum_{ijn} M_{ijn} S_{ijn} \,. \tag{3.4}$$

The time dependence of the receptor concentration c is a result of the time dependence of the source emissions, i.e. the source terms, as well as the time dependence of the accordant SRS value representing the meteorological conditions. Two approaches exist to simulate the transport and dispersion of particles in the atmosphere: The Eulerian and the Lagrangian model.

The Eulerian model divides the globe or the area of contemplation into grid boxes and calculates the in- and out-flux as well as additional local sources (or sinks) s:

$$\frac{\partial X}{\partial t} + v\nabla X = s\,, \tag{3.5}$$

with X being the mass mixing ratio and v being the wind vector. This means that in the Eulerian model the coordinate system is defined by the grid cells, which typically depict latitude and longitude degrees. Examples of an Eulerian model is the GEOS-Chem Model [`http://www.geos-chem.org/`], which is mainly applied to solve atmospheric composition problems, and the general circulation model ECHAM5, which for example can be used for a long term ^{85}Kr background analsis [Ros10].

The Lagrangian model on the other hand follows the trajectory of each simulated particle. It solves the trajectory equation for each particle [Sto10]:

$$\frac{dX}{dt} = v\left[X\left(t\right)\right]\,. \tag{3.6}$$

What is called particles in the Lagrangian model, does not necessarily represent real particles, but rather infinitesimally small air parcels. Such a model computes the statistics of a possibly high number of particle trajectories. The main advantage over Eulerian models is that this moving frame reference does not produce numerical diffusion. Also, whereas Eulerian models see point releases immediately distributed over a whole grid cell, Lagrangian models can interpolate between grid points when calculating the statistical behaviour of particles and have therefore a potentially infinitesimally high resolution. The quality of a Lagrangian simulation heavily depends on the number of simulated particles; higher number of particles usually not only result in higher computation times, but also in higher accuracy of the predictions [Ros10]. Examples for Lagrangian models are CLaMS (Chemical Lagrangian Model of the Stratosphere, [Kon04]) and FLEXPART, as described in the following section and in [Sto10].

In any way the applied model needs meteorological data to to perform the transport calculations. The meteorology can be calculated by deriving prognostic equations including the physical principles like energy and momentum conservation and on the basis of variables describing the state of the atmosphere; on the other hand the model can rely on externally generated meteorological data [Fei02], like described in Section 3.2.2.

Normally, trace gas concentrations are given in mixing ratios of mass m or volume V, because the concentration in mass or particles per volume depends on the parameters of the ideal gas law / van der Waals equation. However, concentrations of radioactive tracers are also given in activity per volume, i.e. $^{\mathrm{Bq}}/_{\mathrm{m}^3}$, while referring to standard temperature 0°C and pressure 1000 hPa.

Independent from the applied model (Eulerian or Lagrangian) ATM can be operated in forward mode or in adjoint mode [Wot03a]. While the resulting SRS fields of the forward model describe the dispersion of particles originating from a given source, the adjoint mode reconstructs the composition of a given detection, i.e. lists all contributions from all grid points and time steps. The adjoint model simply makes use of the temporally reversed model. The mathematical operators that are used to describe diffusion, deposition and radioactive decay processes are the same for forward and adjoint models. Adjoint modelling shall not be confused with inverse modelling, which means to locate previously unknown sources [Sei99]. However, within the context of this work adjoint modelling may also be called backward modelling.

Since forward and backward mode are basically both fulfilling the same purpose, i.e. calculating the atmospheric link between two grid points at a certain time, it is a question of efficiency which mode to select. The forward mode is usually for cases, when the impact of a limited number of known sources on a large or undefined number of receptors have to be simulated. The backward mode is more appropriate when the number of known receptors is limited and the possible sources are many or unknown. In the case of CTBT atmospheric monitoring with 40 noble gas monitoring stations and numerous background sources as well as all possible, unknown sources the backward mode is preferred. The same is valid for the total of 80 radionuclide stations compared to all possible source locations. The total number of possible and unknown sources depends on the spatial grid resolution. Furthermore, as the CTBT scenario calls for backward simulations of an adjoint tracer from a point measurement the Lagrangian model is favoured [Wot03a].

3.1.2 The Lagrangian Dispersion Model FLEXPART

The Norwegian Institute of Air Research (NILU) provides the Lagrangian particle dispersion model FLEXPART as a free software that is formally established by releasing the code under the GNU General Public License (GPL) Version 3. The first version has been released in 1996 by Andreas Stohl and is under steady development ever since. It is currently used by 35 working groups in 17 countries. In the frame of this research the FLEXPART software v8.2 has been utilised [Sto10].

The FLEXPART software allows to run forward and backward simulations of sources and receptors with point, line, area or volume dimensions. FLEXPART uses a zero acceleration scheme to simulate the particle trajectories, which is accurate to the first order:

$$X\left(t+\Delta t\right)=X\left(t\right)+v\left(X,t\right)\Delta t\,, \tag{3.7}$$

with t being time, Δt the time increment and X the position vector. This equation is used by FLEXPART to integrate the trajectory Equation 3.6 with

$$v=\bar{v}+v_t+v_m \tag{3.8}$$

being the wind vector composed of the grid scale wind $\bar{v}$, the turbulent wind fluctuations v_t and the mesoscale wind fluctuations v_m. Several removal processes are included in the FLEXPART code. When being subject to a removal process, the accordant particle

is simply removed from further trajectory simulations. Radioactive decay is included accordant to a given decay constant:

$$m\left(t+\Delta t\right)=m\left(t\right)\exp\left(-\Delta t/\beta\right)\,. \tag{3.9}$$

Since radioactive decay is only dependent on the particles characteristics, i.e. age and half-life, it can also be taken into account after computation of the SRS field. Further loss processes regard mainly chemical processes and are not only dependent on the particle's characteristics, but also on meteorological conditions. Therefore, these can only be simulated by the software itself.

For wet deposition it must be distinguished between in-cloud and below-cloud scavenging [Sto10]. The occurrence of clouds is deducted from local humidity and temperature given in the atmospheric input data. The in-cloud scavenging process differs for gases and particles, but both cases rely on the Hertel scheme

$$\Lambda=\frac{S_i I}{H_i}\,, \tag{3.10}$$

with $\Lambda\ \left[s^{-1}\right]$ being the scavenging coefficient, $I\ \left[mmh^{-1}\right]$ the precipitation rate and H the height over which scavenging takes place. The factor S_i is different for gases and particles and is accordingly inserted by FLEXPART. The below-cloud scavenging process is simulated by an exponential decay process:

$$m\left(t+\Delta t\right)=m\left(t\right)\exp\left(-\Lambda\Delta t\right)\,. \tag{3.11}$$

The scavenging coefficient Λ depends non-linearly on the precipitation rate.

Also for dry deposition it has to be distinguished between gases and particulates. In general dry deposition is included in FLEXPART by the deposition velocity

$$v_d\left(z\right)=-\frac{F_C}{C\left(z\right)}\,, \tag{3.12}$$

depending on the flux F_C and the concentration C of a species at height z within the constant flux layer.

Processes like re-suspension, i.e. formerly on the surface deposited particles that are re-released into the atmosphere, are outside of the frame of ATM and are therefore not included in FLEXPART. However, due to their inert character the noble gases such as radioxenon are not subject to deposition processes and can only be removed from the transport model by radioactivity.

The concentration in each grid cell is finally calculated by summarizing the product of particle mass m_i and the fraction of the mass f_i of particle i in the attributed grid cell over the total number of particles N and dividing by the volume V of the grid cell [Sto10]:

$$c=\frac{1}{V}\sum_{i=1}^{N}\left(m_i f_i\right)\,. \tag{3.13}$$

The FLEXPART v8.2 software has been ported to the local grid computer of the University Roma Tre/INFN and the European Mediterranean Grid (EUMEDGRID) in order to take advantage of parallel computation for fast production of SRS fields. Since the FLEXPART code itself is highly linear, the advantage of grid computing lies not in the acceleration of single jobs, but in the parallel execution of multiple jobs.

3.1.3 Usage and Validation of FLEXPART Output

When simulating the arriving concentrations at IMS stations any FLEXPART backward simulation is conducted with parameters as similar as possible to what is actually used at the CTBTO. This means a simulation time of two weeks, a spatial resolution of one degree and a time resolution of three hours. If not stated otherwise all FLEXPART backward simulations that are executed here assume an ideal tracer without radioactive decay, not being subject to chemical or physical removal processes during the transport. This approach allows it to do simulations only once and subsequently introduce radioactive decay for different isotopes, when analysing the data. However, it is impossible to introduce other removal processes after the simulation is completed. This approach is valid for noble gases as they are like the ideal tracer not subject to other removal processes.

The FLEXPART output is originally not human-readable, but can easily be converted with a Fortran script that was supplied from the Austrian Weather service (Zentralanstalt für Meteorologie und Geodynamik, ZAMG, Vienna). The new output contains the source-receptor matrix in a human-readable format [Wot03b]. The sensitivities are given for all coordinates and time steps with non-zero values. Each entry contains the latitudinal and longitudinal coordinate, the age of the contribution and the SRS itself. The SRS value represents the meteorological link between the source at the given coordinate and time step, and the receptor. The decay factor can be calculated from the age and a half-life of choice. Since the age is only given in integer time steps, the time resolution of three hours is also the time resolution for the radioactive decay. The contribution to the concentration at the receptor can be calculated from the assumed source term, the SRS value and the decay factor. The produced source-receptor matrix (SRM) lists all non-zero SRS values in relation to the source (for forward simulations) or the receptor (for backward simulations).

The radioactive decay depends on the transport time of each air parcel and the isotope's half-life and the reduced concentration can be calculated. However, radioactive decay can not only decrease concentrations, but decay chains can also contribute to an increase. The time development of relations between mother and daughter isotopes is taken into account by the Bateman equations [Bat10] in order to calculate the number N_n of atoms of the isotope n with decay constant λ_n:

$$N_n(t) = \sum_{k=1}^{n} N_{k_0} \cdot \sum_{j=k}^{n} \frac{\lambda_j}{\lambda_n} \cdot \prod_{i \neq j = k}^{n} \frac{\lambda_i}{\lambda_i - \lambda_j} \cdot e^{-\lambda_j t} \,. \tag{3.14}$$

In the case of radioxenon background sources not much is known about other precursor isotopes. When the emissions of the radioxenon isotopes of mass number 133 are known,

Table 3.1: Validation parameters for comparison of atmospheric transport simulations with experimental data.

Name	Abbreviation	Ideal value
Pearson correlation coefficient	r	1
Normalized Mean Square Error	NMSE	0
Fractional Bias	FB	0

the decay from ^{133m}Xe to ^{133}Xe can be included with the simplified Bateman equation for one mother isotope. In the case of N_1 : ^{133m}Xe and N_2 : ^{133}Xe, and only initial concentrations and no feeding after $t = 0$,

$$N_2(t) = N_2(0)\, e^{-\lambda_2 t} - N_1(0)\, \frac{\lambda_1}{\lambda_2 - \lambda_1} \left(e^{-\lambda_2 t} - e^{-\lambda_1 t} \right) . \tag{3.15}$$

The SRS matrices have to be folded with a source field in order to calculate the concentration at the receptor. For each source the location must be given within the used global grid. It is distinguished between constant and varying sources. Constant sources are described by their average emissions, e.g. in one year. Then the code automatically assumes this emission as constant for each time step. Varying sources are additionally described by a start and a stop time. The emissions of all four radioxenon isotopes can be included in the analysis.

In ATM the uncertainty of the SRS output is usually not directly determinable. Of course, this does not mean that the results are necessarily precise or correct. In order to generally validate atmospheric transport models so-called ensemble simulations are conducted. This means a simulation is conducted repeatedly, each time with slightly different parameters. The results are all equally weighted as no set of parameters within the ensemble can be identified with a higher probability of depicting reality [Pef11].

The concentration c at the receptor is given by the measurements c_m and the simulations c_s, and both time series can be compared with each other to check the quality of the model. The prediction quality can be checked with the Pearson correlation coefficient r, which is a measure of the linear dependence between two variables, resulting in a value between $+1$ and -1. High positive values result from a high linear dependence, i.e. a good correlation, while a high negative value results from samples lying on opposite sides of their respective means. A value close to zero means that no correlation is found between measurements (c_m) and simulation (c_s).
The Pearson correlation coefficient is given by

$$r = \frac{\sum_{i=1}^{n} (c_{m,i} - \overline{c_m})(c_{s,i} - \overline{c_s})}{\sqrt{\sum_{i=1}^{n} (c_{m,i} - \overline{c_m})^2} \sqrt{\sum_{i=1}^{n} (c_{s,i} - \overline{c_s})^2}} . \tag{3.16}$$

The Normalized Mean Square Error $NMSE$ describes the scatter in the entire data. It is normalized to assure that it is not biased for over- or under-predicting models. A smaller

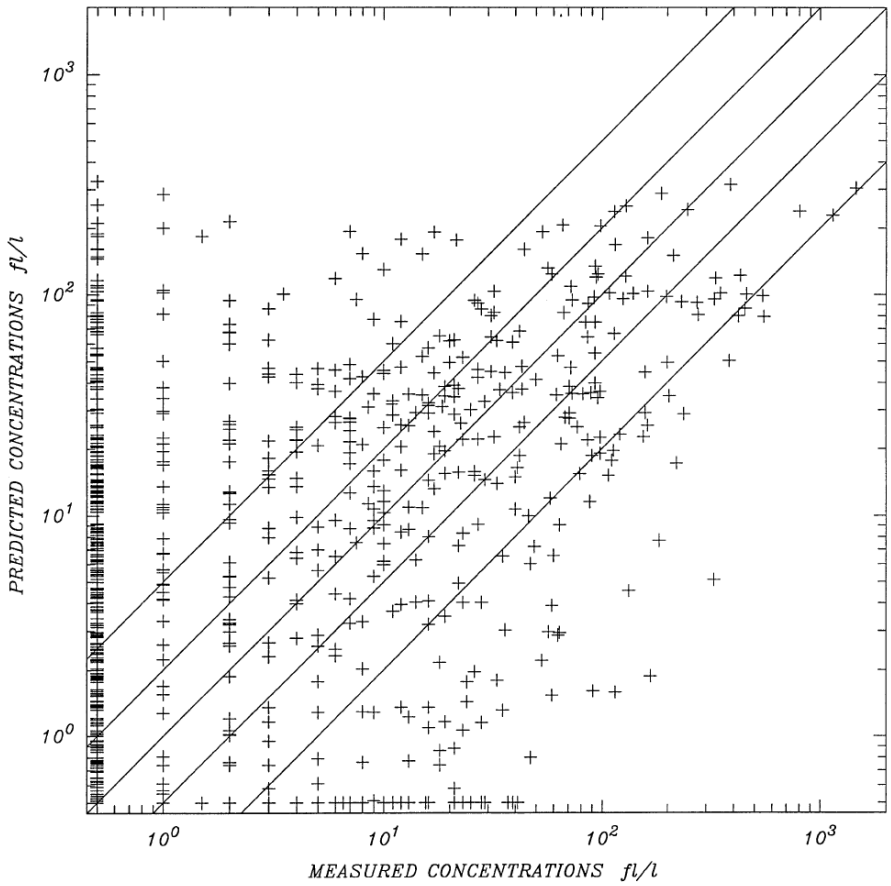

Figure 3.2: Correlation plot between simulated and measured concentrations for the CAPTEX experiment. **[Sto98]** Shown are also the ideal prediction line $x = y$ and the lines with factors 2 and 5 between both values. The data rely on 1,928 samples with a fractional bias of $FB = 0.00$, a normalized mean square error $NMSE = 22.6$ and a correlation of $r = 0.49$.

NMSE means a better model performance. It is defined by

$$NMSE = \frac{1}{n}\sum_{i=1}^{n}\frac{(c_m - c_s)^2}{(\overline{c_m}\cdot\overline{c_s})}\,. \tag{3.17}$$

The Fractional Bias FB denotes, if the simulation is over- or under-predicting. It varies between $+2$ and -2. The ideal value of 0 means that the deviation from the ideal prediction is symmetric. It is defined by

$$FB = \frac{1}{n}\sum_{i=1}^{n}2\cdot\frac{(c_{m,i} - c_{s,i})}{(\overline{c_m} + \overline{c_s})}\,. \tag{3.18}$$

These parameters have been proven to be valid for the comparison of atmospheric transport simulations with tracer experiments [Sto98]. The simulation of three tracer experiments - the Cross-Appalachian Tracer Experiment (CAPTEX, 1986), the Across North America Tracer Experiment (ANATEX, 1991) and the European Tracer Experiment (ETEX, 1996) - has shown good results, i.e. good prediction quality and neither over- nor under-estimation by the model itself. The results of the comparison with the CAPTEX experiment are shown in Figure 3.2. A correlation of $r = 0.49$ denotes a quite good agreement between model and experiment; a fractional bias of $FB = 0.00$ means that the model is generally neither over- nor under-predicted.

3.2 Sources of Data

For every step in the chain of emission→transport→detection independent data are needed. The following subsections contain descriptions of the data types and sources for radioxenon emissions, atmospheric fields and radioxenon sampling.

3.2.1 Radioxenon Emission Inventory

Legitimate sources of radioxenon included in the simulations are NPPs and IPFs. Other legitimate sources are not included. Since the SRS field from the FLEXPART output, which has to be folded with the emission inventory, is given with a one degree resolution, the location of each emitter is approximated to be on the nearest grid cell coordinates. In the usual case, when no time-dependent emission reports are available, continuous emissions have to be assumed.

3.2.1.1 Nuclear Explosions

When introducing hypothetical nuclear explosions into ATM, each explosion is characterised by the emitted activity (optionally for each isotope) and its time and location. The activity emission depends on bomb type, yield and leakage. These have been discussed in Section 2.1.1. The time and location can be freely chosen, but must fit into the discrete grid of the simulation. Time is handled by the simulations with a resolution of three

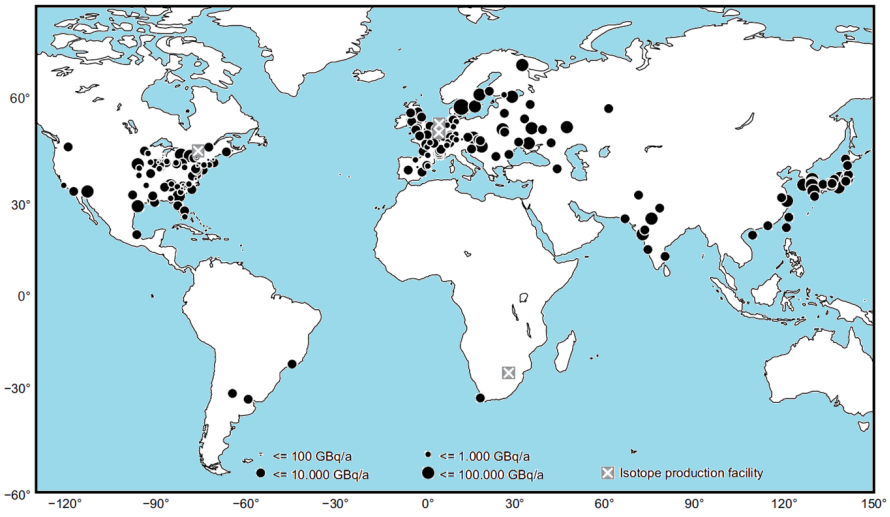

Figure 3.3: Global distribution of legitimate radioxenon emitters. [**Kal09**] Shown are NPPs scaled to their average emissions of ^{133}Xe and locations of known IPFs. Sources of radioxenon are clustered in North America, Europe and East Asia.

hours and thus each event can only last multiples of three hours. The location must be defined within the one degree latitude/longitude grid.

Releases and especially operational releases of radioxenon have been described in the Schoengold report [Sch96]. The duration of these operational releases are often stated to be in the order of one or a few days, but it is not referred to how long after the explosion the releases have been performed. The time of the original event can be reconstructed from the isotopic activity ratios. However, the radioxenon releases from this emission report have not been used in this work due to the fact that it only covers operational releases often days after the original event. When in this work presuming a hypothetical nuclear explosion, a standardised, conservative scenario is applied:

- The explosion has a yield of 1 kt TNT equivalent.
- A 1 kt nuclear explosion creates 10^{16} Bq of ^{133}Xe.
- An atmospheric or underwater explosion releases 100% of its noble gas outcome into the atmosphere.
- An underground explosion releases 1% of its noble gas outcome into the atmosphere.
- The products of an atmospheric explosion are directly released into the atmosphere.
- For underwater and underground scenarios a leakage within 3 h or less is assumed.

The choice of a conservative scenario ensures that the outcoming results regarding the detectability are reliable also under suboptimal conditions.

3.2.1.2 Isotope Production Facilities

For IPFs no publicly available emission reports exist. In the context of this work estimated annual emission data of ^{133}Xe for each IPF have been gathered, mainly during the Workshop on Medical Isotope Production in June 2011. Five IPFs have been considered as regularly emitting sources of radioxenon. They are located in Sydney, Australia, in Fleurus, Belgium, in Chalkriver, Canada, in Petten, Netherlands, and in Pelindaba, South Africa. Except for the facility in Petten, the IPFs have much stronger emissions of radioxenon compared to NPPs. An overview about their locations and emissions is given in Appendix B. Beside the estimated annual emissions, some IPFs supported this research with on-site monitoring data of emissions. The Belgium National Institute for Radioelements (IRE) has provided monthly emission data of ^{133}Xe for the time period 2007-2009 [Sch12a]. The Australian Nuclear Science and Technology Organisation (ANSTO) has provided the emission data from their reactor in the vicinity of Sydney, Australia, for the time period of November 2008 - December 2010. The latter data set is examined in an own section, see Section 4.2.

Recent research has shown that the applied radioxenon emission inventory leads to simulated receptor concentration that are on average lower than the accordant experimental measurements [Wot10, Sch12b]. The results conclude the underestimation within the model can be most likely attributed to an underestimation of the radioxenon emission inventory. A linear regression analysis has shown that the underestimation of the emission inventory is partly due to unaccounted sources and partly due to higher emissions from known emitters [Wot10]. Additionally to the five IPFs mentioned above, others exist, e.g. in Argentina and Indonesia, but no official information about their emissions is available. It is assumed here that their emissions are irregular and generally lower than those of the five better known IPFs due to a lower production rate of isotopes. Although at the moment only few actors exist, during the next years new actors will emerge on this market, while existing ones may also close down or vary their production rate or reduce their emissions.

3.2.1.3 Nuclear Power Plants

As of end of 2012 there are 435 nuclear power reactors worldwide in operation and 64 nuclear power reactors under construction [Iae12]. However, the most comprehensive, available compilation of NPP radioxenon emissions [Kal09] includes all operational reactors as of November 2007. This radioxenon emission inventory of NPPs worldwide is based on emission reports from several NPP sites, especially US-American and European ones. From these a global radioxenon emission inventory has been compiled [Kal09] for all operational reactors, including estimations for reactor sites without reliable emission reports. This global inventory gives estimations for generic annual emissions for each site, i.e. how much of each of the four relevant radioxenon isotope is emitted by each reactor site on average during one year, see Appendix B. In Figure 3.4 the number and duration of NPP batch emissions are plotted. Only few facilities operate in the regime of continuous emissions. Some can be approximated with a semi-continuous operation

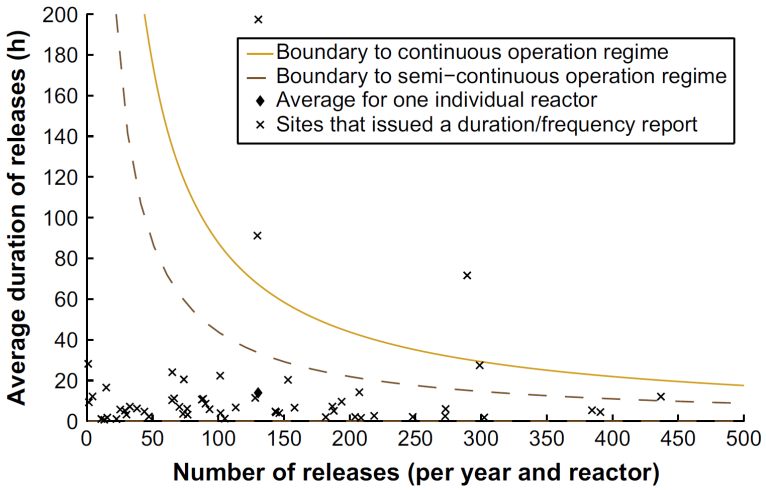

Figure 3.4: Number and duration of NPP radioxenon batch releases. [**Kal09**] Each mark represents one NPP site with available emission reports from November 2007. Only few operate in the continuous operation regime.

regime. However, most available duration/frequency reports indicate operations that can not be interpreted with continuous emissions. This may have a significant, negative impact on the prediction quality of the simulations. On the other hand, in regions with existing NPPs, their density suggests that they approximately can be handled as continuously emitting area sources, see also Figure 3.3. Nevertheless, it is believed that actual emission reports would improve the prediction quality of ATM.

3.2.2 Atmospheric Fields

In order to conduct ATM detailed information about the atmospheric conditions and movements are a basic prerequisite. Digital files containing such information about a certain time period are called atmospheric fields. They can be provided by national and international weather services. The FLEXPART software can utilise atmospheric fields from either the National Centers for Environmental Prediction (NCEP, USA) or the the European Centre for Medium-Range Weather Forecasts (ECMWF, UK).

The atmospheric fields containing the meteorological data used by the FLEXPART software are provided by the ECMWF [Per11]. It archives large quantities of atmospheric fields with various parameters for different applications. The input data for the FLEXPART software must include [Sto10]:

Two-dimensional fields: Surface pressure, total cloud cover, 10 m horizontal wind components, 2 m temperature and dew point temperature, large scale and convective precipitation, sensible heat flux, east/west and north/south surface stress, topography, land-sea mask and sub-grid standard deviation of topography[1].

[1]The land-use inventory is provided with the FLEXPART software in an extra file [Bel99].

Three-dimensional fields: Horizontal and vertical wind components, temperature and specific humidity.

The input data must be conform with the ECMWF η levels and its hybrid coordinate system, where the heights of the η surfaces at the kth level are defined by

$$\eta_k = \frac{A_k}{p_o} + B_k \,, \tag{3.19}$$

with $p_0 = 1.01325\,\mathrm{bar}$, and A_k and B_k coefficients to define the lowest level closest to the topography and the highest level equal to the pressure surfaces. All three-dimensional data are interpolated linearly from the ECMWF model levels to the terrain-following Cartesian coordinate system $\tilde{z} = z - z_t$, where z_t is the height of the topography. The FLEXPART software converts the vertical wind speeds from the η coordinate system into the terrain-following coordinate system:

$$\dot{\tilde{z}} = \dot{\eta}\frac{\partial p}{\partial \eta}\left(\frac{\partial p}{\partial z}\right)^{-1} + v_h \cdot \nabla_\eta \tilde{z} + \left.\frac{\partial \tilde{z}}{\partial t}\right|_\eta \,. \tag{3.20}$$

The last term on the right hand sight is much smaller than the others and is therefore neglected in the FLEXPART transformation.

The atmospheric fields provided by the ECMWF have been locally stored in a 3h time and a $1^\circ \times 1^\circ$ spatial resolution on the local grid computer at the Department of Phyics at the University of Roma Tre in cooperation with the Italian National Institute for Nuclear Physics (INFN).

3.2.3 Radioxenon Sampling Data

In order to support scientific studies that are based on IMS data the PTS established an electronic platform called virtual Data Exploitation Centre (vDEC) [vDe12]. Besides data from the IMS waveform components it currently contains noble gas data gathered by INGE from the years 2008 to 2010. The vDEC also offers access to noble gas and radionuclide data for the time period following the Fukushima accident. As explained in Section 2.2.2 the noble gas data is not comprehensive for all 39 stations due to planning, construction work, down-times etc. An overview over the current status of the IMS noble gas component is given in Appendix A. Available time periods of the year 2010 are given in Figure 3.5 for all data-delivering IMS stations.

When using the provided radioxenon sampling data and comparing it to simulations, one has to be aware of nuclear incidents in the time period of regard. Since most of the following simulations and analysis refer to the year 2010, it has to be mentioned that during May 2010 four IMS stations in Eastern Asia made detections of elevated concentrations of several radionuclide and radioxenon. One explanation could be a decoupled, but uncontained nuclear test of low yield on 11 May 2010 at the North Korean nuclear test site [DeG12].

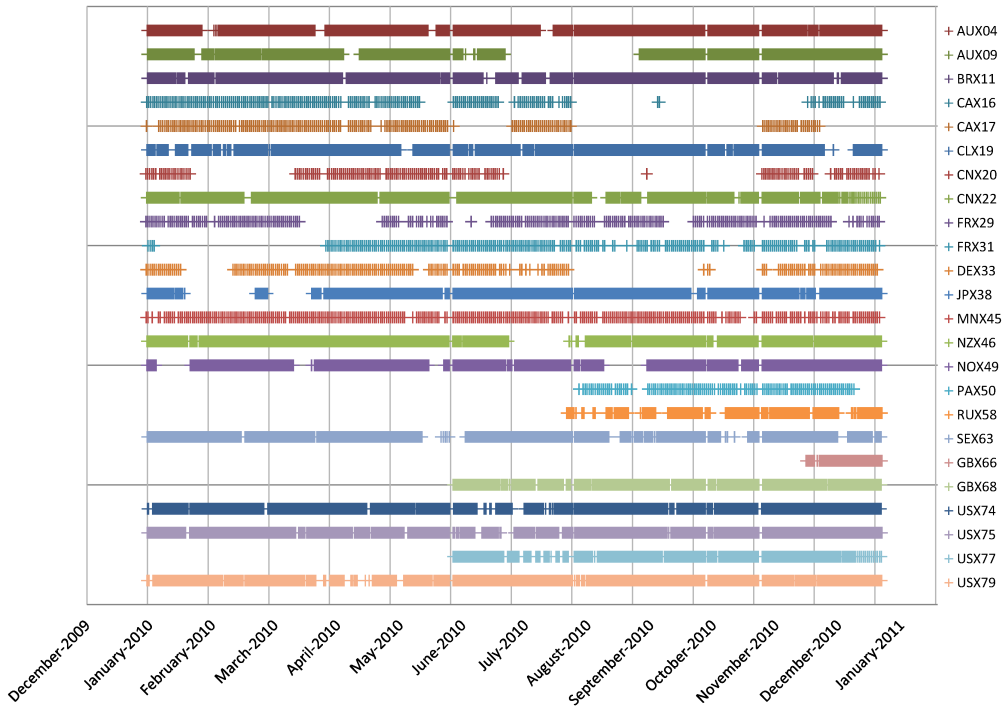

Figure 3.5: Available, experimental INGE data from 2010. [**vDe12**] Shown are all sampling periods (12h or 24h, depending on the detection system) in which the atmospheric radioxenon activity concentration has been measured.

Chapter 4

4 Simulation and Analysis of the Radioxenon Background

The worldwide emissions of radioxenon are characterised by many weak and few strong emitters, namely NPPs and IPFs, as presented in Section 3.2.1. The impact of these emissions on the IMS noble gas component is analysed in the following chapter.

4.1 Characterisation of Radioxenon Detections

4.1.1 Simulation of the Global Background

Due to the spatial distribution of radioxenon emitters in the world and particular meteorological conditions between emitters and IMS noble gas stations, the time series of radioxenon detections vary from station to station. As the IMS noble gas component is not fully built, tested and certified yet, the experimental data is not available for all stations and time periods. The radioxenon emission inventory can be used together with ATM to simulate the time series that are to be expected at IMS stations. As a first step to characterise the global radioxenon background the concentrations at the IMS stations are simulated for the course of one year. The simulations take into account the detection system that is used at each station with the accordant collection time of 12 or 24 hours, compare Table 2.1 and Appendix A. For those stations that are still in their planning phase and have no designated system yet, a SPALAX system with a collection time of 24 hours is assumed. The samples of all 39 IMS noble gas stations have been simulated for the whole year of 2010 with FLEXPART backward runs as described in Section 3.1.3. The time period of one year can only balance out the seasonal variations of this year, but not annual variations. Thus the following calculations primarily relate to the year 2010.

These simulated one-year time series of all IMS noble gas stations are presented in a box-and-whisker diagram[1] in Figure 4.1. As seen there, the predicted levels of ^{133}Xe vary over many orders of magnitude for the different stations. For most stations large parts of their distribution are found below the lower end of the MDC range, i.e. 0.2 $\mathrm{mBq/m^3}$. For

[1] For information on box-and-whisker diagrams see the box on the following page.

Box-and-whisker diagram
The length of the central box represents the spread of the central 50% of the data, i.e. the dispersion of the measurements. The central bar within the box represents the median value. The whiskers extend to the 5th and 95th percentiles; the "×" mark the 1st and 99th percentiles. The minimum and maximum values are represented by "–". The small square-box is found at the mean value of the distribution.

certain stations even the upper outliers are below this value. Only few stations have the median of their simulated data above this threshold, namely CAX17, DEX33, JPX38, SEX63 and USX75, i.e. these stations should detect ^{133}Xe in more than half of the taken samples. In the box-and-whisker diagram it can be observed how the rate of detections will be for each station according to the simulations. As seen for the simulated, one-year time series the concentrations at each station follow a certain probability distribution. For each station it has been tested which commonly known distribution is best suited to fit the simulated data. The following distributions were considered.

Distributions: Beta, Burr (also known as Singh-Maddala), generalized Pareto, generalized Gamma, inverse Gaussian, Kumaraswamy, log-normal, log-Pearson III, Pearson, Pearson VI, Weibull, and Weibull III.

These distributions have been originally developed each in different fields of research, but can be used in various applications. For each station-specific time series these distributions were validated with

1. the Kolmogorov-Smirnov test,
2. the Anderson-Darling test and
3. the Pearson's chi-squared test.

For each set of simulated data the distributions have been ranked by their goodness of fit according to these three tests. The one distribution with the best average rank has been chosen as the most fitting one. The determination of each probability distribution is important for the calculation of the standard deviation, which depends on the kind of distribution. The fitted probability distribution and the accordant standard deviation are given in Table 4.1 for the ^{133}Xe simulations of each IMS noble gas station. For most stations the distribution-specific standard deviation is below the upper range limit of the station-specific MDC.

As expected, especially for stations in regions with high density of NPPs or an IPF present the standard deviation is above the MDC, i.e. for

- DEX33, RUX61 and SEX63 in Europe and
- CAX16, CAX17, USX74 and USX75 in North America.

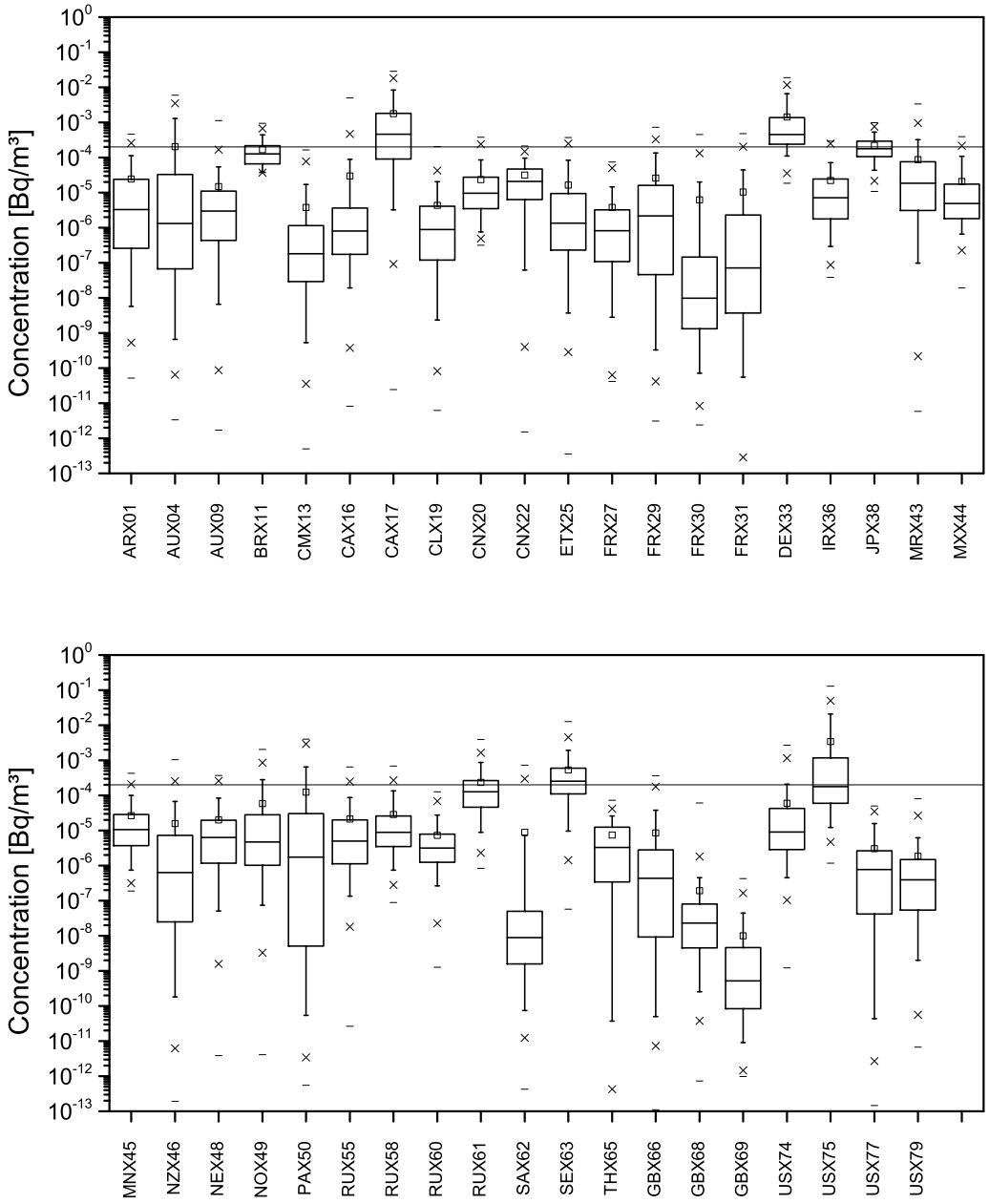

Figure 4.1: Box-and-whisker diagram of simulated ^{133}Xe activity concentrations for all IMS noble gas stations for the year 2010. The time series of each station has a typical distribution. Due to the theoretical nature of the simulations also concentrations below the MDC are included. Depending on the noble gas system the MDC can vary between $0.2 - 0.6\,^{\mathrm{mBq}}/_{\mathrm{m}^3}$; the common lowest value of $0.2\,^{\mathrm{mBq}}/_{\mathrm{m}^3}$ is plotted as a horizontal line.

Table 4.1: Distributions and standard deviations of simulated ^{133}Xe time series of IMS noble gas stations. Marked in **bold** is the higher value of either the station-specific, upper-limit MDC or the standard deviation.

Station ID	Distribution	Std. dev. [Bq/m³]	MDC [Bq/m³]
ARX01	Weibull	1.71E-04	**3.00E-04**
AUX04	Weibull	**1.89E-03**	4.00E-04
AUX09	Weibull	3.28E-05	**4.00E-04**
BRX11	Log-normal	1.51E-04	**4.00E-04**
CMX13	Gen. Gamma	2.42E-05	**6.00E-04**
CAX16	Log-normal	**9.21E-04**	6.00E-04
CAX17	Weibull	**4.70E-03**	6.00E-04
CLX19	Gen. Gamma	1.03E-05	**4.00E-04**
CNX20	Log-normal	6.63E-05	**6.00E-04**
CNX22	Gen. Gamma	3.38E-05	**4.00E-04**
ETX25	Gen. Gamma	8.32E-05	**6.00E-04**
FRX27	Pearson VI	2.41E-05	**6.00E-04**
FRX29	Weibull	1.66E-04	**6.00E-04**
FRX30	Gen. Gamma	5.56E-05	**6.00E-04**
FRX31	Kumaraswamy	4.19E-05	**6.00E-04**
DEX33	Log-Pearson III	**9.32E-03**	6.00E-04
IRX36	Log-normal	1.39E-04	**6.00E-04**
JPX38	Burr	1.66E-04	**4.00E-04**
MRX43	Weibull	1.97E-04	**6.00E-04**
MXX44	Inv. Gaussian	7.23E-05	**4.00E-04**
MNX45	Log-normal	8.65E-05	**6.00E-04**
NZX46	Pearson	3.54E-05	**4.00E-04**
NEX48	Burr	8.07E-05	**6.00E-04**
NOX49	Weibull III	1.52E-04	**4.00E-04**
PAX50	Gamma	3.99E-04	**6.00E-04**
RUX55	Burr	6.52E-05	**3.00E-04**
RUX58	Log normal	9.69E-05	**3.00E-04**
RUX60	Gen. Pareto	2.35E-05	**3.00E-04**
RUX61	Burr	**4.56E-04**	3.00E-04
SAX62	Log-normal	**7.77E-04**	6.00E-04
SEX63	Burr	**9.04E-04**	4.00E-04
THX65	Gen. Pareto	1.32E-05	**6.00E-04**
GBX66	Kumaraswamy	3.98E-05	**4.00E-04**
GBX68	Burr	3.97E-07	**4.00E-04**
GBX69	Gen. Gamma	6.23E-08	**6.00E-04**
USX74	Log-normal	**4.63E-04**	4.00E-04
USX75	Inv. Gaussian	**2.04E-02**	4.00E-04
USX77	Kumaraswamy	9.44E-06	**4.00E-04**
USX79	Weibull	4.09E-06	**4.00E-04**

Beside these also two stations in regions with no or low number of NPPs fall in this category. However, both are in regional vicinity to IPFs, namely:

- AUX04 in Melbourne, Australia with an IPF in Sydney, and
- SAX62 on Marion Island, South Africa, with an IPF in Pelindaba.

The prediction quality of each sample's concentration depends on the correct interpretation of the meteorological transport mechanisms by ATM as well as the applied radioxenon emission inventory. However, ATM may over- as well as under-predict the concentration of single samples, but on average is not biased for time series with a larger number of samples, as shown in Section 3.1.3. Therefore, the prediction quality of a larger data set, e.g. of one year, depends primarily on the applied radioxenon emission inventory. The presented results so far are based solely on simulations; these are compared to experimental data in the following section.

4.1.2 Comparison with Experimental Data

Unlike the simulations the experimental data are not available for all IMS noble gas stations for all time periods since not all of these are fully operational yet. Some stations are still in their planning phase and no detections have yet been made. Other stations are in their testing phase and in principle are able to deliver data. Also certified stations that should deliver data continuously can have downtimes due to maintenance, mechanical failures etc. Thus, the available experimental data is not necessarily as consistent as the simulated time series.

When comparing the simulated with the experimental data it has to be considered that only data points of the same sampling periods are comparable. Furthermore, only samples for which an experimental detection of a non-zero ^{133}Xe concentration has been made are used in the comparison. These experimental data are compared only to the accordant selection of simulated sample concentrations. Many IMS stations, especially in the southern hemisphere, are located in areas with a low radioxenon background. Though sampling data may be available, see Figure 3.5, these data do not necessarily include many detections. The following, comparative box-and-whisker diagram in Figure 4.2 presents experimental and simulated distributions of 15 selected stations with sufficient data basis next to each other. It has to be considered that the simulations can produce concentration values below the experimental MDC. As seen in the diagram, for some stations the predicted distribution follows the experimental data in reasonable agreement. Others have well enough overlaps between their experimental and simulated distributions. On the other hand, certain stations are clearly under-predicted in their simulated data, including some stations for which no detections at all are predicted (i.e. all simulated data is below the MDC). Accordingly the stations can be categorised:

Reasonable agreement: AUX04, CAX17, DEX33, NZX46 and USX75.

Overlapping distributions: BRX11, JPX38, NOX49, SEX63 and USX74.

Under-predicted: CNX20, CNX22, FRX29, MNX45 and RUX58.

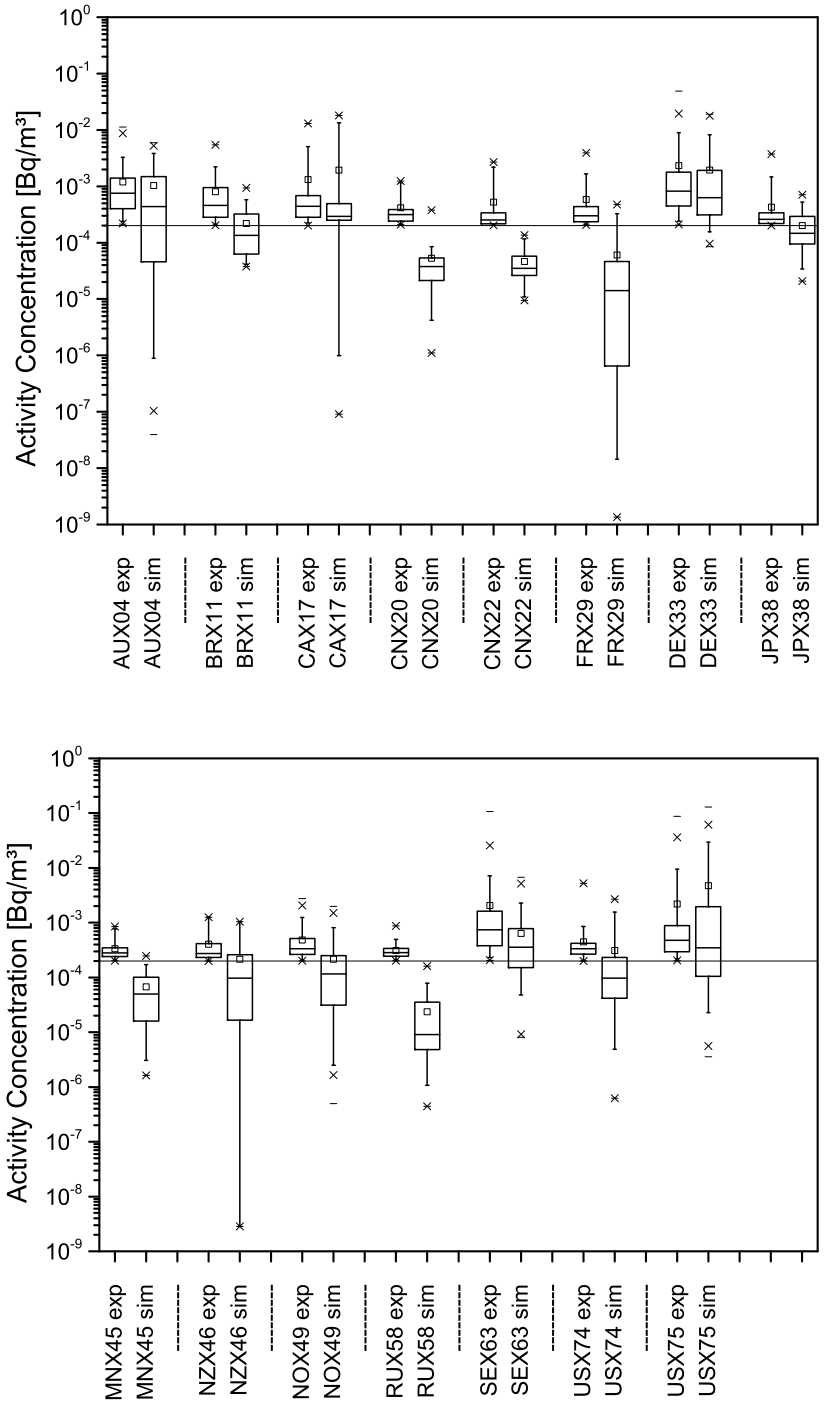

Figure 4.2: Box-and-whisker comparison of experimental and simulated ^{133}Xe activity concentrations at various IMS noble gas stations. Only actual experimental detections are considered, while samples with no measured concentration are excluded.

Besides that it is remarkable that for no station the distribution of xenon concentrations is clearly over-predicted. The possible reasons for this tendency towards under-prediction have been identified as fourfold:

1. The atmospheric transport model,
2. the applied emission inventory of legitimate radioxenon sources,
3. unaccounted emissions of mother isotopes of ^{133}Xe, and
4. unaccounted sources.

The experience with the FLEXPART model, see Section 3.1.3, and the fact that some stations are well and others are under-predicted suggest that the model itself is not biased. Following the categorisation for the stations, a regional dependence is noticeable. The prediction quality shows rather good results for Europe, North America and Oceania, while rather under-predicted results for the Asian region. This indicates that for certain regions the level of radioxenon emissions are well presumed, while for other regions a lack of emissions can be assumed. Whether this is mainly due to underestimated emissions from known plants, emissions of mother isotopes, newly built facilities or a mixture of these, cannot be answered with this analysis. The most likely contributor from decay chains is ^{133}I, which emissions strength are currently not well known [Sae10b]. Monitoring data from the IPF facility ANSTO in Australia [Hof12] indicate an activity emission rate of ^{133}I of six to seven orders of magnitude below that of ^{133}Xe, which would result in a negligible impact on the ^{133}Xe detections. Even when emitted in the same activity rate as ^{133}Xe, with an half-life of 20.8 h the feeding process from ^{133}I to ^{133}Xe increases the amount of ^{133}Xe by a factor of around 2 at maximum peak after about 2-2.5 days.

With fast developing countries in Asia it seems more likely that new nuclear facilities have been built that are not listed in the emission inventory, or existing NPPs have increased their electrical power output and thus also the radioxenon emissions. Of the contemplated Asian IMS stations the background at JPX38 is predicted best, probably because Japan is a long-standing producer of nuclear energy that allowed for better estimations of its radioxenon emissions.

A linear regression analysis has been used before for 12 IMS stations to distinguish between model bias and underestimation of emissions [Wot10]. A separated linear regression analysis for each continent could give answer to the newly found regional dependence of the prediction capability. Unfortunately the data basis is not large enough to handle only three to four IMS stations separately for each region.

Overall, it can be concluded that the quality of understanding the ^{133}Xe background is clearly regionally dependent. The distribution of ^{133}Xe concentrations is reasonably well understood for stations with available data in Europe, North America and Oceania. On the other hand, concentrations at stations in Asia and at FRX29 in the Indian Ocean are clearly under-predicted.

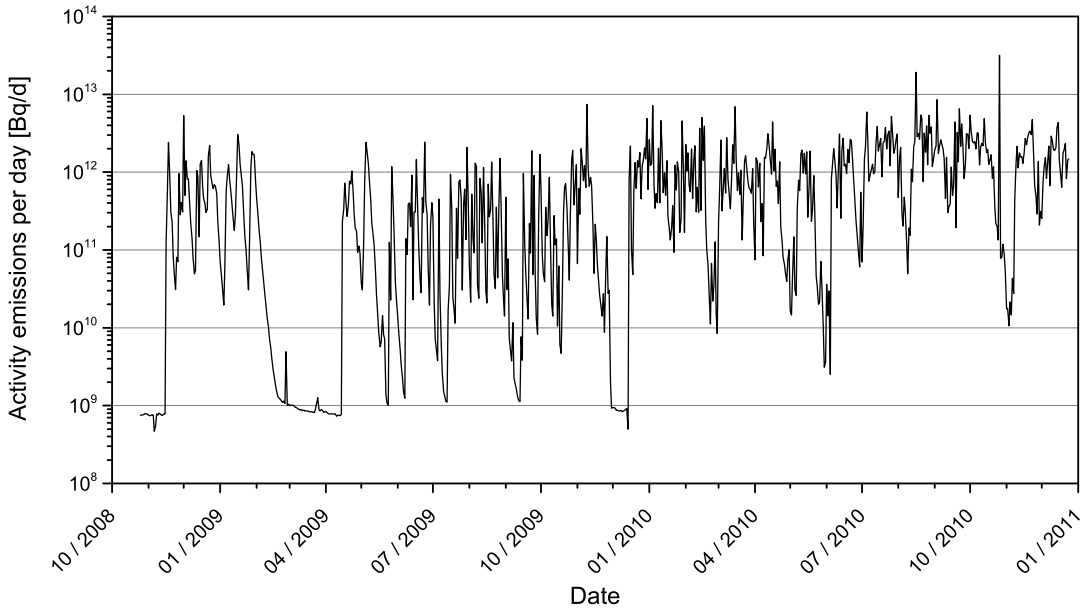

Figure 4.3: Time series of Ansto ^{133}Xe emissions. [**Hof12**] The source term varies over about four orders of magnitude in the course of two years and often has day-to-day variations of one order of magnitude.

4.2 Influence of Source Term Time Resolution

The used radioxenon emission inventory relies on reports and estimations of average, annual emissions. In reality NPPs and IPFs alike tend to operate with batch emissions with various frequencies and durations. In ATM these time dependent emissions can only be realised with accordant emission reports. It is assumed that availability of such data improves the quality of ATM-based predictions of radioxenon concentrations. Due to their high emission rates especially the emission reports from IPFs could have a measurable, positive impact on the prediction quality.

In order to quantify the improvement in the predictions different emission data sets based on different time resolutions of emission data can be compared. The IPF Ansto in Sydney, Australia, has provided daily resolved emission data for the time period of November 2008 to December 2010. The emission data is based on monitoring the active ventilation duct with NaI gamma ray detectors. All planned and unplanned emissions from the ^{99}Mo process are captured in this ventilation and monitoring system [Hof12]. However, such stack monitoring usually has an uncertainty of $\pm 20 - 30\%$ due to the gamma ray spectrum of ^{133}Xe and other fission products. In order to safely comply with governmental discharge limits this leads to an assumed overestimation of the emissions by about $\approx 20\%$.

As seen in Figure 4.3, the source term varies over four orders of magnitude overall and can have day-to-day variations of one order of magnitude. The general effect of emissions from the Ansto (Sydney, Australia) facility on the IMS noble gas component

has been subject of research before [Sae10c, Tin10]. In any case the emissions result in doses considerably below the annual limit for public exposure of 1 mSv. In the following the impact of source terms with different time resolutions from ANSTO is examined.

Parallel to the emission data the matching detection data are needed. The detection data from two nearby IMS noble gas stations have been available:

- AUX04, the Australian IMS station near Melbourne, about 700 km in a south west direction from the ANSTO facility;
- NZX46, the New Zealand station on Chatham Island, about 3,000 km in an east south-east direction from the ANSTO facility.

Both stations use a SAUNA system with a beta-gamma coincidence detector to monitor the radioxenon concentration in 12h cycles. In total 1,395 samples including 470 detections of ^{133}Xe from AUX04 and 1,555 samples with 204 detections from NZX46 were available for the time period of November 2008 until December 2010. As typical for the southern hemisphere the radioxenon background at both stations is usually around or below 1 $^{\mathrm{mBq}}/_{\mathrm{m}^3}$. The smallest, common MDC that is reached by both stations is 0.12 $^{\mathrm{mBq}}/_{\mathrm{m}^3}$ for ^{133}Xe. In order to exclude false-positive detections from the time series only samples with a concentration of 2σ above this value are taken into the analysis. The final data set that is used for the following discussion consists of 152 detections from AUX04 with an average concentration of 1.16 $^{\mathrm{mBq}}/_{\mathrm{m}^3}$ and 9 detections from NZX46 with an average concentration of 0.82 $^{\mathrm{mBq}}/_{\mathrm{m}^3}$. Due to the quantitative difference in the data sets the results for the two stations are not comparable with each other; a direct comparison would be biased, and no significant conclusion about the near- or far-field capabilities of ATM can be deducted from this.

With both - emissions and detections - being available the impact of various time resolutions can be investigated. From the daily resolved data three additional data sets with lower time resolution have been created: Daily, weekly, monthly and annual time resolutions of the ANSTO source term. For each of the four selected time resolutions the time series of ^{133}Xe concentration has been simulated for the time period of November 2008 until December 2010 at the AUX04 and NZX46 station. Each of the four simulated time series is separately compared to the experimental detection data of that period. For the statistical validation the three parameters that were presented in Section 3.1.3 are applied, namely the Pearson correlation coefficient, the normalized mean square error and the fractional bias.

The statistical results are presented in Table 4.2. The correlation for the Australian station AUX04 improves slowly from annual to weekly time resolution. For daily time resolution it improves significantly to 0.67, which is a sign for a considerable correlation. The NMSE shows only small increases that does not improve significantly. Also the fractional bias does not show a clear dependence on the time resolution.

For the New Zealand station NZX46 the correlation is close to zero and shows no significant change for varying time resolutions. The NMSE slightly improves with increasing time resolution. The fractional bias only improves significantly from annual

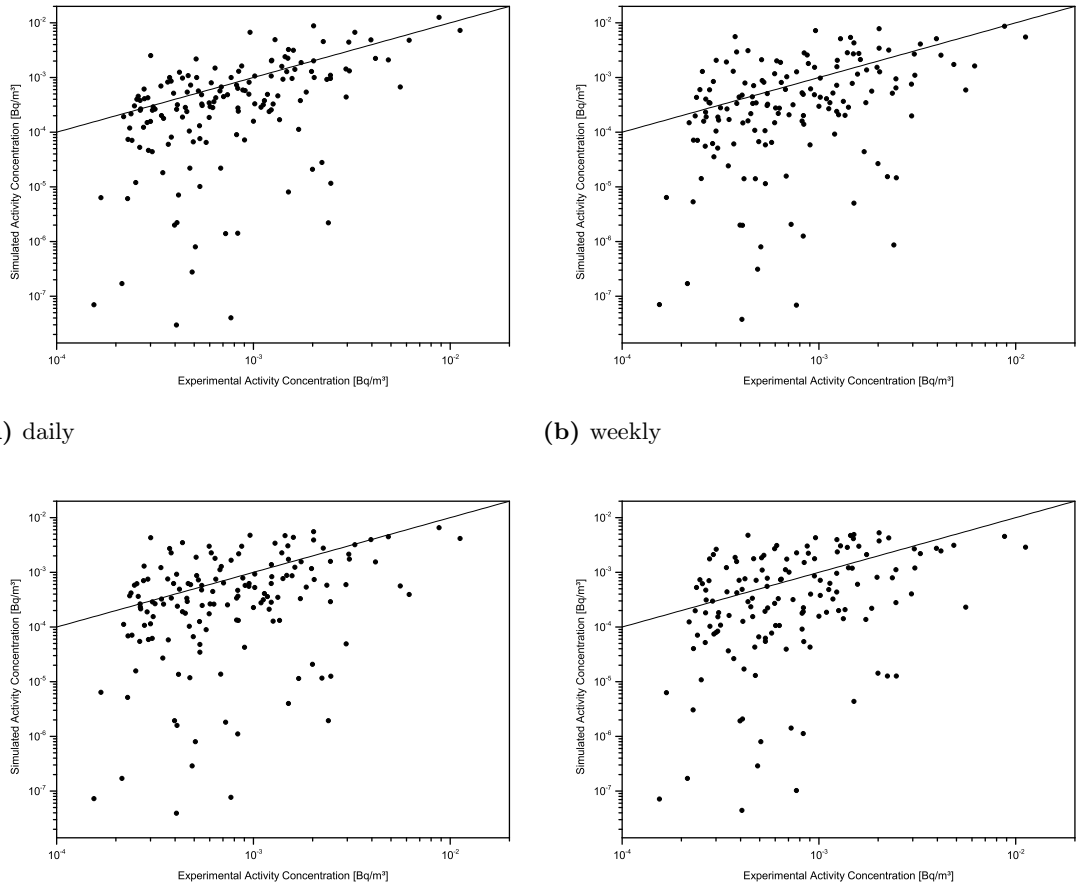

(a) daily

(b) weekly

(c) monthly

(d) annual

Figure 4.4: Correlation plots for AUX04 simulations based on different source term time resolutions. The differences are barely visible with the human eye, but are in the statistics. Since the plots rely on the same experimental data, the location of points change only in the vertical direction due to different simulated data. For some points, e.g. the two data points with the highest experimental concentration it can be observed how they are closer to the ideal prediction line for higher time resolutions.

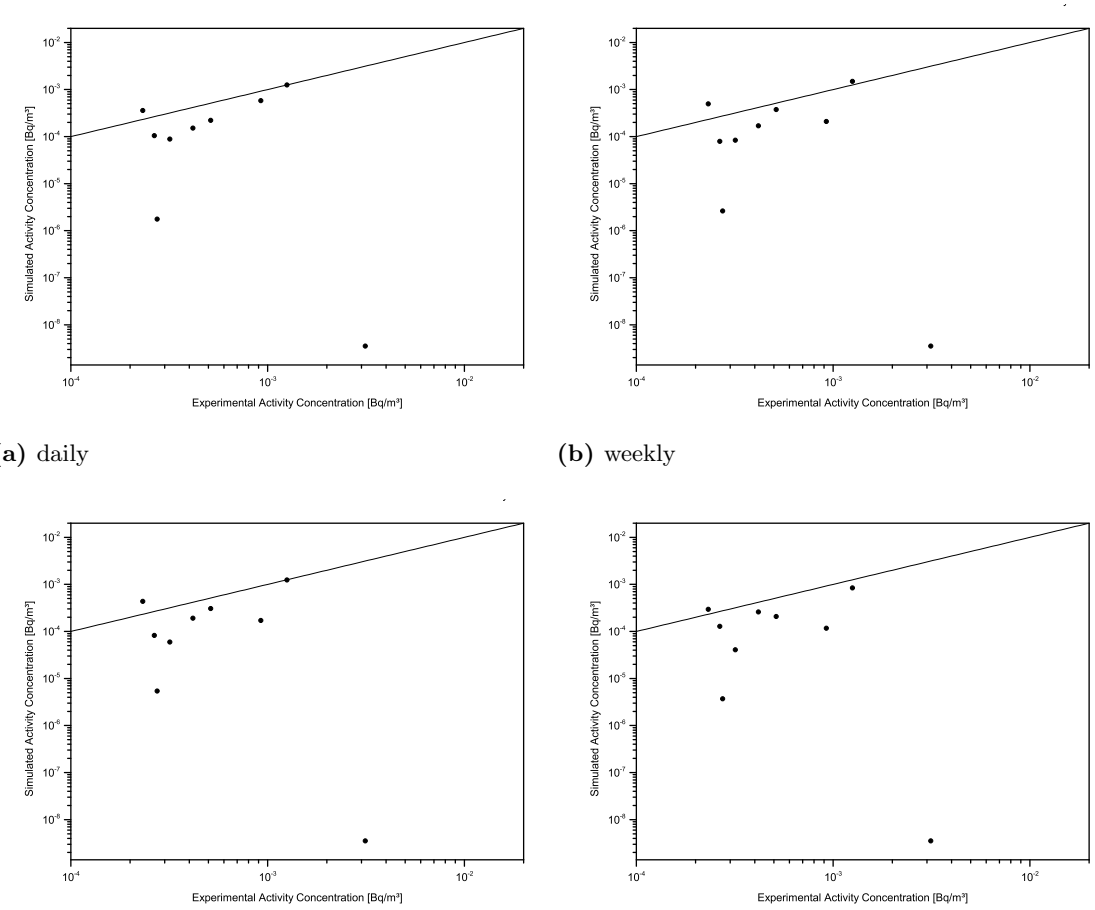

(a) daily **(b)** weekly

(c) monthly **(d)** annual

Figure 4.5: Correlation plots for NZX46 simulations based on different source term time resolutions. There are only few reliable, experimental data available for NZX46, but they show a good correlation with the simulations and also a positive correlation on the source time resolution as expected. The data point with the highest experimental concentration (and the lowest simulated concentration), is well under-predicted and shows no dependence on the time resolution since it contains no contributions from ANSTO according to the simulations.

Table 4.2: Statistical results of the time series analysis with four different emission data sets. The simulations are based on emission data from ANSTO (Sydney) and detections at AUX04 (a) and NZX46 (b).

(a) AUX04, Melbourne.

	daily	weekly	monthly	annual
Correlation	0.67	0.49	0.47	0.39
NMSE	1.13	1.45	1.42	1.63
Fractional Bias	0.16	0.12	0.23	0.15

(b) NZX46, Chatham Island. (In brackets statistics without the under-predicted outlier.)

	daily	weekly	monthly	annual
Correlation	0.06 (0.92)	0.04 (0.77)	0.02 (0.76)	-0.02 (0.73)
NMSE	0.20 (0.01)	0.20 (0.02)	0.23 (0.03)	0.31 (0.04)
Fractional Bias	0.90 (0.41)	0.86 (0.36)	0.98 (0.51)	1.18 (0.75)

to monthly time resolution, denoting less under-predicted simulations, but it does not improve much from a further increased resolution.

For both stations and all time resolutions a positive fractional bias indicates that the concentrations cannot be fully explained with the applied model. The experimental data from NZX46 includes a sample with an exceptional high concentration of $3.13\,^{\mathrm{mBq}}/_{\mathrm{m}^3}$, which is under-predicted by the model by about six orders of magnitude, see Figure 4.5. The accordant SRS field does not indicate any contributions from the ANSTO facility, but it is possible that in reality a non-zero sensitivity existed that was not resolved by ATM. When excluding this data point from the statistical analysis, the NZX46 simulations yield different results, which are shown in brackets in Table 4.2. All statistical parameters drastically improve, and partly exceed the results for the much closer AUX04 station. The correlation clearly increases, especially for daily time resolution of the source term. The NMSE decreases by about one order of magnitude. The fractional bias suggests a lesser under-prediction.

In Oceania the ANSTO facility is a strong and well known emitter of radioxenon [Tin10], and no other known sources are found in this geographical region. Due to these beneficial conditions from the monitoring point of view, it can be assumed that the prediction quality of ATM-based simulations is strongly influenced by available emission data from ANSTO. The results showed that over short distances, i.e. about 700 km for AUX04, the daily source term time resolution yields the best statistical results. The accuracy of a daily resolved source term directly reflects on the prediction capability at AUX04. On the other hand, for medium distances, such as 3,000 km for NZX46, no clear improvement is observed for different time resolutions. Only when excluding one under-predicted outlier, the statistics show a positive dependence for higher resolutions.

For both stations the predicted time series of ^{133}Xe are generally under-predicted. In this case the under-estimation can have a number of reasons:

1. The atmospheric transport model,
2. the ANSTO source term,
3. the emission inventory of other legitimate sources,
4. unaccounted mother isotopes of ^{133}Xe from known sources, and
5. unknown sources of ^{133}Xe.

As previously discussed, although for single samples the model can produce estimations that can deviate to up to one order of magnitude, FLEXPART is not biased for larger data sets. The source term describing the ANSTO emissions has been provided directly from the operator and is taken to be accurate within the range of uncertainty as discussed above. On the other hand, only ^{133}Xe emissions were reported as time resolved data and the time dependent influence of mother decay products, such as ^{133}I and ^{133m}Xe, cannot be quantified directly. Reports indicate that the annual emission rate of ^{133}I is in the range of six to seven orders of magnitude below of ^{133}Xe [Hof12] and, thus, in this case insignificant to the total concentration.

However, a general underestimation of the global emission inventory has been concluded previously [Wot10]. Besides that, a possible unaccounted source of radioxenon in this region could be found e.g. in Indonesia, a nuclear developed country with intentions and existing infrastructure to produce medical isotopes [Ima12]. In a recent research collaboration with the the Australian Radiation Protection and Nuclear Safety Agency (ARPANSA) it has been shown that the contribution of assumed ^{133}Xe emissions from this facility to the background level over the Australian landmass generally does not lead to measurably increased concentrations [Orr12].

Apart from the general effect of under-prediction, the availability of source term data with daily time resolution significantly improves the prediction quality in terms of correlation, scattering and bias. Similar studies for dominant radioxenon sources in Europe and North America would further help the understanding of the impact of available source term time resolution data and radioxenon background in general. Further improvements can also be expected for higher source term time resolution up to 3h, which would correspond to the SRS field time resolution.

4.3 Reconstruction of Source Term from Detections

When only a single source with a known location is contributing to the concentration at the receptor, the relation between source and receptor may not be linear, but has significantly less degrees of freedom than in multiple source scenarios. Inverse modelling can be used to locate an unknown source, or to restrict possible source locations, and to gain information about the emissions [Sei99, Sei00]. In the following section it is described how to reconstruct information about the time dependence of emissions from a known

location. This is done exemplary on the basis of the 2011 Fukushima nuclear accident. Other reconstructions of the source term by means of inverse modelling have been published [Sto11]. In order to establish an automated procedure on the grid computer of the University of Roma Tre in the following the basic steps are described of how to transform the problem into a set of linear equations, which would simplify the automation of source term reconstruction.

4.3.1 Practical Test

The Fukushima Dai-ichi NPP[2] was severely damaged in the following of the Tōhoku earthquake and the tsunami on 11 March 2011. Multiple reactors reached critical conditions and released large parts of their radioactive inventory into the environment. The emissions are assumed to have been strongly time dependent and being related to events such as explosions, emergency venting or cooling attempts, but were extremely difficult to determine in situ. Due to the radioactive and unstable environment on-site of the NPP no reliable assessment of the emissions could have been done. It is expected that they somehow correlate with external observations such as explosions, smoke or manual venting. These are comprehensively described in the publicly available database of the IAEA (`http://www.iaea.org/newscenter/news/tsunamiupdate01.html`).

In the following it is described how the Fukushima source term can be approximated by usage of ATM. It is a manual approach that potentially can be automated, which will be discussed the following Section 4.3.2. The pre-requisites for the following method are that

1. the location (latitude/longitude) of the emitter is known, and
2. the emitter is assumed to be the only source of the contemplated isotopic tracer.

The first step of the manual approach is to assume a constant source term from the known source [Pla11]. Backward simulations are used to determine the time series at the receptor from the constant source term. A reconstruction of the source term has been previously accomplished with a similar method and based on forward simulation [Sto11]. Here the results from the backward simulations are compared with the experimental measurements. The simulated time series of activity concentrations differs from the experimentally detected one, and the difference can be summarized in the sum of square errors of each data pair. However, since atmospheric activity concentrations often vary over orders of magnitude, it is appropriate to calculate the square error on a logarithmic scale,

$$e = \sum_i \left(\log_{10} c_{M,i} - \log_{10} c_{S,i}\right)^2 \tag{4.1}$$

$$= \sum_i \left(\log_{10} \frac{c_{M,i}}{c_{S,i}}\right)^2 \tag{4.2}$$

[2] In the following also abbreviated as Fukushima.

The detected concentration in a single sample may be composed of particles from different emission time intervals, and vice versa the emission of one time interval may contribute to the detected time series on multiple occasions. Thus, by varying the release of a single emission time interval, the detection time series may response in multiple detection time intervals. This also changes the sum of square log errors and therefore, the source term can be iteratively adjusted in a way that minimizes the value e.

The Fukushima nuclear accident allows for an exercise in source term reconstruction as its emissions are magnitudes above other sources. Therefore, also the data that are taken at downwind IMS stations report concentrations with magnitudes above the usual background. For the time series with elevated concentrations from these stations the Fukushima NPP can be handled as a single and only source.

Detections have not only been made for ^{133}Xe, but also particulate radioisotopes such as ^{137}Cs and ^{131}I. The activity concentration data have been made available through vDEC. When selecting suitable data from IMS stations the available time periods, their continuity and the distance to the Fukushima Dai-Ichi NPP are to be considered. For the purpose of source term reconstruction the detection time series should be continuous with as few gaps as possible. Also, for remote stations the quality of ATM-based prediction usually decreases since longer transport times and distances have to be simulated.

The ^{133}Xe data from two IMS stations that are in close and medium distance to Fukushima were available for the time period following the accident:

- The Chinese station CNX22 close to Hong Kong is in about 3,000 km distance in south-west direction from Fukushima. Its ^{133}Xe data is available starting from 24 March 2011. Previous to the nuclear accident common detection levels at this station were below $1\,^{\mathrm{mBq}}/_{\mathrm{m}^3}$, while at the end of March and the first half of April 2011 levels of $0.1 - 1\,^{\mathrm{Bq}}/_{\mathrm{m}^3}$ have been detected.

- The Japanese station JPX38 close to Tagasaki is located about 250 km in south-west direction from Fukushima. Its ^{133}Xe data is available from 04 April 2011 onwards. Also for this station detections of ^{133}Xe prior to the Fukushima accident were typically below $1\,^{\mathrm{mBq}}/_{\mathrm{m}^3}$, while the detected concentrations during April are also in the order of $0.1 - 1\,^{\mathrm{Bq}}/_{\mathrm{m}^3}$.

Both stations are operated with SAUNA systems and may therefore be subject to a certain memory effect as described in Section 2.2.1.2. The exact reasons for the detector down-times in the first days after the accident are unknown.

To establish the sensitivity between Fukushima and the two IMS stations with regard to ^{133}Xe the backward simulations have been conducted as described in Section 3.1.3. For ^{137}Cs and ^{131}I special simulations, including their chemical properties in the atmosphere, have been performed.

When applying the above described method to reconstruct the source term for each station and isotope separately, each station-isotope combination delivers an own point of view of how the Fukushima source term looks like. These four reconstructions are presented in Figure 4.6. With regard to the total emissions the magnitude of the

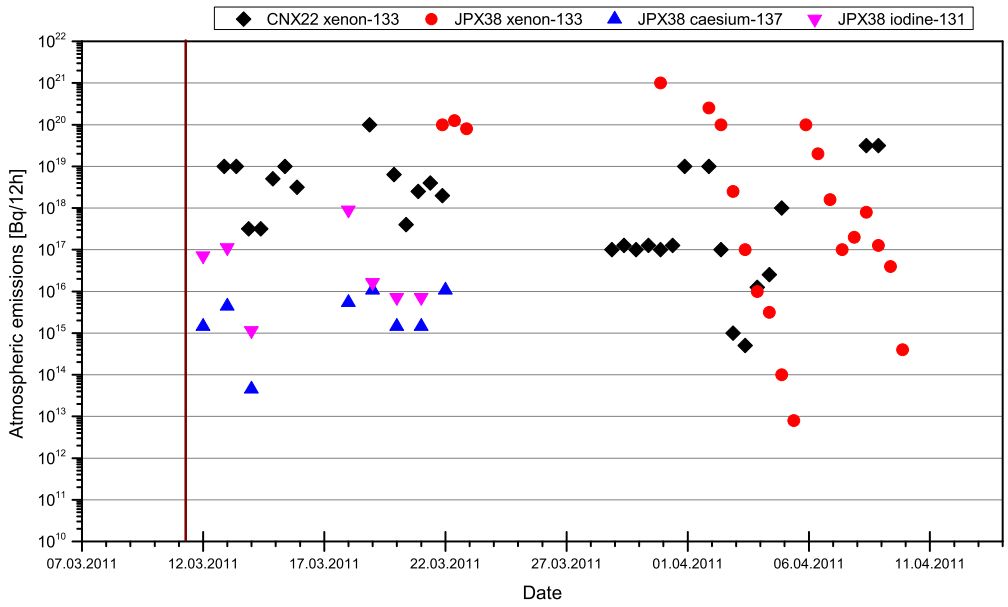

Figure 4.6: Fukushima source term reconstructions. The emissions per time interval as seen from the Chinese station CNX22 (^{133}Xe) and the Japanese station JPX38 (^{133}Xe, ^{137}Cs and ^{131}I). According to the meteorological data the gaps are due to non-existing source-receptor sensitivities in these time intervals. The vertical line represents the initiation of the nuclear accident at the Fukushima Dai-ichi NPP.

reconstructed ^{133}Xe releases is slightly higher than previously estimated releases of $13.4 - 20.0$ EBq [Sto11].

However, the different reconstructed source terms show certain common characteristics in the time series. Heightened emissions are observed for 13th and 15th March with a with local minimum between the two, a peak between the 17th and 18th and again around the 20st/22nd. These coincide approximately with observed explosions on 12th, 14th and 15th March. Also large emissions of smoke were reported for 18th March with lower amounts on the following days.

For the second part of the time series only the ^{133}Xe data allowed for a reconstruction. The gap of data between the two parts is due to meteorological conditions that did not produce any non-zero source-receptor sensitivities in the simulations. In that time period the focus of on-site activity was mainly on water-cooling the damaged reactors. During that time leakages of water from the reactor into the sea were reported, but neither further explosions nor further obvious atmospheric releases. Thus, the peaks in the second part of the reconstructed source term seem overestimated, especially when compared to the first part when explosions and smoke releases were observed. This overestimation probably results from a contamination of the detectors. Also, in the second part a common decline in the emission strength from 2nd to 5th of April is observed, although the time series

seems to be shifted against each other by one day. This time shift could be due to the chosen time resolution in the reconstructed source term of 12 h for ^{133}Xe (and 24 h for the other radionuclides), so that a peak could easily be attributed to a neighbouring time slot. It seems unlikely that in this approach a one-source/one-receptor scenario the time resolution of the reconstruction could reliably increased beyond the time resolution of the sampling data. However, a higher source term time resolution may be achieved in a one-source/multiple-receptor scenarios. Anyway, although the reconstructed source suggests higher emissions than presented in other publications [Sto11], the derived time dependent characteristics are in reasonable agreement.

If a single source is assumed and the source location is known, the method for source term reconstruction as presented above could be potentially used for various applications. Possible scenarios are

1. nuclear accidents, e.g. like Fukushima and Chernobyl, but also smaller incidents on the INES[3] could be possible,

2. strong emitters like regionally dominant IPFs, given that the emissions are much higher than those of NPPs in the same region, and

3. nuclear explosions, e.g. from an underground test, given that the emissions into the atmosphere are strong enough.

The presented method is less suited to reconstruct radionuclide and particulate source terms than noble gas source terms, because non-noble gas radionuclides and particulates are subject to more complicated transport mechanisms and especially deposition effects when being airborne in the atmosphere. Special cases with particular boundary conditions have been developed and discussed . Furthermore, effects that are out of the scope of ATM, such as re-suspension into the atmosphere of once surface-deposited particles, can make reliable predictions difficult. However, the comparison shows similar features in the source terms from various isotopes and stations.

4.3.2 Mathematical Description

In the previous section an iterative approach has been tested when minimising the sum of square errors between simulated and detected concentrations. That is taken as a concept study for the case of one single source with known location. As mentioned above similar methods have been previously delevoped [Sei99, Sei00] and enhanced [Sto09, Sei11].

The original equation describing the source-receptor sensitivity, see Equation 3.4, is

$$c = \sum_{ijn} M_{ijn} S_{ijn} \,, \tag{4.3}$$

and in the case of backward simulations it calculates the concentration for a single sample with the summed contributions for all time intervals n from all known source at locations

[3] International Nuclear Event Scale.

i, j. This can be rewritten for the case of a single known source ($i, j = const.$), but still all emission time steps n that contribute to the detection time interval m:

$$c_m = \sum_n M_{mn} S_n \,. \tag{4.4}$$

It has to be distinguished between the time interval m, when the sample is taken, and the time interval n, that represents the time interval of the emissions. For subsequent time intervals, i.e. a time series of detections, the source-receptor sensitivities can be written as

$$\begin{pmatrix} c_1 \\ \vdots \\ c_m \end{pmatrix} = \begin{pmatrix} M_{11} & \cdots & M_{1n} \\ \vdots & \ddots & \vdots \\ M_{m1} & \cdots & M_{mn} \end{pmatrix} \cdot \begin{pmatrix} S_1 \\ \vdots \\ S_n \end{pmatrix} . \tag{4.5}$$

This is a system of linear equations and, depending on the numbers m and n, it can also be over- or under-determined. It describes how receptor concentrations c_m are composed of emissions of various emission intervals S_n.

The concentration time series is given by the detection data and the SRS matrix is given by ATM, while the emission time series is unknown. The time resolution of the vector c is given by the sampling time of the detection system. In the case of one receptor and one source the time resolution of the emission time series is chosen here to be same as the time resolution of the sampling time series. This means a 12 h time resolution for ARIX and SAUNA systems, and 24 h for SPALAX systems. In ATM as applied in this work and by the CTBTO the backward simulations cover 14 days. Thus, in case of a 24 h sampling time the dimensions m and n follow the restriction $n = m + 13$, and in case of a 12 h sampling the $n = m + 27$; e.g., when having 14 samples with a sampling time of 24 h available, the matrix $\mathbf{M}$ has the dimensions 14×27. In any case $n > m$ and the equation in matrix notation is:

$$\mathbf{c}_{\mathrm{m}\times 1}(t) = \mathbf{M}_{\mathrm{m}\times \mathrm{n}}(\mathbf{S}(t)) \cdot \mathbf{S}_{\mathrm{n}\times 1}(t) \,. \tag{4.6}$$

Thus, the problem of source term reconstruction has been reduced to a system of linear equations. Including the boundary conditions of n and m results in an overdetermined system, i.e. a system that most likely has no exact solution. This equation seems similar to Equation 3.4, but now contains the detection sample m as an additional dimension.

There are various methods to automatically solve overdetermined systems of linear equations, which could also include the method of minimizing the sum of square errors as applied in the previous section. Future research could show which method yields the best results for this kind of matrix elements (dilutions in the order of $10^{-14} - 10^{-15}$) and matrix structures (e.g. distribution of zero elements). Further improvement could be achieved by a factorisation of $\mathbf{S}$, if any boundary conditions about the source term are known. These could concern minimum or maximum emissions, or any information about the time dependence of the source term such as start/stop time or characteristic frequencies.

The description above is also meant to serve as a guidance for the future to establish such an automated inversion algorithm at the Physics Department at the University of Roma Tre.

Multiple Sources, Multiple Receptors. As the right hand side stands for the contribution from one, known source, in the case of multiple source the right hand side has to be summed over the number of sources with coordinates i and j:

$$\mathbf{c}_{m\times 1}(t) = \sum_{ij} \mathbf{M}_{ij}\mathbf{S}_{ij}(t) \ . \tag{4.7}$$

Although also the SRS matrix is time dependent, it is defined by the time intervals of emission and detection as well as the location of the emitter. Mathematically this approach can easily be adapted to the case of a multitude of sources, but due to the inherent uncertainties of ATM the results that have been theoretically well determined may not represent the reality. Since the degrees of freedom increases with the number of included sources, especially due to the inherent uncertainty of ATM, the result's correlation with reality is expected to drastically decrease with a higher number of sources. On the other hand, a similar method could be developed to reconstruct one source term from detections at multiple stations in order to increase the reliability.

Chapter 5
5 Roles of Atmospheric Transport Modelling in Categorisation

The categorisation of radioxenon samples is supposed to aid human analysts in the assessment of a sample, and ATM can play various roles in it. The CTBTO has not yet adapted a certain categorisation scheme and, as presented in Section 2.3, various options exist. In general ATM can be utilised for categorisation purposes in two ways; it can be used:

1. to optimise the parameters of a categorisation scheme that by itself does not include ATM, e.g. by simulating the impacts of hypothetical events, or

2. as a method within the categorisation to assess each sample, for which the accordant SRS field must have been calculated.

This chapter gives an overview over possible directions and is meant to be a groundwork for future research.

5.1 Training of Methods based on Absolute Concentrations

When a certain categorisation mechanism relies on absolute sample concentrations, ATM can be used to determine thresholds for categorisation levels. Also, as long as the IMS noble gas component is not completed, it can be used to determine the expected background for not yet existing or newly build stations with small statistical history.

The Nevada Test Site (NTS) hosted the majority of the US nuclear tests, especially underground. It has been shown that the IMS stations that are most influenced by NTS emissions are USX74 in Ashland, Kansas, and USX75 in Charlottesville, Virginia [Pos12]. The nearest grid point of the NTS is 37° of latitude and -116° of longitude; the distance to USX74 is 1,400 km and to USX75 it is 3,300 km. Results from Section 4.1 have shown that both stations have an above average background of ^{133}Xe. In the following the impact of emissions from an NTS underground test on USX74 and USX75 are simulated. In the first step the impact of standardised emissions of 10^{14} Bq due to an 1% leakage

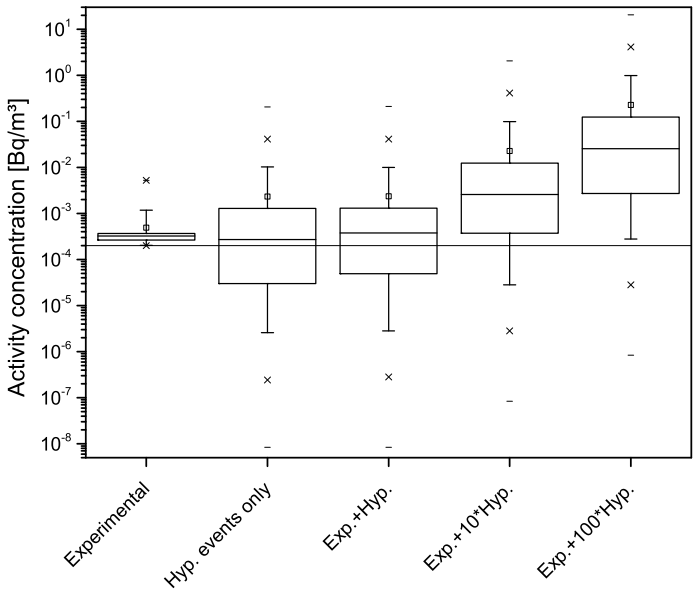

(a) USX74

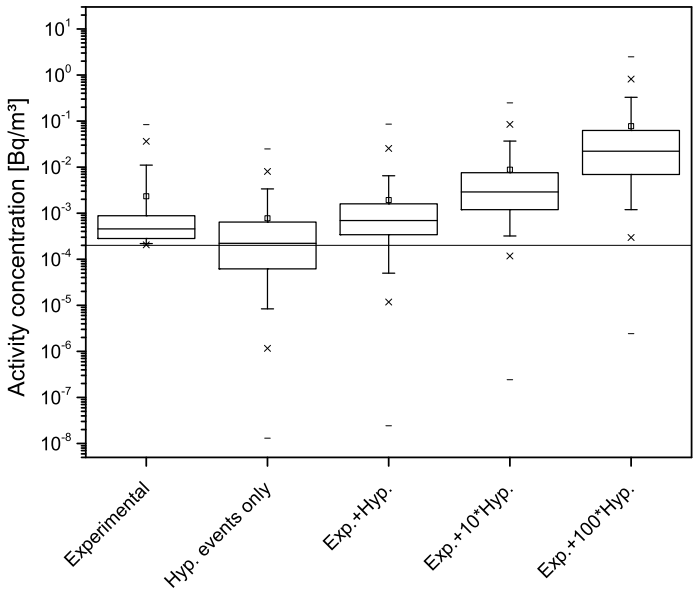

(b) USX75

Figure 5.1: Impact of hypothetical events from NTS on USX74 and USX75 signals. Shown are from left to right box-and-whisker plots of (1) the experimental data, (2) the data from all hypothetical events at NTS with assumed leakage of 1%, (3) sum of 1. and 2., (4) sum of 1. and 2. assuming 10% leakage, and (5) sum of 1. and 2. assuming full leakage.

as introduced in 3.2.1.1 are simulated for every 3h time step of the year 2010. For each of these 2,920 hypothetical event the time series of concentrations is deduced from the collective SRS fields of USX74 and USX75. Each event can cause several (or none), simulated concentrations at the receptors, which can also be below the MDC. Since here it is about absolute sample concentrations and not about time series analysis, for each event only the highest contribution to each of the two stations is selected for further analysis. In order to compare these highest contributions with the experimental data, only the detections from the accordant samples are taken into account.

This leads to several time series for both stations that can be compared with each other:

- The experimental data of the samples, which coincide with the highest concentrations from each hypothetical event,
- the highest concentrations from each hypothetical event without experimental background,
- the sum of the simulated contribution and the experimental concentration, and
- the same as the latter, but with up-scaled emissions from the NTS hypothetical events.

These time series are compared in a box-and-whisker[1] diagram, see Figure 5.1. The experimental box-and-whisker plot does not include the samples with no detection as these cannot be shown on a logarithmic scale. However, these non-detections are included in the time series when adding concentrations from hypothetical events. The box-plot of the impact of only hypothetical events (the second from the left) indicates that for both stations about half of the concentrations would be below the MDC and therefore, even with a clean background, undetectable. The following three box-plots show the distributions of the sums of the highest impact from each hypothetical event and the accordant experimental concentration. The first of the three plots shows the case of a 1% leakage, the following for 10% and 100% leakage. The latter can also be imagined as an atmospheric 1 kt explosion. For both stations it is observed that only the distributions with 10% and 100% leakage yield significantly higher concentrations than the original, experimental one.

As seen even for the closest IMS station (USX74) to NTS a high concentration does not necessarily come from a nuclear explosion, and a low concentration does not exclude the presence of one. The distributions of scenarios with different leakages overlap with the standard experimental data. This makes an absolute accurate categorisation scheme based on absolute thresholds, without false-positive and false-negative results, impossible to realise for emissions of low magnitudes such as 10^{14} Bq. This suggests that a level of acceptance has to be determined, as possible with station specific thresholds.

[1] For information on box-and-whisker diagrams see the box on page 46.

Application in Categorisation

Since the data series of each station follows a certain distribution, it is possible to determine the likelihood with which a certain detected concentration belongs to the standard distribution of the station. For each station with a history of experimental detections, e.g. more than one year, the kind of distribution could be determined, as shown in Section 4.1.1 for the case of simulated data. The accordant probability distribution can be used to check whether a sample is within certain boundaries, e.g. 68% or 97%. If such a boundary would be chosen, e.g. by the CTBTO, this could be included in a flag that states whether or not the sample is within standard range.

Besides that, the probability itself of the sample to be part of the station's typical distribution could be used as a floating number carrying more information than one flag.

5.2 Categorisation including Atmospheric Transport Modelling

Furthermore, ATM can be included as a categorisation mechanism itself. As presented above in Section 2.3, one example of this is to simulate the expected concentration for each sample and assign a certain level depending on absolute thresholds to the sample. In that example the flag may help to explain samples with a high, legitimate concentration, if it has been predicted well.

In any case, when including legitimate radioxenon sources in an ATM-based analysis, the applied radioxenon emission inventory is of high importance for the quality of the categorisation. As demonstrated in Section 4.1.2, for some stations this leads to well predicted distributions, while for others to underestimated ones.

The prediction quality of each sample can be formulated by the ratio of simulated to measured concentration. Since this prediction quality has an ideal ratio of one and can easily be off of the ideal value by one or even two orders of magnitude, it is useful to calculate it on a logarithmic scale for each sample:

$$d = \log_{10}\left(\frac{c_s}{c_m}\right) . \tag{5.1}$$

Then an ideal prediction would result in $d = 0$, while a value of d above (below) 0 denotes an over- (under-) estimation[2]. The average value $\overline{d}$ of a time series can be used to compare the prediction quality of different time series. The value $\overline{d}$ is calculated for the simulated data based on the emission inventory of legitimate radioxenon sources paired with the original, experimental data. Similar to the approach in the previous section the original, experimental data can be altered by the impacts on USX74 and USX75 samples from hypothetical explosions of various emission strengths from the NTS. The altered time series are in each case paired with the same simulated data based on the standard emission inventory.

[2]Opposed to the fractional bias the value d is suited not only for comparing data sets, but also single samples. This will be of importance in the following section.

Table 5.1: Average prediction quality for original, experimental and three altered time series. The prediction quality refers to the logarithmic ratio of simulations based on the standard radioxenon emission inventory to the experimental (or altered experimental) data. The experimental data has been altered by adding the simulated contribution from NTS 1 kt nuclear explosions with 1%, 10% and 100% leakage.

	USX74	USX75
$\overline{d}\,(exp)$	-0.68 ± 0.93	-0.13 ± 0.89
$\overline{d}\,(exp + hyp)$	-1.91 ± 1.07	-0.47 ± 0.85
$\overline{d}\,(exp + 10 * hyp)$	-2.46 ± 1.20	-1.05 ± 1.00
$\overline{d}\,(exp + 100 * hyp)$	-3.17 ± 1.31	-1.89 ± 1.11

The results for 1%, 10% and 100% leakage scenarios are presented in Table 5.1. As seen there the prediction quality gets more and more under-predicted for each scenario. In general the results for USX74 are subject to a stronger under-prediction than USX75. The magnitude of the average under-prediction increases clearly for increasing leakage scenarios, especially for USX74, which is located in vicinity of the NTS.

Application in Categorisation

The magnitude of average under-prediction shows clear dependence on contributions from nuclear explosions to nearby stations, even in distances of 3,300 km. Thus, potentially the prediction quality d of a specific sample could be used to validate it by comparing d to $\overline{d}$. However, as also seen in Table 5.1, the standard deviation $\sigma_{\overline{d}}$ is relatively high compared to $\overline{d}$ and for low emission scenarios even exceeds $\overline{d}$. This means that due to the high standard deviation even for low emission scenarios the sample may be over-predicted. Thus, this criteria is rather suited for categorisation when the sample contains high contributions from a nuclear explosion. It may help to identify such samples with unexpectedly high concentrations, but the reliability of such a method suffers due to the high standard deviation. Anyway, in the following section it is presented how this reliability can be improved.

5.3 Influence of Sample Composition

This section extends the analysis of the data concerning the source term time resolution presented in Section 4.2. By using ATM it is possible to determine the composition of a sample from the calculated SRS fields and a radioxenon emission inventory, i.e. how the total sample concentration is composed of concentrations from contributing sources. If emission data from a regionally dominant radioxenon emitter (in this case the Ansto facility as presented in Section 4.2) are available, the share of this source with regard to the total sample concentration can be calculated for each sample with

$$a = \frac{c_s\,(\text{Ansto})}{c_s\,(\text{Ansto}) + c_s\,(\text{other})}\,. \tag{5.2}$$

Table 5.2: Statistical results of simulations arranged by sample composition.

Share:	$\geq 99\%$	90-98%	<90%
Correlation r:	0.68	0.67	-0.04
Fractional Bias FB:	0.03	0.88	1.19
Prediction quality $\overline{d}$:	-0.22±0.57	-0.63±0.69	-1.56±1.34

This number can be calculated from the SRS field of each sample. Naturally, a can take values between 0 and 1. Also, as demonstrated in the previous section the prediction quality for each sample can be determined by:

$$d = \log_{10}\left(\frac{c_s}{c_m}\right) . \tag{5.3}$$

In Figure 5.2 a comparison between a and d for the AUX04 data is presented. The samples are sorted by the sample's share of ANSTO-related ^{133}Xe, which is plotted in black and with decreasing values from left to right[3]. The prediction quality of each sample is plotted in red. As seen, the quality of the prediction tends to go down along with decreasing values of a. It is also observed that the spread of the prediction quality is higher for lower shares a.

The correlation between a and d can also be found in the correlation plot that can be re-aligned according to each sample's share of ^{133}Xe from ANSTO[4]. In Figure 5.3 the samples have been categorised into three groups; one group with samples that theoretically consist of equal or more than 99% of ^{133}Xe from ANSTO, a second group with shares between 90-98%, and a third group with a share of less than 90%. In this case data with daily source term time resolution has been applied.

As seen directly in the plot the samples with a high share of ANSTO-originated ^{133}Xe rather tend to be found along the ideal prediction line as opposed to samples with lower shares. On the one hand this is due to the fact that sources other than ANSTO are in greater distance to the detector and therefore are subject to more uncertainties in the simulation. This is most likely also the reason for the spread of d in the right-hand side in Figure 5.2. On the other hand it is due to the fact that ANSTO is a regionally dominant and relative strong emitter when compared to regular NPPs. The latter is also the case for other IPFs in the world, e.g. CRL in Canada and IRE in Belgium. Similar results have been found for the relation between IRE, Belgium, and the German IMS station DEX33 [Sch12a].

This particular behaviour of each group of samples is confirmed by their statistics, see Table 5.2. For the $a \geq 99\%$ and the 90-98% group the correlation shows a good agreement between model and experimental data, but close to none for group of samples with $a < 90\%$. The fractional bias is close to zero for $a \geq 99\%$, i.e. denoting neither over- nor under-estimation, but shows clearly higher values for groups of lower a. Positive values of the fractional bias signify a general underestimation in the simulation.

[3] Values of $a = 0$ cannot be plotted on a logarithmic scale.

[4] The small data basis that is available for NZX46 would make such an analysis for this station insignificant.

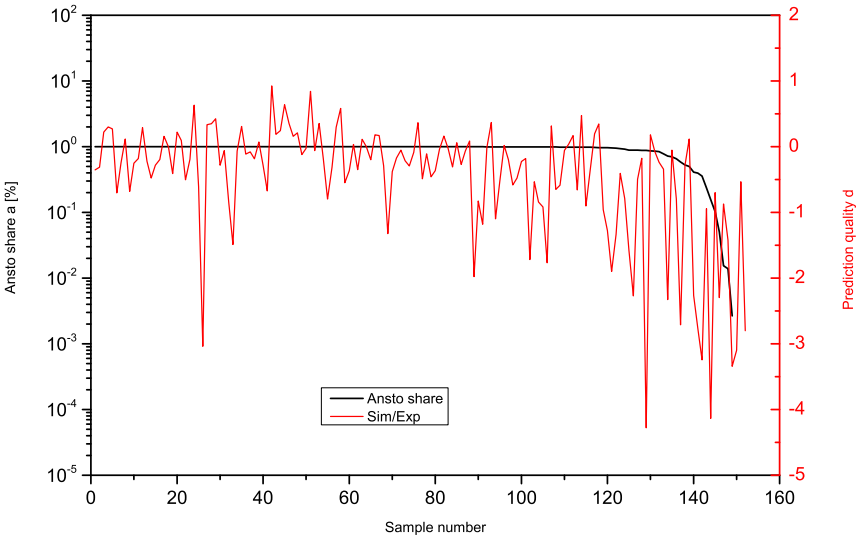

Figure 5.2: Comparison between prediction quality and share of Ansto-related ^{133}Xe. The samples are sorted from left to right by their share of ANSTO-related xenon (black). Also shown for each sample is the prediction quality $d = \log_{10} {}^{c_s}/_{c_m}$ (red). On average the prediction quality decreases with declining shares of ANSTO-related xenon.

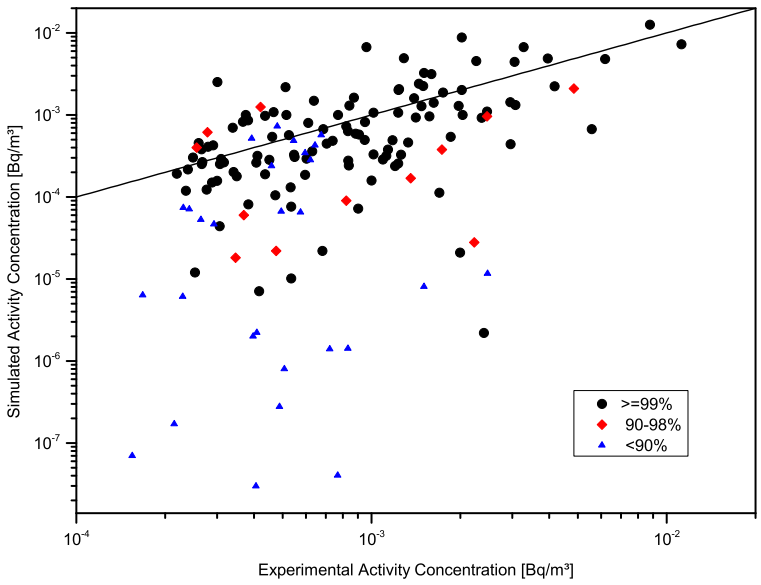

Figure 5.3: Correlation diagram for AUX04 by sample composition. The percentage represents the share of ^{133}Xe from ANSTO facility in the sample. The shares have been determined from the simulations based on the standard radioxenon inventory extended by daily emission data from ANSTO. Samples with high shares of ANSTO-related xenon are generally closer to the ideal prediction line $y = x$.

This demonstrates for a scenario with a main contributor to the signal that the standard deviation of d correlates with the sample composition; a higher share from the dominant source results in a lower standard deviation.

Application in Categorisation

This correlation between composition of the sample and its tendency in prediction quality could be potentially used for categorisation purposes. For each sample taken by the IMS noble gas network its composition could be determined from ATM backward simulations, e.g. for each single IPF and all NPPs together. The comparison with the prediction quality would allow to check how likely or unlikely this prediction quality is found in the accordant distribution of sample compositions. In case of a CTBT-related event, i.e. the emissions of a nuclear explosion, leading to an increase in the detected concentration, the sample would be under-predicted by ATM despite its sample composition suggesting a better prediction quality.

This could even be feasible without time-resolved emission data from strong sources, but in that case less reliable. However, this method must be thoroughly tested also for other regions in the world, especially with higher density of radioxenon background sources.

6 Chapter 6
Computation of the Network Coverage

This chapter deals with the effectiveness of the IMS noble gas component in detecting nuclear explosions worldwide. The capability to detect low yield nuclear explosions is parametrised so that a quality coefficient - the network coverage - can be attached to the current network design. This network coverage is a main quality parameter for the design of the IMS noble gas component and is approximated with ATM in the following.

6.1 Method

6.1.1 Definition

The IMS noble gas component has been designed to provide a 90% detectability of a 1 kt nuclear explosion within 14 days [Sch00]. The following work is supposed to determine the capability of the IMS to provide this coverage and to make suggestions how to improve it. So far the term *network coverage* has been used in a general meaning when describing the overall ability of the IMS to detect nuclear test explosions. Previously the spatial distribution of threshold yields of nuclear explosions that would trigger a detection has been researched [Wot10]. In the following for the network coverage η a new definition is established.

Definition. The network coverage η is the percentage of all possible 1 kt nuclear explosions, evenly distributed in global space and time, that are successfully detected by the IMS noble gas component.

The exact and real value of this number would only be determined by an infinite number of nuclear test explosions over an infinite time. Here the network coverage is approximated by simulating a multitude n of nuclear explosions evenly distributed in space and time. For each hypothetical event it is checked whether a detection within the IMS noble gas component is evoked or not. The total share of successfully detected events gives the network coverage:

$$\eta = \frac{n_{detected}}{n_{detected} + n_{undetected}} \,. \tag{6.1}$$

When using simulations to approximate the network coverage, certain boundary conditions have to be applied, where the results depends on the used parameters:

$$\eta_{reality} \simeq \eta_{sim} = \eta_{sim}(...)\,. \tag{6.2}$$

In the following these parameters are identified and determined.

6.1.2 Parameters

The parameters must provide an unbiased approach to determine the network coverage. In the presented method the general guideline for choosing the parameters is a conservative approach that is meant to represent a realistic - or even bad case - scenario with low emissions, strict detection criteria and today's network of noble gas monitoring stations. The following parameters have been considered in this approach to determine the network coverage.

Spatial distribution: An equal, spatial distribution of hypothetical, nuclear explosions is desired, where no region is a priori excluded or weighted in its likelihood to host a nuclear test explosion. The applied ATM runs on a global latitude-longitude grid with a $1^\circ \times 1^\circ$ resolution. The absolute length of a degree of latitude and longitude depends on the radius of a circle of given latitude [Osb08]. Taking the earth as an ellipsoid[1] the arc distances of one degree can be calculated dependent on the latitude ϕ as

$$\triangle^1_{Lat}(\phi) = \frac{\pi r_{eq}\left(1-e^2\right)}{180\left(1-e^2\sin^2\phi\right)^{\frac{3}{2}}} \tag{6.3}$$

and

$$\triangle^1_{Lon}(\phi) = \frac{\pi r_{eq}\cos\phi}{180\left(1-e^2\sin^2\phi\right)^{\frac{1}{2}}}\,. \tag{6.4}$$

This latitudinal dependence results in a variation of only up to 1% in the absolute length of one degree latitude, i.e. between $\triangle^1_{Lat}(0^\circ) = 110.57\,\text{km}$ and $\triangle^1_{Lat}(90^\circ) = 111.69\,\text{km}$, but results in large variations for the longitude, i.e. from $\triangle^1_{Lon}(0^\circ) = 111.32\,\text{km}$ over $\triangle^1_{Lon}(45^\circ) = 78.85\,\text{km}$ to $\triangle^1_{Lon}(90^\circ) = 0\,\text{km}$. This means that, if all grid points are treated equally, the spatial density of nuclear explosions would increase from the equator to the poles.
Therefore, for circles of latitudes that are higher or lower than the equator only a certain percentage p_{valid} of longitudinal grid points have to be considered for hypothetical, nuclear explosions in order to preserve an equally distributed field of events:

$$p_{valid}(\phi) = \frac{\triangle^1_{Lon}(\phi)}{\triangle^1_{Lon}(0^\circ)} = \frac{\cos\phi}{\left(1-e^2\sin^2\phi\right)^{\frac{1}{2}}}\,, \tag{6.5}$$

[1] The earth is taken as an ellipsoid with equatorial radius $r_{eq} = 6,378\,\text{km}$, polar radius $r_{pol} = 6,357\,\text{km}$ and eccentricity $e^2 = \frac{r^2_{eq}-r^2_{pol}}{r^2_{eq}} \approx 6.57 \cdot 10^{-3}$.

and an accordant percentage of grid points has to be skipped:

$$p_{skipped}(\phi) = 1 - p_{valid}\,. \tag{6.6}$$

The skipped grid points are to be equally distributed along each circle of latitude and are different for each one. Instead of $360 \cdot 181 = 65,160$ grid points only a total of $\sum_{\phi} 360 \cdot p_{valid} = 41,408$ grid points has to be considered, if one wants to provide an approximately equal spatial distribution.

Temporal distribution: For the choice of a certain time period it is reasonable to take a whole year (or multiples of one) in order to balance seasonal variations. For the time resolution of 3 h, the course of one year and 41,408 grid points a total of $365 \cdot 8 \cdot 41,408 = 120,911,360$ hypothetical events are considered.

Radionuclides: Only ^{133}Xe is considered in this approach to determine the network coverage. Due to its fission yield and half-life it is the isotope of choice, when simulating emissions from hypothetical nuclear explosions as well as from legitimate sources. For the background that is created by the latter the previously presented emission inventory is applied. In the future also the other three relevant radioxenon isotopes can be considered. Also other radionuclides or particulates can be included, if own simulations including dry and wet deposition are carried out.

Assumed network: The current network design foresees 40 IMS stations with noble gas monitoring equipment. Today only the locations of 39 stations have been appointed. The 40th station (RNX35, see Appendix - A) is supposed to be located in India, but is still subject to negotiations. To determine the network coverage today's network with known locations of 39 stations has been considered.

Assumed emissions: Emissions from underground, underwater and atmospheric nuclear test explosions can differ widely in amount and type of released radionuclides. As described in Section 3.2.1.1, a conservative, standardised approach is used to describe the emissions nuclear explosions. Atmospheric and underwater explosions are taken into account with full release within the first time interval, i.e. 10^{16} Bq in 3 h; underground explosions with a leakage of 1%, i.e. 10^{14} Bq in 3 h. In order to decide whether a grid point has to be considered as covered with water or landmass, the a land-sea mask has been extracted from ECMWF meteorological data and interpolated for a 1° resolution.

Detection criteria: Whether a concentration can be correlated to a nuclear explosion, depends on the MDC and the background activity concentration at the detector during the sampling time. For the MDC the system-dependent higher-end value is assumed; the values for ARIX, SAUNA and SPALAX systems are given in Table 2.1 on page 18. Clean background scenarios are discussed in Sections 6.2 and 6.3; a scenario including a radioxenon background in Section 6.4.

As the network coverage depends also on the assumed emissions and the emissions themselves depend on the environmental surroundings of the explosion, it is distinguished in the following between explosions above and under the earth's surface. For the scenario with subsurface explosions also a radioxenon background is included.

The basis for the determination of the network coverage are the backward simulations of the 39 IMS noble gas station of the year 2010 as described in Section 4.1.1. For each hypothetical event these SRS matrices are filtered for matching coordinate/time matches. For all matches it is checked, if at least one fulfils the detection criteria so that the event can be counted as a detection or as a non-detection. From this the ratio of detected to total events can be calculated.

6.2 Surface Nuclear Explosions

6.2.1 Scenario Conditions

Historically surface nuclear explosions have been detonated in military attacks twice[2] and in many cases for testing purposes until the PTBT entered into force in October 1963. Also full-leakage scenarios as well as peaceful, nuclear explosions are imaginable, e.g. for geoscaping. When considering only explosions on the earth's surface the emission strength is equal for each of the hypothetical events.

Assumed emissions: For surface explosions it is assumed that the full amount of radioxenon is released within the first time step of the simulation. This means that a source of

$$S = 10^{16}\,\mathrm{Bq} \tag{6.7}$$

is simulated that releases evenly over the course of one time interval, i.e. 3 h.

Background: No other sources of radioxenon are included in these simulations.

Detection criteria: For a clean background scenario with no other radioxenon sources a successful detection of a nuclear explosion is assumed to be made when the arriving concentration at a detector site is above the MDC:

$$c_{hyp} \geq MDC_{detector}\,. \tag{6.8}$$

6.2.2 Results

The presented approach and the clean background scenario for surface explosions of 1 kt are used to calculate the network coverage on a daily basis[3]. The total network coverage is averaged from the the daily values over the course of one year. This results in a network coverage of

$$\eta_{atmo} = (85.8 \pm 3.5)\ \%. \tag{6.9}$$

[2] On 6 August 1945 in Hiroshima, and on 9 August 1945 in Nagasaki.
[3] The underlying simulations still run with a frequency of one hypothetical events per 3h.

The daily values, each including the global coverage, have a minimum value of 78.3% and a maximum of 92.8%. This means that in this conservative scenario of surface explosions the targeted capability of detecting 90% of nuclear explosions is not constantly achieved. However, this reflects the overall value averaged over all locations and time steps. For a certain latitude-longitude coordinate or certain regions the statistics are different, e.g. events from a location in close, upwind distance to an IMS station lead more often to detections than e.g. locations in larger distance.

This spatial dependence can be displayed by summing the successful detections for each (included) grid point over the total time period and calculating the accordant success rate per grid point, see Figure 6.1a. As seen the meteorological patterns around the equator play a major role for the detection capability. Trade winds carry air masses from lower/higher latitudes towards the equator; Hadley cells keep air masses trapped in loops between the equator and the circles of $\pm 30°$ latitudes. The Intertropical Convergence Zone (ITCZ) is a low pressure belt of a few hundred kilometres width close to the equator, where the trade winds collide. This leads to the formation of zones with low air velocities or even windless regions. For latitudes beyond $\approx \pm 30°$ the detection probability is clearly higher and more uniformly distributed. The effects of reoccurring meteorological patterns especially in the equatorial region are seen in Figure 6.1a and can be identified as the main reason for lowering the total network coverage in this basic scenario.

6.3 Sub-surface Nuclear Explosions

6.3.1 Scenario Conditions

Sub-surface, nuclear explosions - whether underground or underwater - are more likely to be military tests.

Assumed emissions: Underground explosions are considered here with a 1% leakage within the first time interval, i.e. 10^{14} Bq within 3 h. This emission is assumed where underground explosions are possible, i.e. when the grid point is located on land. Where no solid ground is present, an underwater explosion is assumed. The noble gas release from an underwater explosion into the atmosphere is approximated with a full release of 10^{16} Bq within 3 h.

Background: No other sources of radioxenon are included in these simulations.

Detection criteria: When assuming a clean background the detection criteria is again for the concentration arriving at the detector to be above the MDC of the used detection system:

$$c_{hyp} \geq MDC_{detector} \,. \tag{6.10}$$

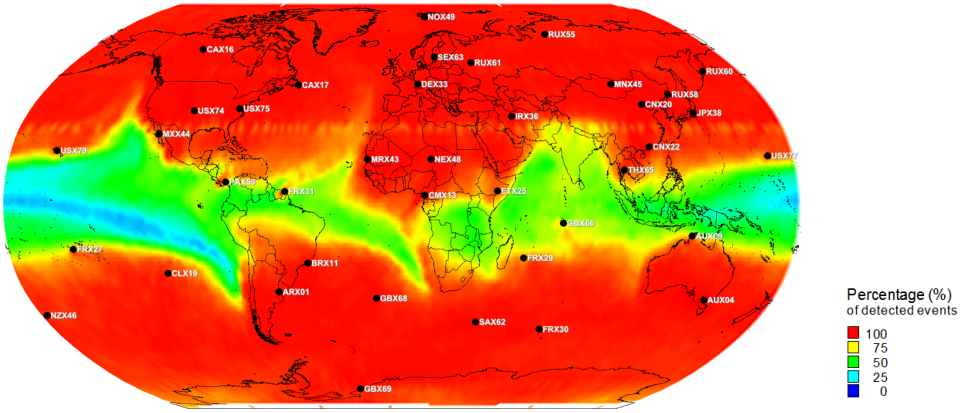

(a) Atmospheric, hypothetical explosions without radioxenon background.

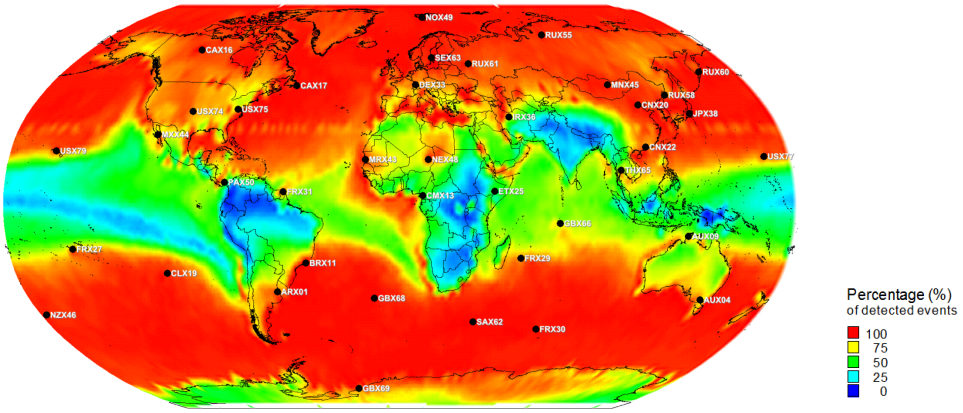

(b) Subsurface, hypothetical explosions without radioxenon background.

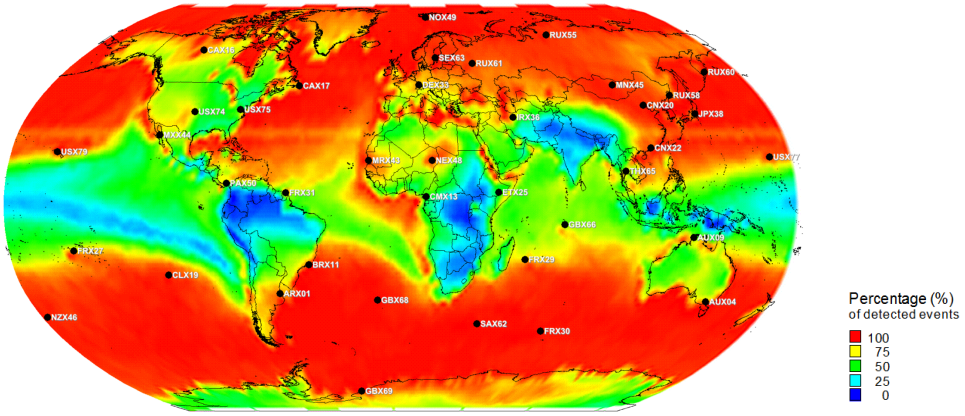

(c) Subsurface, hypothetical explosions including radioxenon background from known, legitimate sources.

Figure 6.1: Spatial dependence of network coverage for different scenarios, averaged over one year for each grid point. In each scenario the meteorological patterns surrounding the equator have a major influence.

6.3.2 Results

Averaged over each day as described in the previous section, this results in a network coverage for subsurface explosions of

$$\eta_{subs} = (77.9 \pm 2.8)\ \%. \tag{6.11}$$

This means that the relocation of nuclear explosions from above-surface to the subsurface decreases the theoretical network coverage by 7.9%. The daily values include a minimum of 71.5% and a maximum of 84.0%. The underlying land-sea mask describes the water coverage of the used grid points with about 71%. Thus, when comparing with the above-surface scenario, the reduced emissions from the remaining 29% of land-based grid points are responsible for this decrease in the network coverage. This is also displayed in Figure 6.1b, where the distribution over sea grid points is the same as for the previously discussed scenario of surface events. This includes again the effects of the ITCZ over large parts of the Atlantic, the Indian and particular the Pacific Ocean.

When comparing Figures 6.1a and 6.1b nearly all land masses show a reduction in the local detection capability. However, the reduced emissions form sub-surface nuclear explosions in equatorial regions together with the peculiar meteorological patterns lead to a clear decrease of the detection probability especially in East Africa, in the northern regions of South America, the Indian Subcontinent, Antarctica and parts of South East Asia.

Additionally to regions with oceanic water also some smaller seas, such as the Mediterranean, the Caspian Sea or the Great Lakes in Northern America can be identified in Figure 6.1b via their heightened detection probability. Their size exceeds the distances between the local grid points and therefore would theoretically prevent a contained, underground nuclear explosion.

6.4 Influence of the Radioxenon Background

6.4.1 Scenario Conditions

The most realistic scenario for calculating the network coverage is not only to assume sub-surface explosions where possible, but also to take into account the heterogeneous background. When including the radioxenon background, as analysed in Section 4.1, a detection of radioxenon does not necessarily imply the event of a nuclear explosion. Any concentration that comes from such an event and arrives at a detector adds with the background that is present at the given location and time. An applicable detection criteria would have to be aligned with the minimum, explosion-related concentration that is necessary to elevate the local concentration to an unusual level.

Assumed emissions: Where possible, underground explosions with a 1% leakage, i.e. 10^{14} Bq, are assumed. Otherwise an underwater explosion with 100% release of 10^{16} Bq is simulated. In both cases any emission lasts for one time interval in the simulations, i.e. 3 h.

Background: In this scenario the standard radioxenon emission inventory of legitimate sources, i.e. NPPs and IPFs as listed in Appendix B, are included.

Detection criteria: For a scenario with a radioxenon background coming from legitimate sources the detection criteria cannot be a simple threshold as before. The concentration that arrives from a hypothetical nuclear explosion has to be detected against a time dependent background concentration. The time series at each station are diverse and depend on many factors. The long-term distribution of concentrations is different for each station due to their geographical location and the time-dependent emissions of background sources. Accordant to the type of distribution the standard deviation is calculated for each station. It is assumed that when the contribution from the hypothetical explosion is higher than the standard deviation, the total signal is an unusual high concentration that stands out from the average time series. Thus the impact from the simulated, nuclear explosion must exceed the MDC as well as the standard deviation of the time series of one year:

$$c_{hyp} \geq MDC_{detector} \qquad \wedge \qquad c_{hyp} \geq \sigma_{station} \tag{6.12}$$

This means that a hypothetical, nuclear explosion must at least cause one detection of elevated concentration in order to be counted as detected. If this is not the case, it is counted as not-detected.

As in the previous scenario the upper-limit MDC is applied for each detector-specific system. The standard deviations for annual time series of the different stations have been presented in Table 4.1 on page 48.

6.4.2 Results

The application of these stricter detection criteria results in a lowered global network coverage of

$$\eta_{back} = (76.4 \pm 2.8)\ \%. \tag{6.13}$$

The time series of daily values include a minimum of 70.2% and a maximum of 82.7%. As to be expected the further reduction is mainly caused by reduced detection capabilities for events in Northern America and Western Europe, see Figure 6.1c. This is due to the regional higher density of NPPs and IPFs. Surprisingly events in East Asia that are likely to be detected by JPX38 in Japan are not that much negatively affected by the legitimate background.

However, the results from Chapter 4 and previous research [Wot10, Sch12a] suggest that the applied radioxenon emission inventory may generally and regionally be underestimated. Thus the real impact might be higher in certain regions and result in a further decrease of the total network coverage.

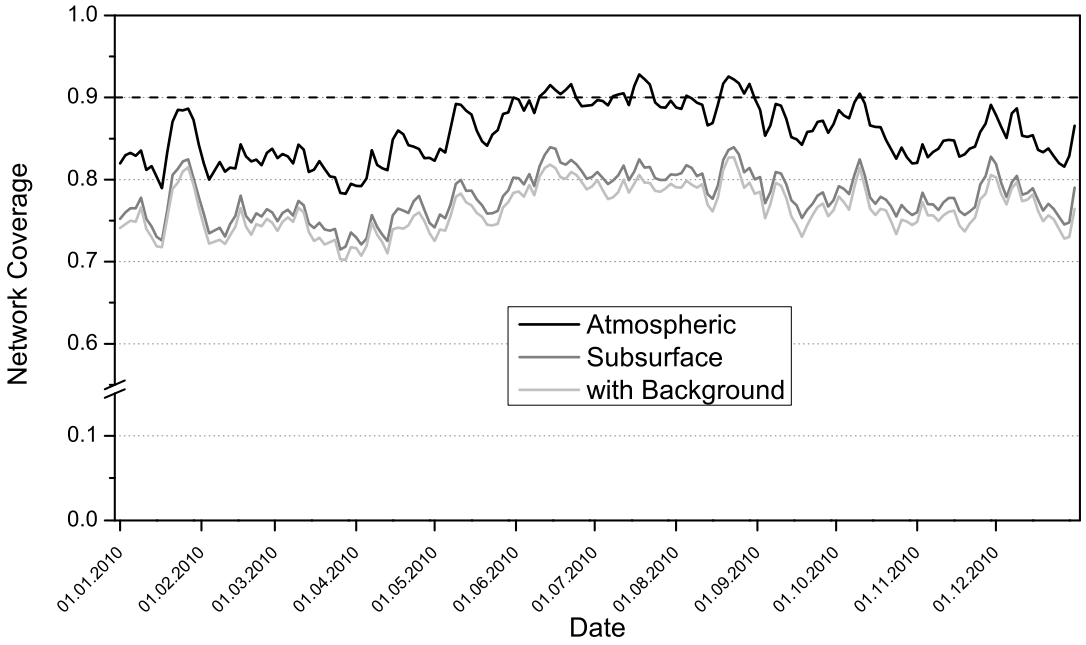

Figure 6.2: Time series of network coverages for the year 2010. The three scenarios produce time series with very similar characteristics. Moving from above-surface to subsurface explosions reduces the network coverage clearly, while the introduction of the background has an additional (but smaller) negative effect.

6.5 Time and Spatial Distribution of Network Coverage

6.5.1 Seasonal Dependence

The general time dependence over the course of one year behaves very similar for all three of the above scenarios. As seen in Figure 6.2 they share most characteristic peaks on a day-to-day basis, e.g. the positive peak at the end of January 2010, and also medium-term developments, e.g. the high plateau between June and August 2010.

Large parts of the areas with low detection probability are found in the tropical Pacific. This part of the world is not only subject to the aforementioned trade winds, but also to the El Niño and La Niña Oscillations[4]. El Niño is most notably marked by an increased surface temperature of the western Pacific, while La Niña by lowered surface temperature of the equatorial eastern Pacific, both with temperature differences of at least $\pm 0.5\,\mathrm{C}^\circ$. In the year 2010 the maximum surface temperature differences were $\pm 1.5\,\mathrm{C}^\circ$ with regard to the average. The effects, however, can be globally observed with impact on pressure in the Indian Ocean, on trade winds in the south Pacific, and on general climate, e.g. also in Europe and Africa. In the year 2010 El Niño peaked during January and ended in March, while from April to July the surface temperatures normalised [Noa12]. From August onwards for the rest of the year La Niña was predominant.

[4]El Niño and La Niña are quasi-periodic meteorological patterns occurring across the tropical Pacific.

During the last third of January 2010 the network coverage exhibits a 5-7 days lasting positive peak with a maximum value of about 10% above the previous and following local minima, as seen in the plot in Figure 6.2. The spatial relocation of the the network coverage is shown in Figure 6.3a; in order to better compare meteorological effects the surface explosion scenario has been chosen. It is seen that the equatorial zones with typical low detections have contracted. However, a short term peak of a few days cannot be explained with a climate pattern lasting for months. On the other hand, since El Niño peaked in January, the turn of the development might have an effect on the transport mechanisms in the Pacific.

Exemplary, also the spatial distribution of the minimum of the network coverage from 26 to 30 March has been plotted in Figure 6.3b. It is seen that the zones of lower detection probability are still connected, having an extremely low detection probability in wide areas of down to 0%, and cover significantly larger areas than on average.

The spatial distribution of detection probabilities of the network coverage's high plateau from June to August 2010 has been plotted separately in Figure 6.3c. When comparing this three month period with the annual distribution in Figure 6.1a, it is seen that the higher probability between June and August 2010 is due to a different distribution of the equatorial meteorological patterns; the low-probability zones around the equator are smaller and even separated from each other by zones of high detection probability. This change of detection probabilities is believed to be caused by a particular behaviour of the ITCZ. During these months, i.e. during the Northern summer, the ITCZ tends to move farther away from the equator and thus allows hypothetical emissions to be more effectively transported. This meteorological behaviour of the ITCZ is generally not observed during Southern summers, i.e. during Northern winter times, which is congruent with the generally lower simulated detection probability from January to March 2010, as seen in the plot in Figure 6.2. Furthermore, the occurrence of La Niña during these months may have influenced the detection capability, especially for events in the Pacific area.

It is summarised that the seasonal dependence of the network coverage can be attributed to meteorological effects around the equator and to the seasonal dependence of transport mechanisms of the ITCZ.

6.5.2 Non-detectable Events

In the previous sections the spatial as well as the seasonal dependencies of detections have been discussed. In order to understand the parameters influencing the network coverage it is necessary to also discuss the spatial distribution of the *non*-detections. In the above described simulations of hypothetical nuclear explosions an event can remain undetected due to

1. the activity concentration arriving at an IMS noble gas station does not fulfil the necessary detection criteria, or

2. the simulated plume of the emissions from the event does not reach any IMS noble gas station within 14 days.

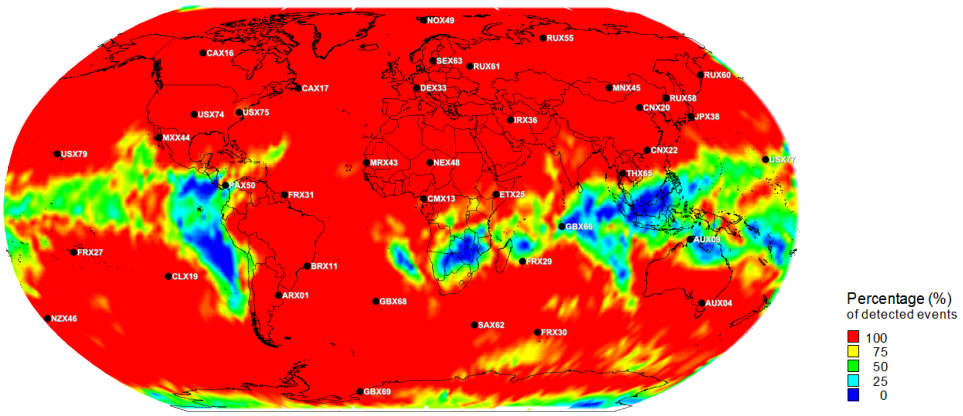

(a) Heightened network coverage during 23-27 January, 2010.

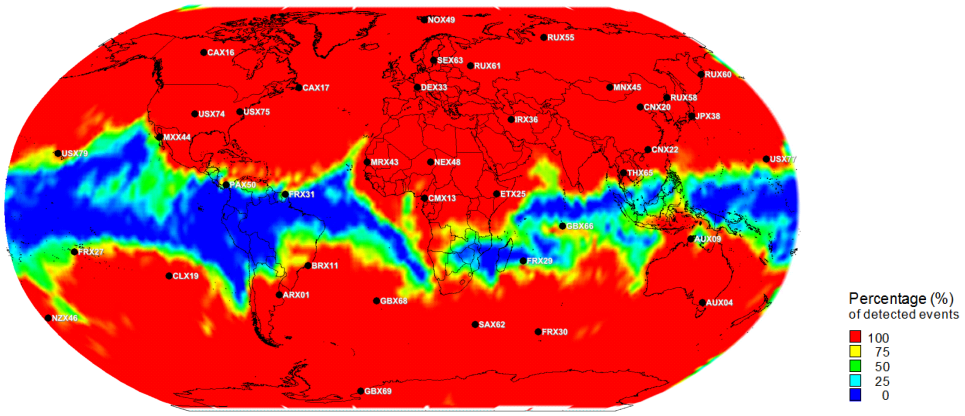

(b) Lowered network coverage during 26-30 March, 2010.

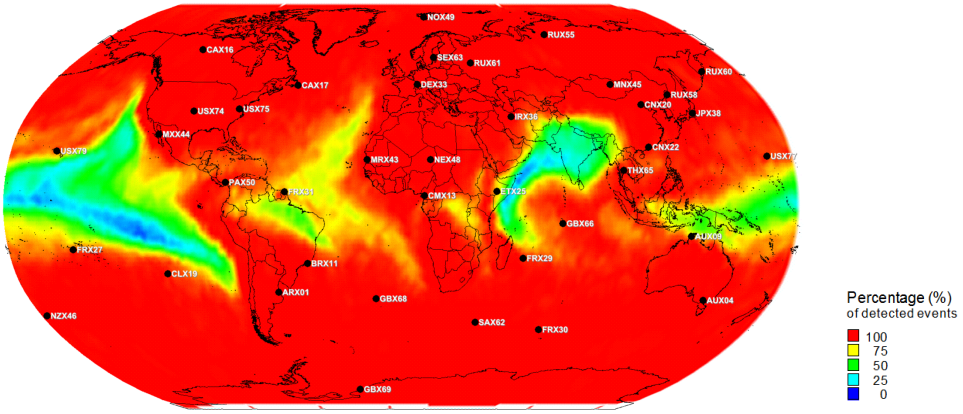

(c) Heightened network coverage during June-August, 2010.

Figure 6.3: Spatial dependence of network coverage during selected time periods. During June-August the network coverage of surface nuclear explosions without background is heightened, see Figure 6.2. When compared to Figure 6.1a, it is due to a partly reduced ITCZ.

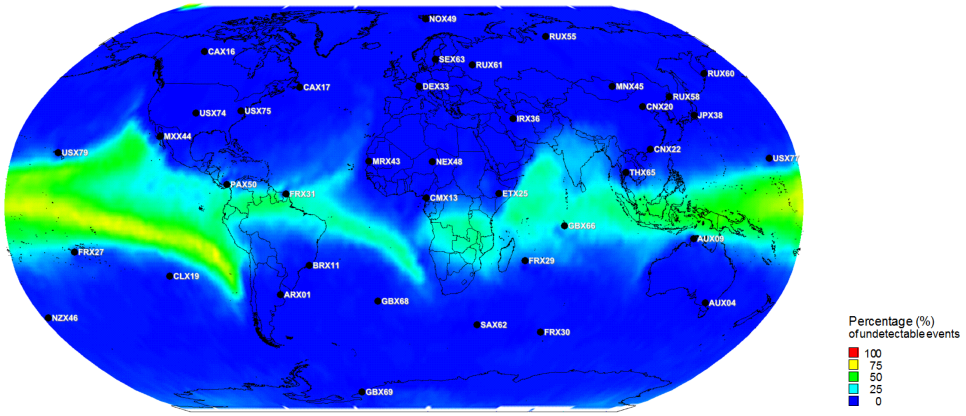

Figure 6.4: Probability distribution of non-detectable events, whose emissions do not reach the IMS noble gas component. The spatial distribution is very similar to the scenario shown in Figure 6.1a, where also the meteorological patterns surrounding the equator are mostly responsible for the characteristics.

In cases of (1.) the emission strength and/or the leakage of radioxenon versus the legitimate background is the main factor in determining whether the event can be detected or not. In cases of (2.) the simulations predict that the radioxenon emissions of the event will stay undetected in any case within the simulation time of two weeks, i.e. they are non-detectable independent of their emission strength.

For every grid point, for which explosions have been simulated, the number of non-detections due to (2.) are counted for the whole time period. Scaled to the total number of simulated events per grid point, the percentage of non-detectable events is calculated for each grid point. This results in a total percentage of non-detectable events of 13.2%. Naturally, this value is identical for all three of the presented scenarios. The global distribution is plotted in Figure 6.4, where it is observed that the spatial distribution is very similar to that of the basic, surface explosion scenario presented as seen in Figure 6.1a. Taking into account the total network coverage for the surface scenario of 85.8% and the share of non-detectable events of 13.2%, only 1% of the above-surface events did not evoke a detection due to the emission strength being too small. The analogue calculation for subsurface events without background results in a share of 8.9% of events that are in principle detectable by today's network (10.4% for subsurface events with additional background). In these cases one or a combination of the following factors prevent a detection: too low emission strength, too high atmospheric dilution and/or too high detection criteria.

The global impact of the legitimate radioxenon background seems rather small, but on a regional scale it can have significant effects as seen when comparing Figures 6.1b and 6.1c. However, the presented approach treats by definition all grid points equally, including points above sea. In a CTBT scenario of a clandestine (or faked) nuclear test, one might be more interested in land-based (and especially underground), hypothetical nuclear explosions.

Table 6.1: Network coverage η and shares of non-detections for global, land-based and sea-based events. Non-detectable events have emissions that do not reach an IMS noble gas station within 14 days. The remaining share denotes events, for which a simulated concentration reaches at least one IMS noble gas station, but do not fulfil the detection criteria, i.e. the concentration is too low.

	Scenario:	Surface	Subsurface	w/ Background
total	Netw. cov. η	**85.8%**	**77.9%**	**76.4%**
	Non-detectable (const.)	13.2%	13.2%	13.2%
	Remaining	1.0%	8.9%	10.4%
land	Netw. cov. η	**91.1%**	**64.4%**	**60.2%**
	Non-detectable (const.)	5.9%	5.9%	5.9%
	Remaining	3.0%	29.7%	33.9%
sea	Netw. cov. η	**83.5%**	**83.5%**	**83.0%**
	Non-detectable (const.)	16.2%	16.2%	16.2%
	Remaining	0.3%	0.3%	0.8%

6.5.3 Landmass Coverage

As seen in Figures 6.1a and 6.4 the events on sea-based grid points in all scenarios tend to have either a very high detectability (due to the high emissions) or they are non-detectable (independent of the emission strength). The differences of η in the three described scenarios are caused rather by a changing detectability of land-based events.

If, for example, assuming a scenario with a secretly conducted nuclear test, it is more likely that this event will be underground. Therefore, it can be a reasonable consideration to handle the land-based network coverage separated from the total network coverage. In this case the network coverages of the three scenarios are shifting from the previous values:

$$\begin{aligned} \eta_{atmo,land} &= 91.1\% \ (\nearrow)\,, \\ \eta_{subs,land} &= 64.4\% \ (\searrow)\,, \\ \eta_{back,land} &= 60.2\% \ (\searrow)\,. \end{aligned} \tag{6.14}$$

For the surface-event scenario without background the land-mass network coverage is 5.3% higher than the total network coverage. This is caused by the fact that the global distribution of non-detectable events is mainly found on the Pacific Ocean, i.e. on grid points above sea, and that the emissions of the land-based events are in most cases strong enough to be detected. When moving to the scenario of underground events (again without background) the network coverage is 13.5% less than for land- and sea-based events combined. This means that the land-based network coverage is sensitive to the assumed emission (or: leakage thereof) of underground tests. Also the coverage for the background scenario is smaller by 16.2% when compared to the global value, indicating

that land-based events are more impacted by the radioxenon background than sea-based events. This is plausible as also the considered emitters of the radioxenon background are found on land.

Table 6.1 gives a comprehensive overview over how the network coverage behaves for the three different scenarios and how for land- and sea-based events. Additional to the network coverage η also the share of non-detectable and not-detected events are listed. For land-based events the percentage of non-detectable events is reduced to 5.9%. According to Figure 6.4 these events are also located in equatorial regions and are results of the typical meteorological patterns. The remaining share of events that have not been detected is due to the fact that the concentrations that arrive at the receptor have not been identified as unusually high. This share of not-detected events clearly rises to about 30% for both subsurface scenarios. This leads to a network coverage of 60.2% for the scenario of subsurface explosions and existing background. The network coverage for sea-based events remains almost constant and shows only a low dependence on the radioxenon background.

The major part of the not detected, land-based events are found in equatorial regions of South America, Africa and India, as seen when following the development from Figure 6.1a to 6.1c. For the subsurface-with-background scenario these regions are tending to have a detection capability of 25% or even significantly below. Large parts of the landmasses of North America are affected by a less significant, but more uniformly and more evenly distributed loss in the detection capability, most likely due to the high number of radioxenon emitters.

The share of non-detectable events and its spatial distribution can only be counteracted with additional IMS noble gas stations. Additional stations would decrease the average distance between CTBT-relevant events and noble gas stations, and therefore also decrease the dilution factor. This would increase the relative impact of such events on the legitimate radioxenon concentration at noble gas stations. On the other hand, the detection probability for events that affected the IMS network, but are not detected due to non-fulfilled detection criteria, can be potentially improved by additional noble gas stations, a sophisticated categorisation scheme (to decide whether or not a sample signifies a detection), and a reduction of the legitimate radioxenon background.

Chapter 7
Conclusion

7.1 Summary

The modelling of atmospheric transport and particle dispersion to calculate large number of SRS fields has become more practical due to the improvements in computation power during the last decade, the high-resolution meteorological data and the accordant storage capabilities. In particular the role of ATM in the monitoring of nuclear explosions still offers many opportunities for research. Radioxenon in particular plays an important role in the detection of nuclear explosions and due to its inert character especially of underground nuclear explosions.

The prediction of concentrations at IMS stations relies mainly on the used atmospheric transport model and the radioxenon emission inventory including legitimate sources. When characterising the worldwide background the simulations produce different kind of distributions for each station. The calculation of the standard deviation is determined by kind of distribution. Only for stations in regions with high densities of NPPs or in vicinity of IPFs the standard deviations is above the MDC. In the comparison with experimental data, it became clear that for certain stations the background is be well predicted, while for other stations it is partly or even clearly under-predicted. The general underestimation of radioxenon concentrations shows a clear regional dependence when comparing the simulated data with experimental detections. Especially stations in Asia and a few stations in remote locations in the southern hemisphere are subject to under-prediction. This regional-dependent seems most likely to be due to an under-prediction of the radioxenon emission inventory. Regionally dominant emitters of radioxenon, such as IPFs, are main contributors to the global radioxenon background. It has been shown that the availability of radioxenon emission data in a daily resolution can significantly improve the prediction capability of ATM. This is the case not only for nearby stations, but in this study also has been shown valid for a station in a medium range of 3,300 km.

Using the Fukushima nuclear accident it has been exemplarily demonstrated that it is possible to reconstruct information about unknown source terms with known locations. The reconstructions from different isotopes and different stations show some similarities; the differences can be attributed to ATM uncertainties.

Besides in these methods for characterising the radioxenon background, ATM also has potential usage in categorisation of radioxenon concentrations. Simulations for emissions from the NTS have shown that categorisation solely based on absolute thresholds may even miss a relatively close 1 kt nuclear test with a 1% leakage. However, ATM-based methods for categorisation, in particular with regard to the sample composition, showed potential for further usage.

As an important design parameter of the IMS noble gas component design the network coverage has been determined by ATM in an unbiased way and conservative scenarios. The aspired global network coverage of 90% is only achieved for land-based, atmospheric 1 kt nuclear tests. For scenarios with underground, contained nuclear tests of 1% leakage, the network coverage drops to about 76%. Restricted to land-based, underground events the network coverage even reaches about 60%. The main reasons for this decrease have been identified as non-detectable events due to meteorological patterns and as low emissions due to small leakage. Overall the radioxenon background from legitimate sources has only a minor impact, but resulted in a significant decrease on regional scales.

Not only in the research on the network coverage, but also in the work on the opportunities for categorisation, it became clear that the emissions (or the leakage thereof) is the most decisive factor for the detectability of nuclear explosions. Especially when the ^{133}Xe emissions are in the order of 10^{14} Bq, corresponding to a 1% leakage of a 1 kt nuclear test, the existing radioxenon background can prevent detections; according to the simulations this is most likely the case for North America and Europe. However, the comparison of simulated and experimental data has shown that the used emission inventory may be underestimated e.g. for Asia. For higher emissions from nuclear tests, may it be due to higher explosion yields or higher leakage, the detection probability clearly increases in regions that are not affected by the presented equatorial, meteorological patterns. In any case the network coverage offers an unbiased opportunity to validate the capability to detect nuclear explosions and the impact of alternative scenarios.

7.2 Recommendations

Further research on the characterisation of the radioxenon background should include the simulation of longer time series in order to improve the statistics and determinations of station-specific distributions. A comparison of longer time series with experimental data could lead to a better understanding of the regional dependence of the radioxenon emission inventory and thus indirectly lead to an improved inventory. Also, more radioxenon isotopes could be included, although ^{133}Xe is the most promising candidate for detecting a CTBT-relevant event.

More exemplarily studies on the positive impact of available emission data from regionally dominant radioxenon emitters would improve the ATM-based prediction quality in North America and Europe. Promising candidates for such studies are IRE in Belgium and CRL in Canada. Besides, positive results in this area could be used as an argument to convince IPF operators of a more open data policy with regard to their radioxenon emissions. Since it is a difficult physical and legislative process to change the

procedures within existing IPFs, it is especially important for new competitors in this field.

The field of categorisation can benefit significantly from more research including methods of ATM. It can help to test the efficiency of existing schemes, e.g. to optimise the rates of false-positve and false-negative outcomes, by simulating the impact of hypothetical nuclear explosions. If possible, newly developed categorisation schemes should be station-specific as the time series of each station follows an own distribution. New suggestions have been made for categorisation that is not based on integer values, but that includes floating numbers to give a joint validation of the sample on a fuzzy scale. When normalised, multiple floating numbers could be easily combined with each other to give an integrated validation of a sample in one number, e.g. by multiplying them. A set of such floating numbers could include the absolute concentration in relation to the station-specific distribution or with regard to the sample's composition, different radioxenon isotopes and/or the the isotopic activity ratios. Advances in this direction could also be validated with ATM-based methods.

The results from the simulations on the network coverage have implications for future research and the design of the IMS noble gas component. The negative impact from the radioxenon background on the network coverage suggests that still research and efforts should be put into the further understanding and reduction of radioxenon emissions. A better knowledge of the radioxenon emissions would lead to better predictions of IMS detections, which would lead to an improved allocation of detection criteria, which in return would improve the determination of the network coverage.

In order to improve the network coverage itself two direct possibilities can be pursued in parallel. On the one hand the reduction of the background would improve the network coverage, though only in certain regions of the world with a significant density of emissions. However, as desirable a reduction of the background is, it cannot be pursued scientifically, but rather by the operators and national, political guidelines. On the other hand, the large percentage of non-detectable events can only be overcome by increasing the number of noble gas stations. Future research could determine the network coverage in dependence of the number and location of additional stations, e.g. how η would improve if all or some of the remaining 40 radionuclide stations without noble gas systems would be equipped with such.

Beside these direct ways there is an indirect way to improve the network coverage. In the presented approach a simple detection criteria is applied to distinguish between detections and non-detections. A more sophisticated detection criteria, which could also be used in context with a categorisation scheme, could lead to better detection rates of hypothetical explosions. In reverse this could be used to validate a new categorisation scheme by their increase of the network coverage.

Summarising, the detection probability can be potentially improved by

1. additional noble gas stations,
2. a sophisticated categorisation scheme, and
3. a reduction of the legitimate radioxenon background.

For approach (1.) and assuming a CTBT-related scenario, where an underground nuclear test has to be proven or disproven, additional stations are recommended to aim for covering more certain landmasses as shown in Figure 6.1c, i.e. Australia, India and North America, and landmasses in equatorial regions, i.e. Africa and South America. An expansion of the IMS noble gas component like suggested here, would not be driven by issues of international relations, but by the goal to maximise the uniformity of the global network coverage.

In the case of (2.) a more sophisticated categorisation scheme could lead to a better detection criteria of whether a sample is categorised as a detection or not. Beside existing categorisation mechanisms such a scheme should include a time series analysis and ATM in one form or another.

Any efforts in (3.) may rely on and supported by further scientific research, but the implementation of such measures is subject to political will, policy making and (inter)national regulations.

If further details on the legitimate emissions of other radioxenon isotopes except ^{133}Xe are provided, especially by IPF operators, it would also allow to calculate the network coverage for these isotopes. The presented approach to determine the network coverage can be used in the future to validate the impact of various parameters on the detection capability of the noble gas component, e.g. from IMS design parameters to different scenarios for the radioxenon background or leakage from nuclear tests.

Appendices

A - The Radionuclide Component of the International Monitoring System

Once completed the IMS radionuclide component will consist of 80 stations around the world of which 40 will be equipped with noble gas detection systems. In the following the radionuclide component is presented with Station ID, geographical latitude and longitude, location (closest city or landmark) and focus on the included noble gas component.

Station ID	Lat	Lon	Location	Noble gas system	Sampling time	Status
ARX01	-34.5	-58.5	Buenos Aires	ARIX	12h	testing
ARP02	-24.0	-65.0	Salta			
ARP03	-41.1	-71.3	S.Carlos deBariloche			
AUX04	-37.7	145.1	Melbourne	SAUNA	12h	testing
AUP05	-67.6	62.5	Mawson			
AUP06	-19.3	146.8	Townsville			
AUP07	-54.0	159.0	MacQuarie Island			
AUP08	-12.2	96.8	Cocos Islands			
AUX09	-12.4	130.9	Darwin	SAUNA	12h	testing
AUP10	-32.0	116.0	Perth			
BRX11	-23.0	-43.4	Rio de Janeiro	SAUNA	12h	certified
BRP12	-8.0	-35.0	Recife			
CMX13	3.8	10.2	Douala	SPALAX	24h	testing
CAP14	49.3	-123.2	Vancouver			
CAP15	74.7	-94.9	Resolute			
CAX16	62.5	-114.5	Yellowknife	SPALAX	24h	testing
CAX17	47.6	-52.7	St. John's	SPALAX	24h	testing
CLP18	-53.1	-70.9	Punta Arenas			
CLX19	-27.1	-108.4	Hanga Roa	SAUNA	12h	testing
CNX20	39.8	116.2	Beijing	SPALAX	24h	testing
CNP21	35.8	103.3	Lanzhou			
CNX22	23.0	113.3	Guangzhou	SAUNA	12h	testing
CKP23	-21.2	-159.8	Rarotonga			
RNP24	-1.0	-89.2	S.Cristobal Island			
ETX25	5.5	42.7	Addis Ababa	tbd		planned
FJP26	-17.8	177.4	Nandi			
FRX27	-17.6	-149.6	Papeete	SPALAX	24h	testing

Station ID	Lat	Lon	Location	Noble gas system	Sampling time	Status
FRP28	17.0	-62.0	Pointe-a-Pitre			
FRX29	-21.1	55.6	St. Denis	SPALAX	24h	certified
FRX30	-49.4	70.3	Port-aux-Francais	SPALAX	24h	planned
FRX31	5.2	-52.7	Cayenne	SPALAX	24h	certified
FRP32	-66.0	140.0	Dumont d'Urville			
DEX33	47.9	7.9	Schauinsland	SPALAX	24h	testing
ISP34	64.1	-21.8	Reykjavik			
RNX35	tbd	tbd	India	tbd		
IRX36	35.0	52.0	Tehran	tbd		planned
JPP37	27.9	126.5	Okinawa			
JPX38	36.3	139.0	Gunma	SAUNA	12h	testing
KIP39	2.0	-157.4	Kiritimati			
KWP40	29.3	47.9	Kuwait City			
RNP41	32.5	15.0	Misratah			
MYP42	4.5	101.4	Kuala Lumpur			
MRX43	18.1	-15.9	Nouakchott	SPALAX	24h	planned
MXX44	28.0	-113.0	Baja California	SAUNA	12h	testing
MNX45	47.9	106.3	Ulan-Bator	SPALAX	24h	testing
NZX46	-43.8	-176.5	Chatham Island	SAUNA	12h	testing
NZP47	-35.1	173.3	Kaitaia			
NEX48	18.0	13.0	Bilma	tbd		planned
NOX49	78.2	15.4	Spitsbergen	SAUNA	12h	testing
PAX50	9.0	-79.5	Panama City	SPALAX	24h	testing
PGP51	-2.6	150.8	New Hanover			
PHP52	14.6	121.4	Quezon City			
RNP53	37.4	-25.4	Ponta Delgada			
RUP54	58.6	49.4	Kirov			
RUX55	69.4	88.1	Norilsk	ARIX	12h	planned
RUP56	59.6	112.6	Peleduy			
RUP57	68.0	166.4	Bilibino			
RUX58	43.7	131.9	Ussuriysk	ARIX	12h	testing
RUP59	53.9	84.8	Zalesovo			
RUX60	53.1	158.8	Petropavlovsk	ARIX	12h	planned
RUX61	56.7	37.3	Dubna	ARIX	12h	testing
SAX62	-46.5	37.0	Marion Islands	tbd		planned
SEX63	59.2	17.6	Stockholm	SAUNA	12h	testing
TZP64	-6.8	39.2	Dar es Salaam			
THX65	13.8	100.5	Bangkok	SPALAX	24h	planned
GBX66	-7.3	72.4	Diego Garcia	SAUNA	12h	certified
GBP67	-15.9	-5.7	St. Helena			
GBX68	-37.0	-12.3	Tristan Da Cunha	SAUNA	12h	certified
GBX69	-76.0	-28.0	Halley	tbd		planned

Station ID	Lat	Lon	Location	Noble gas system	Sampling time	Status
USP70	38.7	-121.4	Sacramento			
USP71	55.3	-160.5	Sand Point			
USP72	28.3	-80.6	Melbourne, FL			
USP73	-64.8	-64.1	Palmer Station			
USX74	37.2	-99.8	Ashland	SAUNA	12h	certified
USX75	38.0	-78.4	Charlottesville	SAUNA	12h	certified
USP76	64.7	-147.1	Salchaket			
USX77	19.3	166.6	Wake Island	SAUNA	12h	testing
USP78	28.2	-177.4	Midway Island			
USX79	21.5	-158.0	Oahu	SAUNA	12h	certified
USP80	13.6	144.9	Guam			

B - Radioxenon Emission Inventory

All of the following emissions are given in GBq/a; all coordinates have been allocated to the nearest point on a 1°x1° latitude-longitude grid.

At the time of the simulations the ^{133}Xe emissions of five Isotope Production Facilities were quantified. The following emission values have been gathered at the Workshop on Signatures of Medical and Industrial Isotope Production (WOSMIP) in June 2011. The radioxenon emissions from Isotope Production Facilities are:

Country	Site Name	Lat	Lon	^{133}Xe
Australia	ANSTO (Sydney)	-34.0	151.0	5.00E+05
Belgium	IRE (Fleurus)	50.0	4.0	1.00E+06
Canada	CRL (Chalkriver)	46.0	-77.0	1.00E+07
Netherlands	NRG (Petten)	53.0	5.0	7.30E+02
South Africa	NECSA(Pelindaba)	-25.0	27.0	4.00E+06

The radioxenon emissions from Nuclear Power Plants are [Kal09]:

Country	Site Name	Lat	Lon	^{131m}Xe	^{133m}Xe	^{133}Xe	^{135}Xe
Argentina	Atucha	-34.0	-59.0	1.09E+02	3.42E+01	1.24E+03	8.97E+02
	Embalse	-32.0	-64.0	1.09E+02	3.42E+01	1.24E+03	8.97E+02
Armenia	Armenia	40.0	44.0	1.09E+02	3.42E+01	1.24E+03	8.97E+02
Belgium	Doel	51.0	4.0	4.36E+02	1.37E+02	4.97E+03	3.59E+03
	Tihange	50.0	5.0	3.27E+02	1.03E+02	3.72E+03	2.69E+03
Brazil	Angra	-23.0	-44.0	2.18E+02	6.84E+01	2.48E+03	1.79E+03
Bulgaria	Kozloduy	43.0	23.0	2.18E+02	6.84E+01	2.48E+03	1.79E+03
Canada	Bruce	44.0	-81.0	6.54E+02	2.05E+02	7.45E+03	5.38E+03

Country	Site Name	Lat	Lon	^{131m}Xe	^{133m}Xe	^{133}Xe	^{135}Xe
	Darlington	43.0	-78.0	4.36E+02	1.37E+02	4.97E+03	3.59E+03
	Gentilly	46.0	-72.0	1.09E+02	3.42E+01	1.24E+03	8.97E+02
	Pickering	43.0	-79.0	6.54E+02	2.05E+02	7.45E+03	5.38E+03
	Point Lepreau	45.0	-66.0	1.85E+01	0.00E+00	3.50E+03	1.38E+03
China	Guangdong	22.0	114.0	2.18E+02	6.84E+01	2.48E+03	1.79E+03
	Lingdao	19.0	109.0	2.18E+02	6.84E+01	2.48E+03	1.79E+03
	Qinshan	30.0	120.0	5.45E+02	1.71E+02	6.21E+03	4.49E+03
	Tianwan	59.0	99.0	0.00E+00	0.00E+00	4.56E+03	0.00E+00
Czech Rep.	Dukovany	49.0	16.0	4.36E+02	1.37E+02	4.97E+03	3.59E+03
	Temelin	49.0	14.0	2.18E+02	6.84E+01	2.48E+03	1.79E+03
Finland	Loviisa	60.0	26.0	0.00E+00	0.00E+00	2.22E+02	7.78E+01
	Olkiluoto	61.0	21.0	0.00E+00	3.02E+01	1.65E+03	1.84E+02
France	Belleville	47.0	2.0	3.75E-01	4.64E-01	7.11E+02	3.49E+02
	Blayais	45.0	0.0	2.21E-01	0.00E+00	9.98E+02	4.88E+02
	Bugey	45.0	5.0	4.82E+02	1.35E-02	4.33E+02	3.21E+02
	Cattenom	49.0	6.0	3.66E+01	7.52E-02	1.76E+03	2.86E+02
	Chinon	47.0	0.0	4.47E-02	1.60E-02	4.84E+02	3.37E+02
	Chooz	50.0	4.0	2.89E+00	1.16E-01	7.64E+02	3.58E+02
	Civaux	46.0	0.0	5.89E-01	0.00E+00	3.74E+02	1.88E+02
	Cruas	44.0	4.0	1.45E+01	3.82E+00	6.63E+03	1.18E+03
	Dampierre	47.0	2.0	2.63E+01	3.75E+00	2.57E+03	4.70E+02
	Fessenheim	47.0	7.0	3.11E-02	0.00E+00	1.98E+02	1.18E+02
	Flamanville	49.0	-1.0	5.17E+00	0.00E+00	5.75E+02	4.31E+02
	Golfech	44.0	0.0	1.93E+00	1.87E-03	2.22E+02	9.41E+01
	Gravelines	51.0	2.0	1.21E+00	0.00E+00	2.50E+03	1.01E+03
	Nogent	48.0	3.0	2.26E+02	2.21E+02	2.12E+03	5.09E+02
	Paluel	49.0	0.0	5.32E+00	7.91E-02	1.18E+03	1.97E+02
	Penly	49.0	1.0	3.20E+00	0.00E+00	5.00E+02	2.61E+03
	Phenix	44.0	4.0	1.09E+02	3.42E+01	1.24E+03	8.97E+02
	St. Alban	45.0	4.0	3.57E+00	1.01E-02	1.33E+03	4.04E+02
	St. Laurent	47.0	1.0	3.39E+02	0.00E+00	1.69E+02	7.41E+01
	Tricastin	44.0	4.0	5.32E+01	0.00E+00	5.59E+03	1.41E+03
Germany	Biblis	49.0	8.0	8.19E+01	1.11E+01	7.59E+02	1.25E+02
	Brokdorf	53.0	9.0	1.37E+02	1.76E+01	6.10E+02	9.37E+01
	Brunsbuettel	53.0	9.0	5.06E+01	1.85E+01	2.30E+02	1.57E+03
	Emsland	52.0	7.0	3.50E+02	1.40E+01	1.70E+01	1.01E+00
	Grafenrheinfeld	49.0	10.0	1.56E+02	8.05E-01	4.58E+01	2.33E+00
	Grohnde	52.0	9.0	3.90E+01	9.82E+00	3.34E+02	9.61E+01
	Gundremmingen	48.0	10.0	7.67E+01	1.17E+00	1.80E+01	9.59E+00
	Isar	48.0	12.0	4.58E+01	5.87E-01	1.73E+01	9.03E+00
	Kruemmel	53.0	10.0	4.65E+00	6.40E+00	2.97E+02	4.88E+02
	Neckarwestheim	49.0	9.0	2.85E+01	3.76E+00	9.44E+01	5.63E+01
	Philippsburg	49.0	8.0	2.69E+01	2.92E+01	5.52E+02	3.91E+02

Country	Site Name	Lat	Lon	^{131m}Xe	^{133m}Xe	^{133}Xe	^{135}Xe
	Unterweser	53.0	8.0	3.13E+02	1.55E+01	1.54E+03	2.41E+02
Hungary	Paks	46.0	18.0	4.36E+02	1.37E+02	4.97E+03	3.59E+03
India	Fbtr	28.0	77.0	0.00E+00	0.00E+00	0.00E+00	0.00E+00
	Kaiga	14.0	74.0	3.27E+02	1.03E+02	3.72E+03	2.69E+03
	Kakrapar	21.0	73.0	2.18E+02	6.84E+01	2.48E+03	1.79E+03
	Koodankulam	8.0	77.0	0.00E+00	0.00E+00	0.00E+00	0.00E+00
	Madras	12.0	80.0	2.18E+02	6.84E+01	2.48E+03	1.79E+03
	Narora	28.0	78.0	2.18E+02	6.84E+01	2.48E+03	1.79E+03
	Rajasthan	24.0	75.0	4.36E+02	1.37E+02	4.97E+03	3.59E+03
	Tarapur	19.0	72.0	4.36E+02	1.37E+02	4.97E+03	3.59E+03
Japan	Fukushima 1	37.0	141.0	6.54E+02	2.05E+02	7.45E+03	5.38E+03
	Fukushima 2	37.0	141.0	4.36E+02	1.37E+02	4.97E+03	3.59E+03
	Genkai	33.0	129.0	4.36E+02	1.37E+02	4.97E+03	3.59E+03
	Hamaoka	34.0	138.0	5.45E+02	1.71E+02	6.21E+03	4.49E+03
	Higashidori	41.0	141.0	1.09E+02	3.42E+01	1.24E+03	8.97E+02
	Ikata	38.0	141.0	3.27E+02	1.03E+02	3.72E+03	2.69E+03
	Kashiwazaki	37.0	138.0	7.63E+02	2.40E+02	8.69E+03	6.28E+03
	Mihama	35.0	135.0	3.27E+02	1.03E+02	3.72E+03	2.69E+03
	Monju	35.0	136.0	1.09E+02	3.42E+01	1.24E+03	8.97E+02
	Ohi	35.0	135.0	4.36E+02	1.37E+02	4.97E+03	3.59E+03
	Onagawa	38.0	141.0	3.27E+02	1.03E+02	3.72E+03	2.69E+03
	Sendai	31.0	130.0	2.18E+02	6.84E+01	2.48E+03	1.79E+03
	Shika	37.0	136.0	2.18E+02	6.84E+01	2.48E+03	1.79E+03
	Shimane	35.0	133.0	2.18E+02	6.84E+01	2.48E+03	1.79E+03
	Takahama	35.0	135.0	4.36E+02	1.37E+02	4.97E+03	3.59E+03
	Tokai	36.0	140.0	1.09E+02	3.42E+01	1.24E+03	8.97E+02
	Tomari	43.0	140.0	2.18E+02	6.84E+01	2.48E+03	1.79E+03
	Tsuruga	35.0	136.0	2.18E+02	6.84E+01	2.48E+03	1.79E+03
Korea	Kori	35.0	129.0	4.36E+02	1.37E+02	4.97E+03	3.59E+03
	Ulchin	37.0	129.0	6.54E+02	2.05E+02	7.45E+03	5.38E+03
	Wolsong	35.0	129.0	4.36E+02	1.37E+02	4.97E+03	3.59E+03
	Yonggwang	35.0	126.0	6.54E+02	2.05E+02	7.45E+03	5.38E+03
Lithuania	Ignalina	55.0	26.0	1.09E+02	3.42E+01	1.24E+03	8.97E+02
Mexico	Laguna Verde	19.0	-96.0	2.18E+02	6.84E+01	2.48E+03	1.79E+03
Netherlands	Borssele	51.0	3.0	1.09E+02	3.42E+01	1.24E+03	8.97E+02
Pakistan	Chasnupp	32.0	71.0	1.09E+02	3.42E+01	1.24E+03	8.97E+02
	Kanupp	24.0	66.0	1.09E+02	3.42E+01	1.24E+03	8.97E+02
Romania	Cernavoda	44.0	28.0	2.18E+02	6.84E+01	2.48E+03	1.79E+03
Russia	Balakovo	51.0	47.0	4.36E+02	1.37E+02	4.97E+03	3.59E+03
	Beloyarsky	56.0	61.0	1.09E+02	3.42E+01	1.24E+03	8.97E+02
	Bilibino	68.0	166.0	4.36E+02	1.37E+02	4.97E+03	3.59E+03
	Kalinin	57.0	35.0	3.27E+02	1.03E+02	3.72E+03	2.69E+03
	Kola	67.0	32.0	4.36E+02	1.37E+02	4.97E+03	3.59E+03

Country	Site Name	Lat	Lon	^{131m}Xe	^{133m}Xe	^{133}Xe	^{135}Xe
	Kursk	51.0	35.0	4.36E+02	1.37E+02	4.97E+03	3.59E+03
	Leningrad	59.0	29.0	4.36E+02	1.37E+02	4.97E+03	3.59E+03
	Novovoronezh	51.0	39.0	3.27E+02	1.03E+02	3.72E+03	2.69E+03
	Smolensk	54.0	33.0	3.27E+02	1.03E+02	3.72E+03	2.69E+03
	Volgodonsk	47.0	42.0	1.09E+02	3.42E+01	1.24E+03	8.97E+02
Slovak Rep.	Bohunice	48.0	17.0	3.27E+02	1.03E+02	3.72E+03	2.69E+03
	Mochovce	48.0	18.0	2.18E+02	6.84E+01	2.48E+03	1.79E+03
Slovenia	Krsko	45.0	15.0	1.09E+02	3.42E+01	1.24E+03	8.97E+02
South Africa	Koeberg	-33.0	18.0	2.18E+02	6.84E+01	2.48E+03	1.79E+03
Spain	Almaraz	39.0	-5.0	1.12E+01	7.89E+00	1.95E+03	4.81E+01
	Asco	41.0	0.0	3.28E+00	5.88E-01	3.89E+03	9.43E+01
	Cofrentes	39.0	-1.0	6.59E-01	5.71E+00	7.97E+02	4.44E+03
	Jose Cabrera	40.0	-2.0	0.00E+00	0.00E+00	0.00E+00	0.00E+00
	S.MariaDeGarona	42.0	-3.0	0.00E+00	0.00E+00	7.29E+01	4.14E+01
	Trillo	40.0	-2.0	0.00E+00	9.43E+00	2.46E+01	1.74E+01
	Vandellos	40.0	0.0	0.00E+00	0.00E+00	2.08E+02	2.75E+01
Sweden	Forsmark	60.0	18.0	8.52E+02	6.31E+01	8.69E+03	2.05E+03
	Oskarshamn	57.0	16.0	4.90E+02	3.69E+02	1.22E+04	5.01E+04
	Ringhals	57.0	12.0	5.38E+02	1.43E+02	1.52E+04	1.77E+05
Switzerland	Beznau	47.0	8.0	0.00E+00	0.00E+00	1.62E+03	2.05E+03
	Goesgen	47.0	7.0	0.00E+00	0.00E+00	2.69E+03	4.40E+02
	Leibstadt	47.0	8.0	0.00E+00	0.00E+00	8.47E+02	1.27E+03
	Muehleberg	46.0	7.0	5.98E+01	0.00E+00	2.11E+02	3.91E+01
Taiwan	Chin Shan	25.0	121.0	2.18E+02	6.84E+01	2.48E+03	1.79E+03
	Kuosheng	25.0	121.0	2.18E+02	6.84E+01	2.48E+03	1.79E+03
	Maanshan	21.0	120.0	2.18E+02	6.84E+01	2.48E+03	1.79E+03
Ukraine	Chernobyl	51.0	30.0	0.00E+00	0.00E+00	0.00E+00	0.00E+00
	Khmelnitski	50.0	26.0	2.18E+02	6.84E+01	2.48E+03	1.79E+03
	Rovno	51.0	25.0	4.36E+02	1.37E+02	4.97E+03	3.59E+03
	South Ukraine	47.0	31.0	3.27E+02	1.03E+02	3.72E+03	2.69E+03
	Zaporozhe	47.0	34.0	6.54E+02	2.05E+02	7.45E+03	5.38E+03
U.K.	Dungeness	50.0	0.0	2.18E+02	6.84E+01	2.48E+03	1.79E+03
	Hartlepool	54.0	-1.0	2.18E+02	6.84E+01	2.48E+03	1.79E+03
	Heysham	54.0	-2.0	4.36E+02	1.37E+02	4.97E+03	3.59E+03
	Hinkley Point	51.0	-3.0	2.18E+02	6.84E+01	2.48E+03	1.79E+03
	Hunterston	55.0	-4.0	2.18E+02	6.84E+01	2.48E+03	1.79E+03
	Oldbury	51.0	-2.0	2.18E+02	6.84E+01	2.48E+03	1.79E+03
	Sizewell	52.0	1.0	1.09E+02	3.42E+01	1.24E+03	8.97E+02
	Torness	55.0	-2.0	2.18E+02	6.84E+01	2.48E+03	1.79E+03
	Wylfa	53.0	-4.0	2.18E+02	6.84E+01	2.48E+03	1.79E+03
U.S.A.	Arkansas One	35.0	-93.0	0.00E+00	0.00E+00	0.00E+00	0.00E+00
	Beaver Valley	40.0	-80.0	7.40E+00	1.09E+00	2.73E+02	4.55E+01
	Braidwood	41.0	-88.0	0.00E+00	0.00E+00	4.10E+02	0.00E+00

Country	Site Name	Lat	Lon	^{131m}Xe	^{133m}Xe	^{133}Xe	^{135}Xe
	Browns Ferry	34.0	-87.0	0.00E+00	0.00E+00	5.64E+02	3.01E+00
	Brunswick	33.0	-78.0	0.00E+00	1.24E+00	2.22E+03	2.07E+03
	Byron	42.0	-89.0	0.00E+00	0.00E+00	3.28E+01	6.50E-03
	Callaway	38.0	-91.0	1.07E+02	2.27E+01	2.52E+03	9.08E+01
	Calvert Cliffs	38.0	-76.0	1.58E+01	1.65E+01	2.86E+03	1.80E+02
	Catawba	35.0	-81.0	0.00E+00	2.52E+00	2.13E+03	2.14E+01
	Clinton	40.0	-88.0	0.00E+00	0.00E+00	8.58E+00	1.98E+02
	Columbia	46.0	-119.0	1.09E+02	3.42E+01	1.24E+03	8.97E+02
	Comanche Peak	32.0	-97.0	1.51E+02	0.00E+00	5.50E+03	3.88E+02
	Cooper	40.0	-95.0	3.66E+00	1.69E+01	6.88E+02	9.13E+01
	Crystal River	28.0	-82.0	1.55E+02	3.64E+01	8.82E+02	4.77E+01
	Davis Besse	41.0	-83.0	1.95E-05	5.41E-01	1.24E+03	2.84E+01
	Diablo Canyon	35.0	-120.0	2.28E+00	1.76E+00	5.62E+02	3.99E+00
	Donald Cook	41.0	-86.0	0.00E+00	0.00E+00	1.39E+03	0.00E+00
	Dresden	41.0	-88.0	1.52E+00	3.09E-01	8.86E+02	2.03E+03
	Duane Arnold	42.0	-91.0	0.00E+00	0.00E+00	2.47E+02	4.47E+02
	Enrico Fermi	41.0	-83.0	0.00E+00	0.00E+00	0.00E+00	5.98E+02
	Farley	31.0	-85.0	0.00E+00	0.00E+00	4.94E+02	5.93E+01
	Fitzpatrick	43.0	-76.0	0.00E+00	0.00E+00	2.28E+01	7.22E+01
	Fort Calhoun	41.0	-96.0	2.87E+02	1.76E+02	1.75E+03	5.56E+01
	Grand Gulf	32.0	-91.0	0.00E+00	2.21E+00	5.84E+02	5.87E+02
	H.B. Robinson	34.0	-80.0	2.47E-02	4.24E-02	1.92E+00	1.59E-01
	Hatch	31.0	-82.0	5.90E+01	1.22E+02	1.49E+04	4.55E+02
	Hope Creek	39.0	-75.0	6.81E+03	8.16E+01	1.44E+04	2.38E+02
	Indian Point	41.0	-73.0	0.00E+00	1.36E-02	1.51E+01	3.98E-01
	Kewaunee	44.0	-87.0	0.00E+00	0.00E+00	0.00E+00	0.00E+00
	Lasalle	41.0	-88.0	1.27E-01	1.05E+02	4.21E+04	6.56E+03
	Limerick	40.0	-75.0	1.08E+01	3.73E+03	3.85E+03	4.04E+03
	Mcguire	35.0	-80.0	0.00E+00	2.23E-04	8.58E-03	0.00E+00
	Millstone	41.0	-72.0	5.92E+00	1.10E+00	6.85E+02	7.43E+01
	Monticello	45.0	-93.0	2.16E+01	9.39E+00	1.79E+03	3.24E+03
	Nine Mile Point	43.0	-76.0	6.73E-05	6.63E-04	1.03E+01	7.79E+00
	North Anna	38.0	-77.0	3.12E-04	7.40E-02	5.38E+02	1.62E+00
	Oconee	34.0	-82.0	8.86E+01	5.69E-01	1.09E+02	1.49E+01
	Oyster Creek	39.0	-74.0	0.00E+00	0.00E+00	2.88E+03	3.63E+03
	Palisades	42.0	-86.0	1.04E+00	7.52E-01	4.20E+02	7.41E-01
	Palo Verde	33.0	-112.0	2.64E+02	8.15E+01	6.55E+03	3.62E+01
	Peach Bottom	39.0	-76.0	0.00E+00	0.00E+00	9.80E+02	4.06E+02
	Perry	41.0	-81.0	1.20E+01	1.79E+01	9.71E+02	2.24E+02
	Pilgrim	41.0	-70.0	0.00E+00	2.32E+01	1.38E+03	1.66E+03
	Point Beach	44.0	-87.0	3.04E-02	8.20E-02	8.27E+00	2.88E-01
	Prairie Island	44.0	-92.0	9.61E+00	9.04E-01	1.59E+02	1.46E+00
	Quad Cities	41.0	-90.0	1.39E+01	3.63E+00	1.07E+03	6.46E+02

Country	Site Name	Lat	Lon	^{131m}Xe	^{133m}Xe	^{133}Xe	^{135}Xe
	R.E. Ginna	43.0	-77.0	4.57E-01	2.76E+00	1.83E+03	3.92E+02
	River Bend	30.0	-91.0	1.92E+01	4.99E+01	5.10E+03	1.80E+03
	Salem	39.0	-75.0	3.64E+03	1.64E+03	1.35E+04	2.64E+02
	San Onofre	33.0	-117.0	3.18E+00	1.64E+01	2.48E+03	1.16E+01
	Seabrook	42.0	-70.0	0.00E+00	0.00E+00	5.37E+01	2.43E-02
	Sequoyah	35.0	-85.0	5.59E-01	0.00E+00	1.13E+03	8.56E+00
	Shearon Harris	35.0	-78.0	0.00E+00	0.00E+00	2.08E+02	2.36E+00
	South Texas	28.0	-96.0	1.13E+01	3.27E+00	1.35E+04	6.17E+00
	St. Lucie	27.0	-80.0	0.00E+00	3.15E+01	8.15E+02	4.69E+02
	Surry	37.0	-76.0	0.00E+00	1.41E-02	1.61E+00	1.74E-01
	Susquehanna	41.0	-76.0	0.00E+00	4.69E+00	8.73E-03	1.79E+01
	Three Mile Island	40.0	-76.0	0.00E+00	0.00E+00	0.00E+00	3.51E-02
	Turkey Point	25.0	-80.0	0.00E+00	0.00E+00	1.65E+02	0.00E+00
	Vermont Yankee	42.0	-72.0	0.00E+00	0.00E+00	0.00E+00	1.57E+01
	Virgil C. Summer	34.0	-81.0	1.53E+01	1.80E+00	1.11E+01	6.63E-01
	Vogtle	33.0	-81.0	0.00E+00	0.00E+00	1.12E+02	2.90E+01
	Waterford	30.0	-90.0	1.25E+02	5.67E+01	5.46E+03	5.38E+01
	Watts Bar	35.0	-84.0	0.00E+00	0.00E+00	1.25E+00	5.55E-04
	Wolf Creek	38.0	-95.0	1.69E+02	0.00E+00	1.54E+02	1.42E+01

C - Used Hardware and Software

Software

- FLEXPART v8.2, available at `http://transport.nilu.no/flexpart`
- OriginPro 8.6.0 (32 bit), © 1991-2012 OriginLab Corporation
- Easyfit Professional 5.5, © 2004-2010 MathWave Technologies
- MapInfo Professional 11.0, © 2011 Pitney Bowes Software Inc.

Hardware and Operating Systems

- User-Interface "ui-01", Scientific Linux 6.2 (64 bit)
  - 500x Intel Xeon CPU X5675 @ 3.07GHz, 2 GB RAM
  - 100x Intel Xeon CPU L5335 @ 2.00GHz, 2 GB RAM
- Sony Vaio VPCF13Z1E/B, Intel® Core™ i7-740QM, aka "Tegola"
  - Windows 7 Professional (64 bit)
  - Scientific Linux 6.1 (64 bit)

Bibliography

[Adu93] Teleseismic Monitoring of Underground Nuclear Explosions at the Nevada Test Site from Borovoye, Kazakhstan - Vitaly V. Adushkina and Vadim A. Ana (Science & Global Security, 1993, Volume 3, pp.289-309)

[Aue10] Ten years of development of equipment for measurement of atmospheric radioactive xenon for the verification of the CTBT - M. Auer, T. Kumberg, H. Sartorius, B. Wernsperger, C. Schlosser (Pure and Applied Geophysics, Vol. 167, 2010, pp. 471–486)

[Aue12] CTBT Overview - Design and Setup of the global RN Monitoring System - M. Auer (Presentation at the Workshop on the Signatures of Medical and Industrial Isotope Production (WOSMIP) on 19 June 2012)

[Bar01] Seismological monitoring of the Comprehensive Nuclear-Test-Ban Treaty - S. Barrientos, F. Haslinger (Kerntechnik 66 (3), 82–89, 2001)

[Bat10] The solution of a system of differential equations in the theory of radioactive transformation - H. Bateman (Proc. Cambridge Phil. Soc. (16), p. 423-427, 1910)

[Bea07] Understanding the Memory Effect in SAUNA's Plastic Scintillator and Its Impact on the Measurement - M. Bean, N. St-Amant, K. Ungar (Poster presented at the Informal Noble Gas Workshop, Las Vegas, 2007)

[Bel99] The IGBP-DIS 1-Km Land-Cover Data Set DISCover: A Project Overview - A. Belward, J. Estes, K. Kline (Photogrammetric Engineering and Remote Sensing , Vol. 65, No. 9, pp. 1013–1020, 1999)

[Bie01] Determining detection limits and Minimum Detectable Concentrations for noble gas detectors utilizing beta-gamma coincidence systems - K. Biegalski, S. Biegalski (Journal of Radioanalytical and Nuclear Chemistry 248, 673-682, 2001)

[Chr01] Detection of atmospheric nuclear explosions. The infrasound component of the International Monitoring System - D. Christie, J. Vivas Veloso, P. Campus, M. Bell, T. Hoffmann, A. Langlois, P. Martysevich, E. Demirovic, J. Carvalho (Kerntechnik 66 (3), 96–101, 2001)

[Cur68] Limits for qualitative detection and quantitative determination - L. Currie (Analytical Chemistry 340, 586-593, 1968)

[DeG02] Basic Nuclear Data for PTS Xenon Analyses - L. De Geer (PTS/IDC/RS/RD, 9 April, 2002)

[DeG12] Radionuclide Evidence for Low-Yield Nuclear Testing in North Korea in April/May 2010 - Lars-Erik De Geer (Science & Global Security: The Technical Basis for Arms Control, Disarmament, and Nonproliferation Initiatives, 20:1, 1-29, March 2012)

[Eng93] T.R. England, B.F. Rider (Los Alamos National Laboratory, LA-UR-94-3106; ENDF-349, 1993)

[Fei02] Modeling chemical constituents of the atmosphere - Feichter, J., Schultz, M., Diehl, T. (Computing in Science & Engineering 4 (5), 56–63, 2002)

[Fon04] Atmospheric xenon radioactive isotope monitoring - J.-P. Fontaine, F. Pointurier, X. Blanchard, T. Taffary (J. Environ. Rad. 72, 129–135, 2004)

[Hei02] Environmental monitoring of radioxenon in support of the radionuclide measurement system of the international monitoring system - T. Heimbigner, J. McIntyre, T. Bowyer, J. Hayes, M. Panisko (24th Seismic Research Review – Nuclear Explosion Monitoring: Innovation and Integration, NNSA, Ponte Vedra Beach, Florida, 2002)

[Hof12] Personal communication - Emmy Hoffmann (Australian Nuclear Science and Technology Organisation ANSTO, 2012)

[Iae12] Power Reactor Information System (PRIS) - International Atomic Energy Agency (`www.iaea.org/programmes/a2/`, last checked as of November 2012)

[Ima12] Status of Radioisotope Production of Mo-99 from FPM using LEU Target and I-131; Current and Increased Production Capacity in the Near Future - Y. Imardjoko (Presentation at the Workshop on the Signatures of Medical and Industrial Isotope Production (WOSMIP) on 20 June 2012)

[Ing03] Noble Gas Monitoring Handbook - International Noble Gas Experiment (INGE) (CTBTO, Version 1.0, 2003)

[Jac99] Introduction to Atmospheric Chemistry - D. Jacob (Princeton University Press, 1999)

[Kal06] Isotopic signature of atmospheric xenon released from lightwater reactors - M. Kalinowski, C. Pistner (Journal of Environmental Radioactivity 88 (3), 215–235, 2006)

[Kal09] Global radioxenon emission inventory based on nuclear power reactor reports - M. Kalinowski, M. Tuma (Journal of Environmental Radioactivity 100, 2009, pp. 58-70)

[Kal10] Discrimination of Nuclear Explosions against Civilian Sources Based on Atmospheric Xenon Isotopic Activity Ratios - M. Kalinowski et al. (Pure and Applied Geophysics 167, 2010, pp. 517-539)

[Kal11] Characterisation of prompt and delayed atmospheric radioactivity releases from underground nuclear tests at Nevada as a function of release time - M. Kalinowski (Journal of Environmental Radioactivity 102, 824-836, 2011)

[Kal12] Implications of Xe-emissions from medical isotope production - M. Kalinowski, M. Grosch, S. Hebel (Pure and Applied Geophysics, Topical Volume Nuclear Explosion Monitoring - Vol. II, 2012)

[Kon04] Mixing and ozone loss in the 1999–2000 Arctic vortex: Simulations with the three-dimensional Chemical Lagrangian Model of the Stratosphere (CLaMS) - P. Konopka, H.-M. Steinhorst, J. Grooß, G. Gebhard, R. Müller, J. Elkins, H. Jost, E. Richard, U. Schmidt, G. Toon, D. McKenna (J. Geophys. Res., 109, D02315, doi:10.1029/2003JD003792, 2004)

[Law01] Hydroacoustic monitoring system for the Comprehensive Nuclear-Test-Ban Treaty - M. Lawrence, M. Galindo, P. Grenard, J. Newton (Kerntechnik 66 (3), 90–95, 2001)

[Mar06] Mid-Latitude Atmospheric Dynamics, A First Course - J. Martin (John Wiley and Sons, Ltd, 2006)

[Mat01] The radionuclide monitoring system of the Comprehensive Nuclear-Test-Ban Treaty Organisation: From sample to product - M. Matthews, J. Schulze (Kerntechnik 66(3), 102– 112, 2001)

[Mat05] The CTBT verification significance of particulate radionuclides detected by the International Monitoring System - K. M. Matthews (National Radiation Laboratory, Ministry of Health, New Zealand, `http://www.nrl.moh.govt.nz`, 2005)

[Nea02] Chernobyl: Assessment of Radiological and Health Impacts, 2002 Update of Chernobyl: Ten Years On - Nuclear Energy Agency (NEA) (Organisation for Economic Co-Operation and Development (OECD) Publications, pp. 155, Paris, 2002)

[Nik11a] Noble Gas Categorization scheme - M. Nikkinen, U. Stoehlker, A. Gheddou, M. Verpelli (Presentation at the Working Group B meeting 36, February 2011)

[Nik11b] Use of Xenon Emission Data to Calculate the Effect of Pharmaceutical Facilities on CTBT Xenon Detections - M. Nikkinen, M. Krysta, U. Stoehlker (Presentation at WOSMIP II, Strassoldo, Italy, June 2011)

[Noa12] ENSO Cycle: Recent Evolution, Current Status and Predictions - National Oceanic and Atmospheric Administration (Climate Prediction Center of the National Centers for Environmental Prediction, `http://www.cpc.ncep.noaa.gov/products/analysis_monitoring/lanina/enso_evolution-status-fcsts-web.pdf`, October 2012)

[Orr12] Detection of radioxenon in Darwin, Australia following the Fukushima Daiichi nuclear power plant accident - B. Orr, M. Schoeppner, R. Tinker, W. Plastino (to be submitted to the Journal of Environmental Radioactivity, 2012)

[Osb08] The Mercator Projections - P. Osborne (Edinburgh, 2008)

[Pef11] Hybrid variational ensemble data assimilation with inital condition and model physics uncertainty - Luke Peffer (PhD thesis, Florida State University, 2011)

[Per11] User guide to ECMWF forecast products - Anders Persson (ECMWF, 2011)

[Pla10] Radioxenon Time Series and Meteorological Pattern Analysis for CTBT Event Categorisation - W. Plastino, R. Plenteda, G. Azzari, A. Becker, P. Saey, G. Wotawa (Pure and Applied Geophysics, Pure and Applied Geophysics 167, 559-573, 2010)

[Pla11] Atmospheric Transport Modeling Based Estimation of Radioactive Release from the Fukushima Dai-ichi Nuclear Power Plant Accident - Wolfango Plastino, Michael Schöppner, Francesco Bella, Mario De Vincenzi, Gerhard Wotawa, Pavel P. Povinec, Antonio Budano, Federico Ruggieri (2011 Seventh International Conference on Natural Computation, 2027-2030, 2011)

[Pos12] Capability to categorise real and hypothetical cases of radioxenon releases for CTBT verification - Frederik Postelt (Diploma Thesis, ZNF, 2012)

[Ric90] Seismic Discrimination of Nuclear Explosions - P.G. Richards, J. Zavales (Annu. Rev. Earth Planet. Sci. 1990, 18:257-86)

[Ric06] Spying on the bomb: American nuclear intelligence from Nazi Germany to Iran and North Korea - J. Richelson (Norton & Company, 2006)

[Rin03] SAUNA—A system for automatic sampling, processing, and analysis of radioactive xenon - A. Ringbom, T. Larson, A. Axelsson, K. Elmgren, C. Johansson (Nucl. Inst. Meth. A 508, 542–553, 2003)

[Rin09] Measurements of Radioxenon in Ground Level Air in South Korea Following the Claimed Nuclear Test in North Korea on October 9, 2006 - A. Ringbom, K. Elmgren, K. Lindh, J. Peterson, T. W. Bowyer, J. C. Hayes,

J. I. McIntyre, M. Paninsko, and R. Williams (Journal of Radioanalytical and Nuclear Chemistry 282, 773–779, 2009)

[Ros10] Simulation of atmospheric krypton-85 transport to assess the detectability of clandestine nuclear reprocessing - Jens Ole Ross (Dissertation, University of Hamburg, 2010)

[Sae07] Technical report on noble gas data processing in support of CTBT verication - P. Saey, L. De Geer (Technical report, Provisional Technical Secretariat (PTS) for the CTBTO, 2007)

[Sae09] The influence of radiopharmaceutical isotope production on the global radioxenon background - P. Saey (Journal of Environmental Radioactivity 100, 2009, pp. 396-406)

[Sae10a] Environmental radioxenon levels in Europe: A comprehensive overview - P. Saey, C. Schlosser et al. (Pure and Applied Geophysics, Vol. 167, 2010, pp. 499-515)

[Sae10b] Isotopic noble gas signatures released from medical isotope production facilities-Simulations and measurements - P. Saey, T. Bowyer, A. Ringbom (Applied Radiation and Isotopes 68, 2010, pp. 1846-1854)

[Sae10c] The influence on the radioxenon background during the temporary suspension of operations of three major medical isotope production facilities in the Northern Hemisphere and during the start-up of another facility in the Southern Hemisphere - P. Saey et al. (Journal of Enironmental Radioactivity 101, 2010, pp. 730-738)

[Sae12] Complexity of radioxenon isotopical ratios in medical and industrial isotope production facilities - P. Saey (Presentation at WOSMIP III, Strassoldo, Italy, June 2012)

[Sal85] Reprocessing of irradiated uranium-235 for the production of Mo-99, I-131, Xe-133 radioisotopes - J. Salacz, (Revue IRE Tijdschrift 9(3), 22–28, 1985)

[Sal12] Physics of the Atmosphere and Climate - M. Salby (Cambridge University Press, 2012)

[Sam87] Production techniques of fission molybdenum-99 - A.A. Sameh, H.J. Ache (Radiochimica Acta 41, 65–72, 1987)

[Sau12] Scienta SAUNA Systems, Uppsala, Sweden, Official Website > About Us > Radioxenon Detection, (`www.saunasystems.se/default.aspx?PID=45`, 2012)

[Sch96] Radiological Effluents Released from U.S. Continental Tests 1961 through 1992 - C. Schoengold, M. DeMarre, E. Kirkwood (United States Department of Energy, Nevada Operations Office, August 1996)

[Sch00] Low level radioactivity measurement in support of the CTBTO - J. Schulze, M. Auer, R. Werzi (Appl. Rad. Isotopes 53, 23–30, 2000)

[Sch11] Estimation of the time-dependent radioactive source-term from the Fukushima nuclear power plant accident using atmospheric transport modelling - M. Schöppner, W. Plastino, P. Povinec, G. Wotawa, F. Bella, A. Budano, M. De Vincenzi, F. Ruggieri (Journal of Environmental Radioactivity, Special Fukushima Edition, 2011)

[Sch12a] Impact of monthly radioxenon source time-resolution on atmospheric concentration predictions - M.Schöppner, M. Kalinowski, W. Plastino, A. Budano, M. de Vincenzi, A. Ringbom, F. Ruggieri, C.Schlosser (Topical Volume II, Nuclear Explosion Monitoring, Pure Appl. Geophys., DOI 10.1007/s00024-012-0499-z, 2012)

[Sch12b] Atmospheric transport modelling of time resolved xenon-133 emissions from ANSTO, Australia - M. Schöppner, W. Plastino, N. Hermanspahn, E. Hoffmann, M. Kalinowski, B. Orr, R. Tinker (under submission to the Journal of Environmental Radioactivity, 2012)

[Sei99] Inverse modelling of sulfur emissions in Europe based on trajectories - P. Seibert (Inverse Methods in Global Biogeochemical Cycles AGU Geophysical Monograph Vol. 114, 147-154, 1999)

[Sei00] Inverse modelling of the ETEX-1 release with a Lagrangian particle model - P. Seibert, A. Stohl (Proc. Third GLOREAM Workshop, Ischia, Italy, September 1999, 2000)

[Sei11] Uncertainties in the inverse modelling of sulphur dioxide eruption profiles - P. Seibert, N. Kristiansen, A. Richter, S. Eckhardt, A. Prata, A. Stohl (Geomatics, Natural Hazards and Risk, 2:3, 201-216, 2011)

[Sow12] Kaye & Laby, Tables of Physical and Chemical Constants - M. Sowerby (National Physical Laboratory, `http://www.kayelaby.npl.co.uk/`, 2012)

[Sto98] Validation of the Lagrangian particle dispersion model FLEXPART against large-scale tracer experiment data - A. Stohl, M. Hittenberger, G. Wotawa (Atmospheric Environment Vol. 32, No. 24, 1998, pp. 4245-4264)

[Sto09] An analytical inversion method for determining regional and global emissions of greenhouse gases: Sensitivity studies and application to halocarbons - A. Stohl, P. Seibert, J. Arduini, S. Eckhardt, P. Fraser, B. Greally, C. Lunder, M. Maione, J. Mühle, S. O'Doherty, R. Prinn, S. Reimann, T. Saito, N. Schmidbauer, P. Simmonds, M. Vollmer, R. Weiss, Y. Yokouchi (Atmos. Chem. Phys., 9, 1597–1620, doi:10.5194/acp-9-1597- 20 2009, 2009)

[Sto10] The Lagrangian particle dispersion model FLEXPART version 8.2 - A. Stohl, H. Sodemann, S. Eckhardt, A. Frank, P. Seibert, G. Wotawa (`http://transport.nilu.no/flexpart`, 2010)

[Sto11] Xenon-133 and caesium-137 releases into the atmosphere from the Fukushima Dai-ichi nuclear power plant: determination of the source term, atmospheric dispersion, and deposition - A. Stohl, P. Seibert, G. Wotawa, D. Arnold, J. F. Burkhart, S. Eckhardt, C. Tapia, A. Vargas, and T. J. Yasunari (Atmos. Chem. Phys. Discuss., 11, 28319–28394, October 2011)

[Tin10] Evaluation of radioxenon releases in Australia using atmospheric dispersion modelling tools - R. Tinker, B. Orr, M. Grzechnik, E. Hoffmann, P. Saey, S. Solomon (Journal of Environmental Radioactivity 101, 2010, pp. 353-361)

[Uns09] Effects of ionizing radiation: United Nations Scientific Committee on the Effects of Atomic Radiation - UNSCEAR 2006 Report, Volume II - report to the general assembly, with scientific annexes C, D, and E - Annex E: sources-to-effects assessment for radon in homes and work places. (Effects of ionizing radiation, 2, UNSCEAR, Vienna, Austria, p.217, 2009)

[vDe12] virtual Data Exploitation Centre - CTBTO (2012)

[Wot03a] Atmospheric transport modelling in support of CTBT verification-overview and basic concepts - G. Wotawa et al. (Atmospheric Environment 37, pp. 2529-2537, 2003)

[Wot03b] New ATM Software layer 2, Software package SRSM-MODEL Version 1.0, Short User Guide - G. Wotawa (CTBTO, 2003)

[Wot10] Computation and Analysis of the Global Distribution of the Radioxenon Isotope 133-Xe based on Emissions from Nuclear Power Plants and Radioisotope Production Facilities and its Relevance for the Verification of the Nuclear-Test-Ban Treaty - G. Wotawa, A. Becker, M. Kalinowski, P. Saey, M. Tuma, M. Zähringer (Pure and Applied Geophysics 167, 2010, pp. 541-557)

[Zäh09] Testing Noble Gas Categorization with IMS data - M. Zähringer, A. Becker, M. Nikkinen (Presentation at the Working Group B meeting, 17 February 2009)

Acknowledgements

The foremost acknowledgement goes to Wolfango Plastino for his supervision, ideas, support and willingness to host this project. On a fundamental level I also want to personally thank Martin B. Kalinowski for the basic idea for this thesis and repeated feedback and guidance.

Without steady communication and exchange with the experts in this field of research this work would have been impossible. My gratitude goes in particular to Gerhard Wotawa for introducing me to ATM and answering my many subsequent questions, and also to Andreas Becker, Paul Saey and Roberto Ferretti for their advice and efforts.

Thanks for the support, openness as well as advice in scientific and legal issues from the PTS within the CTBTO, specifically Mika Nikkinen and Monika Krysta; and in the same regard also to Christian Weihrauch from the ECMWF.

The local implementation of software, job coordination, data storage and general handling of grid computer issues have been made possible thanks to the team of Federico Ruggieri, namely Antonio Budano, Federico Bitelli and Claudio Calvani.

I am also grateful for the opportunities for discussion at the General Assembly of the European Geophysical Union and especially at the Workshop on Signatures of Medical and Industrial Isotope Production, which cannot go unmentioned with the names of Paul Saey and Ted Bowyer.

As it ought to be, the final credits are non-scientific in their nature and are going out to friends and family of whom many had a share in my preservation and motivation, each one in an own, special way and some of them perhaps even unaware of their contribution.